NOVA SCHOOL OF SCIENCE & TECHNOLOGY

DEPARTMENT OF CHEMISTRY

ANA EDUARDA LOPES MELICIANO

Degree in Biochemistry

EMPOWERING THE THERAPEUTICAL POTENTIAL OF CLINICALLY EXPIRED PLATELET CONCENTRATES: A NEW SOURCE OF EXTRACELLULAR VESICLES

MASTER DEGREE IN BIOTECHNOLOGY

NOVA University of Lisboa

December 2021

NOVA SCHOOL OF SCIENCE & TECHNOLOGY

DEPARTMENT OF CHEMISTRY

EMPOWERING THE THERAPEUTICAL POTENTIAL OF CLINICALLY EXPIRED PLATELET CONCENTRATES: A NEW SOURCE OF EXTRACELLULAR VESICLES

ANA EDUARDA LOPES MELICIANO
Degree in Biochemistry

Supervisor: Dr. Margarida Serra, Senior Scientist, iBET/ITQB-NOVA
Co-Supervisor: Dr. Daniela Salvador, Scientist, iBET/ITQB-NOVA

Jury:

President: Prof. Dr. Ana Rita Cruz Duarte
Examiner: Dr. Patricia Raquel Pinheiro Pitrez Pereira
Vogal: Dr. Maria Margarida de Carvalho Negrão Serra

MASTER DEGREE IN BIOTECHNOLOGY

NOVA University of Lisboa
December 2021

Empowering the therapeutic potential of clinically expired platelet concentrates: a new source of extracellular vesicles

Acknowledgements

Primariamente pretendo deixar o meu agradecimento à Dr. Paula Alves e ao Professor Manuel Carrondo pela possibilidade de realizar a minha dissertação de mestrado no laboratório de Tecnologia de Células Animais (TCA) no iBET.

Igualmente, à Dr. Margarida Serra, deixo o meu especial obrigado por ter aceite ser a minha orientadora e me tão bem ter recebido no seu grupo e neste projeto. Pela disponibilidade e orientação, pelo suporte e estímulo demonstrados ao longo deste último ano.

À minha co-orientadora, Dr. Daniela Salvador, fica o meu reconhecimento por todos os ensinamentos científicos que me transmitiu. Pelo incansável apoio nos momentos mais desafiantes, pela dedicação, pelo incentivo e confiança investidos em mim. Pela paciência, sentido crítico e boa disposição constantes.

A todos os colegas do TCA pelo ambiente acolhedor e agradável de trabalho. Pelas amizades que emergiram e que permitiram descontração e boa animação no laboratório. Um agradecimento especial à Filipa Louro, pela opinião crítica que sempre demonstrou em relação a este trabalho e pela cooperação científica prestada. À Marta Paiva, Joana Almeida, Henrique Almeida, Pedro Vicente, Cláudia Diniz e Inês Crespo pela disponibilidade que sempre revelaram ter para me dar apoio e orientação no laboratório. À Margarida Costa pela companhia, amizade e todas as conversas de interajuda ao longo deste período. À Beatriz Gamelas, Marta Costa e Hélio Tomás pela preocupação e interesse que foram demonstrando por mim e pelo meu trabalho.

À Ana Paula Sousa e ao Pedro Mendonça, os responsáveis do IPST pelo fornecimento dos concentrados de plaquetas usados neste trabalho. À Maria João Almeida, da unidade de microscopia eletrónica do Instituto Gulbenkian de Ciência pelo suporte técnico prestado.

Aos meus amigos que indiretamente me deram o seu apoio para enfrentar esta etapa e que compreensão expressaram para comigo sempre que os nossos encontros eram por mim cancelados. Estas palavras são manifestadas com especial enfoco nos meus amigos Sara, Vítor, Beatriz e Joana. O meu agradecimento ao João Pedro, que notavelmente esteve sempre presente nesta caminhada, transmitindo-me confiança, motivação e suporte quando mais precisava.

Aos meus pais e irmãs pela paciência e apoio incondicionais que expressam por mim independentemente da etapa na qual me encontre. Principalmente pelo amparo que me concederam nos momentos mais desafiantes e pelas condições que favoravelmente me proporcionaram no decorrer deste trajeto.

Preface

The present work was performed at the Animal Cell Technology Unit at iBET/ITQB-NOVA (Oeiras, Portugal), under the scope of the Fundação para a Ciência e Tecnologia funded projects PEFPlateletValue (PTDC/BTM-ORG/32187/201), and iNOVA4Health (UIDB/04462/2020 and UIDP/04462/2020), a program financially supported by Fundação para a Ciência e Tecnologia/Ministério da Ciência, Tecnologia e Ensino superior, through national funds.

A manuscript compiling the data herein presented is in preparation. Part of the results described in this thesis was presented in the two conferences:

Daniela Salvador, **Ana Meliciano**, Ana Filipa Louro, Pedro Mendonça, Ana Paula Sousa, Margarida Serra. *Empowering the therapeutic potential of clinically expired platelet concentrates: a new source of regenerative EV*. 10th Annual Meeting of the International Society for Extracellular Vesicles (ISEV), May 2021, Virtual Conference (Poster communication).

Ana Meliciano, Daniela Salvador, Ana Filipa Louro, Pedro Mendonça, Ana Paula Sousa, Margarida Serra. *Empowering the therapeutic potential of clinically expired platelet concentrates: a new source of regenerative EV*. First Meeting of Portuguese Network on Extracellular Vesicles (PNEV), September 2021, Investigação e Inovação em Saúde (i3S), Universidade do Porto, Porto, Portugal (Presenting author, Oral communication).

Abstract

The limited shelf-life of platelet concentrates (PC) produced in blood centers leads to a significant portion of platelet donations being discarded before being purposed for transfusion. Consequently, PC are an enormous financial burden for the healthcare system, so, new applications for expired PC have been growing over the past years. Inspired by the high amounts of platelet-derived extracellular vesicles (pEV) that are released during PC storage and by the natural appetency of pEV to interact with cancer cells, we investigated the efficacy of pEV from expired PC as carriers of paclitaxel (PTX), an anti-angiogenic and anti-cancer drug.

In this thesis, pEV were isolated from expired PC using different methods (density gradient ultracentrifugation (DGUC); size exclusion chromatography and the combination of both methods). The highest EV yield ($2.03x10^{11}$/100 mL PC) was obtained using DGUC, so this was selected as the most suitable protocol. Furthermore, a low level of contaminating protein, together with the detection of specific EV markers (CD9, CD63 and FLOT2) were observed. In addition, a typical EV size distribution profile (100-300 nm) with a typical cup-shaped morphology was achieved. By direct incubation, pEV were loaded with PTX (PTX-pEV), and their functionality was assessed on endothelial and breast cancer cell lines (basal, MDA-MB-231 and luminal B, BT474).

Our findings suggest that PTX-pEV showed higher anti-migratory and anti-angiogenic activity than the free drug. A comparison of the cytotoxic effect of PTX-pEV on breast cancer cells was carried out, which identified a decrease in cell viability (21.05%) and proliferation (41.04%) only in BT474. PTX delivery pathways for MDA-MB-231 and BT474 were also distinctly affected by EV uptake inhibitors, between cell lines, showing that dynamin-dependent endocytosis and heparin sulphate proteoglycan-dependent mechanism were only responsible by the PTX release on BT474.

Keywords: expired platelet concentrates, platelet-derived extracellular vesicles, drug delivery system, paclitaxel, therapeutic effect, breast cancer

Resumo

A data de validade limitada dos concentrados de plaquetas (PC) produzidos nos centros de transfusão de sangue, leva a que uma significante porção de doações de plaquetas seja descartada antes de serem transfundidas. Consequentemente, os PC são um enorme encargo financeiro para o sistema de saúde, e como tal, novas aplicações para PC expirados têm vindo a emergir nos últimos anos. Inspirados pelas elevadas quantidades de vesículas extracelulares derivadas de plaquetas (pEV) que são libertadas durante o período de armazenamento dos PC, e pela sua apetência natural para interagir com células cancerígenas, investigámos a eficácia das pEV de PC expirados como sistemas de entrega de paclitaxel (PTX), um fármaco anti angiogénico e anti cancerígeno.

Neste trabalho, as pEV foram isoladas dos PC expirados através de diferentes métodos (ultracentrifugação em gradiente de densidade (DGUC); cromatografia de exclusão molecular e por combinação dos dois métodos). O maior rendimento em pEV ($2.03x10^{11}$/100 mL PC) foi obtido por DGUC, e como tal, este foi selecionado o protocolo mais adequado. Adicionalmente, através deste obtiveram-se baixos níveis de contaminação proteíca, bem como se detetaram marcadores específicos de EV (CD9, CD63 e FLOT2). Para além disto, obtiveram-se pEV com um perfil de distribuição de tamanho típico (100-300 nm) e com uma morfologia típica. Por incubação direta, as pEV foram encapsuladas com o PTX (PTX-pEV), e a sua funcionalidade foi avaliada em células endoteliais e em duas linhas celulares de cancro da mama (basal, MDA-MB-231 e luminal B, BT474).

Os resultados sugerem que as PTX-pEV apresentaram uma maior atividade anti migratória e anti angiogénica que o fármaco livre. Quando comparado o efeito citotóxico das PTX-pEV nas células de cancro da mama, identificou-se um decréscimo na viabilidade (21.05%) e proliferação (41.04%) celulares apenas para as BT474. Após incubação com inibidores de internalização de EV, as via de internalização celular das pEV foram também diferencialmente afetadas entre MDA-MB-231 e BT474, mostrando-se desta forma que as vias de endocitose dependente de dinamina e dependente de proteoglicanos heparina sulfato estavam apenas envolvidas na entrega do PTX nas BT474.

Palavras-Chave: concentrados de plaquetas expirados, vesículas extracelulares derivadas de plaquetas, sistemas de entrega de fármaco, paclitaxel, efeito terapêutico, cancro da mama

TABLE OF CONTENTS

LIST OF FIGURES

LIST OF TABLES

Abbreviations

AB	Apoptotic bodies
AP	Single-donor apheresis
BAR	Bin/Amphiphysin/Rvs
BC	Buffy-coat
BCA	Bicinchoninic acid
BSA	Bovine serum albumin
CAV-1	Caveolin-1
DAPI	4′,6-diamidino-2-phenylindole
DGUC	Density gradient ultracentrifugation
DMSO	Dimethyl sulfoxide
DPBS	Dulbecco's phosphate-buffered saline
ECL	Enhanced chemiluminescence detection
EDTA	Ethylenediamine tetraacetic acid
EdU	5-ethynyl-2’-deoxyuridine
EGF	Epidermal growth factor
EGFR	Epidermal growth factor receptor
ELISA	Enzyme-linked immunosorbent assay
ER	Estrogen receptor
EV	Extracellular vesicle
FACS	Flow cytometry staining
FBS	Fetal bovine serum
FGF	Fibroblast growth factor
FSG	Fish skin gelatin
GA-1000	Gentamicin/Amphotericin-B
GF	Growth Factors
HBV	Hepatitis B virus
HCV	Hepatitis C virus
HDL	High density lipoprotein
HER2	Human epidermal growth factor receptor 2
HIV	Human immunodeficiency virus
HPL	Human platelet lysate
HPLC	High-performance liquid chromatography
HSP	Heparan sulphate proteoglycans
HUVEC	Human Umbilical Vein Endothelial Cells
IC	Immunocytochemistry
iPSC	induced pluripotent stem cell
ISEV	International Society for Extracellular Vesicles

MFSD2a	Major facilitator superfamily domain containing 2a
MSC	Mesenchymal stromal cells
MV	Microvesicles
NTA	Nanoparticle tracking analysis
PAS	Platelet additive solution
PC	Platelet concentrate
PDGF	Platelet-derived growth factor
PECAM-1	Platelet-endothelial cell adhesion molecule-1
PEG	Polyethylene glycol
pEV	Platelet-derived extracellular vesicle
PFA	Paraformaldehyde
P-gp	P-glycoprotein
PI3P	Phosphoinositide 3-phosphate
PM	Plasma membrane
PR	Progesterone receptor
PRP	Platelet-rich plasma
PS	Phosphatidylserine
PTX	Paclitaxel
PVDF	Polyvinylidene fluoride membranes
qR-PCR	Quantitative reverse transcription polymerase chain reaction
R3-IGF-1	R3-Insulin-like growth factor
RBC	Red blood cells
RIPA	Radioimmunoprecipitation assay
RPMI	Roswell Park Memorial Institute
RT	Room temperature
SEC	Size Exclusion chromatography
SNX	Sorting nexins
TBST	Tris-buffered saline with tween-20
TEM	Transmission electron microscopy
TGF-β	Transforming growth factor-β
TIM	T-cell immunoglobulin mucin
TNBC	Triple-negative breast cancer
UV	Ultraviolet
VEGF	Vascular endothelial growth factor
WB	Western blot
WBC	White blood cells

CHAPTER 1

1. Introduction

Platelet concentrates (PC) are blood-derived products enriched in intact platelets from healthy donors. PC have been widely used to treat or prevent hematological diseases [1], however, their inherent short shelf-life leads to their periodic disposal [2]. In this regard, alternative therapeutic applications have been extensively reported, especially using PC as a growth factor (GF) source for regenerative medicine and cell therapy [3]. Besides, it is known that during PC storage, high amounts of platelet-derived extracellular vesicles (pEV) are released and accumulated, nevertheless, little research has explored its applicability. Concerning the therapeutic potential of pEV, recent trends have been investigated the beneficial use of EV over conventional carries for their application as drug delivery systems [4].

In this chapter, a revision is presented by integrating two research topics - pEV as an alternative therapy for expired PC and pEV as drug vehicles.

1.1. Platelets

Platelets are small non-nucleated blood cells produced from megakaryocytes, with relevant functions regarding inflammation, immunity, and regenerative responses [5]. Due to their limited lifespan in circulation (approximately 7-10 days) [5], new platelets need to be produced every day to maintain a concentration of 150-400 $\times$ 10^9 platelets per liter of blood [6]. Thus, approximately one trillion of circulating platelets are present on a healthy individual [5,6], representing the second most prevalent cell type in human blood [7,8].

Platelets are known to contain three main populations of granules, which differ in their composition, biogenesis and function: α-granules, dense granules, and platelet lysosomes. Platelet α-granules have spherical or oval morphology and represent the predominant population, with around 50-80 granules per platelet [9]. These granules are composed of a vast array of GF, proteins, coagulation factors, proteoglycans, and protease inhibitors. This includes platelet-derived growth factor (PDGF), transforming growth factor-β (TGF-β), fibroblast growth factor (FGF), membrane receptor molecules such as glycoprotein IIb/IIIa and P-selectin (CD62p) and proteins including albumin, factor V and von Willebrand antigen [9,10]. Dense granules, also known as δ-granules, are less abundant than α-granules (3-8 granules per each platelet). These granules have a simpler composition, containing calcium, serotonin, pyrophosphate, ADP, and ATP [11]. Platelet lysosomes are less present in platelets (1-3 lysosomes per platelet) and are filled with digestive enzymes (e.g., glycosidases and proteases) [10,12]

1.1.1. The origin and need of platelet concentrates

The origin of platelet transfusion therapy as a relevant procedure remote to the 1950s and 1960s, with the effective reduction of mortality in children with acute lymphoblastic leukemia. This illness was a major cause of mortality in 1955, given that chemotherapy treatment failure due to severe and frequently fatal hemorrhagic complications. Studies in leukemia patients demonstrate a quantitative relation between the occurrence of hemorrhage and the thrombocytopenia degree (platelet count $< 10 \times 10^9$ platelet/L) [13,14]. Patients with leukemia who had undergone chemotherapy treatments generally had a lower platelet count and consequently had a higher probability of bleeding episodes due to the primary role of platelets in blood clotting. For this reason, Dr. Emil Freireich was a pioneer in the treatment of thrombocytopenia condition and frequent hemorrhages in these children, by establishing the platelet transfusion approach [14,15]. However, the routine clinical practice of platelet transfusions faced obstacles concerning the storage conditions and quality of platelets. In 1969, Dr. Scott Murphy revolutionized platelet transfusion medicine by describing that methods of processing and storage of platelets at room temperature (RT, 22 °C) with continuous agitation were feasible, with maintenance of platelets viability for 1 to 3 days [15,16].

Nowadays, platelet transfusions have become crucial to modern clinical practice. According to the World Health Organization (WHO) [17], PC are considered an essential medical product. An increase platelet demand is expected in the upcoming years [18]. Currently, platelet transfusion therapy is recommended for hemorrhage treatment (therapeutic transfusion) or prevention (prophylactic transfusion) in patients with low platelet quantity or platelet function defects. Specifically, for the treatment of bone marrow failure or malignancies (e.g., leukemia, chronic and acute thrombocytopenia), hemopoietic stem cell transplantation, inherited or acquired function platelet defects (e.g., Glanzmann's thrombasthenia), and patients undergoing invasive procedures (e.g., intracranial surgery) [13].

1.1.2. Platelet concentrates processing and storage

Currently, several PC products are available for transfusion, which can be obtained from whole blood donations or single-donor apheresis (AP). The preparation of pooled PC from whole blood includes the buffy-coat (BC) and platelet-rich plasma (PRP) methods (Figure 1.1) [16]. These blood products are prepared under the healthcare system guidelines to assure the quality of these blood products [19].

For the BC method, initially, the whole blood is centrifuged until it reaches a separation into three layers. A layer with cellular elements from the plasma (platelet-poor plasma), a BC layer, and underneath a layer with red blood cells (RBC). This BC layer contains 90-95% of platelets and white blood cells (WBC) [20,21]. After this first centrifugation, the layers can be separated manually, however, the most common system used is an automated technique so-called top-and-bottom system. The BC enriched in platelets is resuspended in platelet additive solution (PAS), a synthetic medium that supports platelet function, and less often in plasma. Further, four to six BC units are typically pooled and centrifuged to increase purity, removing the remaining WBC and RBC. To ensure a residual concentration of leukocyte content, pooled BC are processed through a filter [20,21].

The PRP method refers to the preparation of autologous plasma with a platelet concentration above the typical value in healthy individuals (1.5×10^8 - 4.0×10^8 platelets/mL) [6]. Currently, PRP has been established to have at least 1.0×10^9 platelets/mL in 5 mL of plasma. In the usual method of PRP preparation, anticoagulant solutions are added (e.g., citrate-based anticoagulants/citrate-phosphate-dextrose) to whole blood, to chelate ionized calcium, inhibiting clotting factors and thrombin production [22]. Following this pre-treatment, two centrifugation steps are performed. The first separates the RBC from the plasma (consisting of platelets and WBC) and the second, consists of a soft spin to concentrate the platelets present in the plasma, resulting in the formation of platelet pellets. Following this, the volume above the pellets (platelet-poor plasma) is discarded and the pellets are resuspended with plasma or PAS to produce the PRP [23–25]. In agreement with the BC method, a therapeutic dose of platelets for the PRP procedure is also provided by pooling four to six units of donor platelets [26].

The production of blood components by AP initially involved manual methods, but due to their limited use since 1960s, they were replaced by automated approaches. The apheresis device draws the blood donor, adds anticoagulant solutions, and afterward, the blood passes through filters and/or centrifuges, resulting in platelet collection [21,26]. The remaining blood components return to the donor and the apheresis platelets are resuspended in plasma or PAS [27]. One of the advantages of the AP method is that platelets derived from a single donor reach up to 10 times more levels than the values achieved by the BC and PRP methods [21,26].

Platelet products represent one of the most expensive blood products [28,29], not only because of the optimal conditions required for platelet collection and processing, but also due to financial expenses necessary to maintain PC quality during storage time. Many factors are vital for maintaining the quality of platelets during an appropriate storing environment. Besides the PC preparation method chosen, an appropriate storage temperature, pH, bag plastic containers and agitation profile can influence the viability and quality of platelets. More specifically, the optimal temperature determined so far for platelet maintenance is 22 ± 2 °C. Moreover, pH values above 6.0 are required to avoid loss of platelet morphology and viability. Platelet plastic storage containers are specially designed to allow high gas permeability and diffusion, which is important to maintain pH values and supply sufficient O_2 for platelet metabolism. Lastly, agitation is essential to certify effective gas exchange (oxygenation and CO_2 removal) during storage [30]. To prevent the contamination of PC with bacteria and/or viruses, pathogen inactivation methods have been developed. These include: (1) psoralen-based method, which exposes PC to a synthetic psoralen, called amotosalen, and a long-wave-length ultraviolet (UV) light, resulting in blocking DNA and RNA replication; (2) gamma irradiation, to prevent transfusion associated to graft-versus-host disease [31,32]; (3) riboflavin-based method, which exposes PC to riboflavin (vitamin B2) [31,32] and to UV light, resulting in irreversible DNA and RNA damage; (4) illumination with short-wave ultraviolet light under agitation [31].

Even though PC are stored under optimal conditions and pathogen inactivation technologies are employed, PC have a limited shelf-life of only 5 to 7 days (expiration date). After this date, questions around PC safety arise, especially owing to the storage conditions that favor the risks of microbial contaminations [33]. Consequently, 10-20% of platelet donations are discarded before they even had a transfusion purpose [2]. Combining the outdatedness with the financial costs involved in PC preparing

and storing, logistical and sustainability concerns are also raised (Figure 1.1). To face PC discarded questions, advances in PC storage methodologies and new alternative applications for these products are necessary.

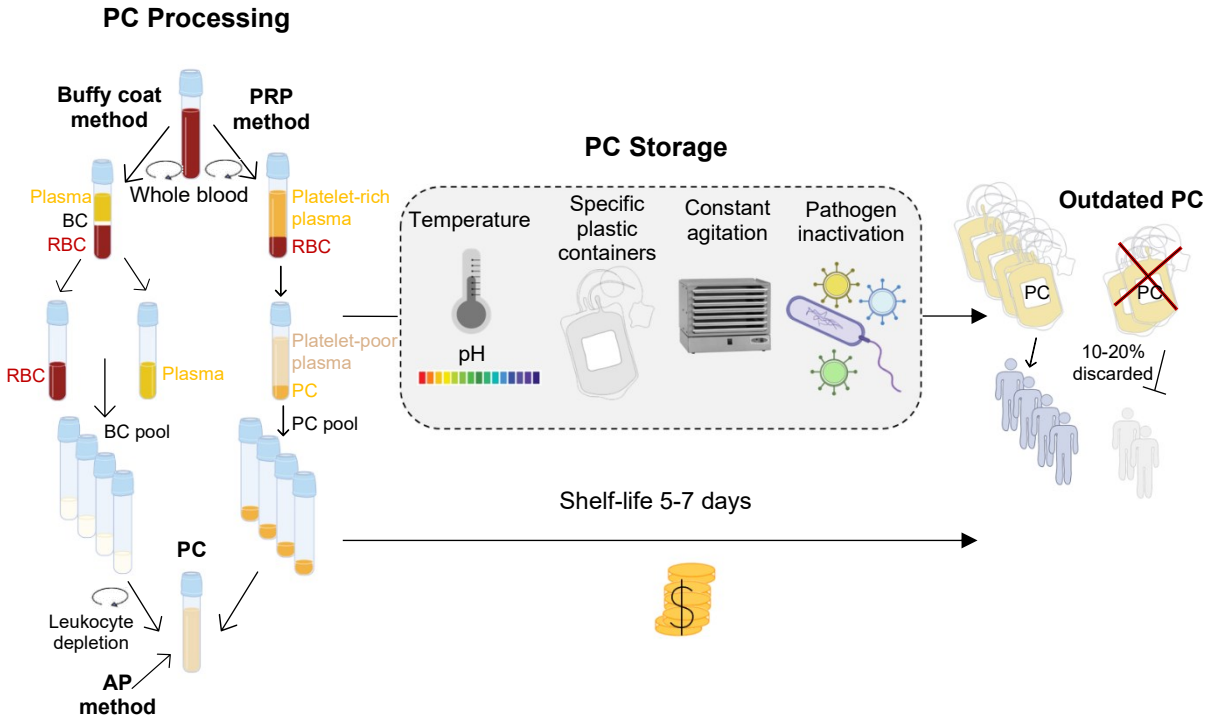

Figure 1.1: Factors that raise awareness of the rate of platelet concentrate discarded in blood centers. Buffy coat (BC) PC are produced by initial centrifugation to separate the whole blood into three layers (plasma, BC, and RBC). BC from 4 to 6 donors are pooled to produce a therapeutic dose and pass through a filter to deplete leukocyte content. For PRP PC, whole blood is centrifuged to first separate the RBC from plasma (enriched in platelets) and the second soft centrifugation to pellets platelets. Four to six doses of platelets for PRP are pooled. PC from BC, PRP, and AP are resuspended in plasma or PAS. After PC preparation, during PC storage, (5 to 7 days, PC shelf-life) an appropriate temperature and pH, such as specific plastic containers with gas permeability and constant agitation to certify effective gas exchange are required. Since PC storage conditions are bacterial growth favorable, pathogen inactivation is required to ensure PC safety. Since PC have a short shelf-life and during PC preparation storage, high financial expenses are required to maintain them transfusible, concerns arise in blood establishments, as expressed by 10-20% of platelets donations that are discarded. BC, buffy coat; PRP, platelet-rich plasma; AP, apheresis; RBC, red blood cells; PC, platelet concentrates; PAS, platelet additive solution.

1.1.3. Alternative applications to outdated PC

1.1.3.1. Cell culture supplements and regenerative medicine applications

Platelets contain α-granules that enclose a variety of GF [e.g., Vascular endothelial growth factor (VEGF), PDGF, TGF-β and FGF] that are well-established for use in *ex vivo* expansion of cells, angiogenesis, and wound healing support. The use of PC as a GF source has been employed as a solution to outdated PC [9,34,35].

Previous studies evidenced that platelet-derived components are a good alternative to xenogenic components, commonly used in cell cultures, due to the GF cargo released during PC storage. Human platelet lysates (HPL) produced from expired human PC have been used as a viable and safe alternative to gold standard fetal bovine serum (FBS) supplementation for *ex vivo* expansion of mesenchymal stem cell culture [36–38], human dermal fibroblasts [39] and adipose-derived stromal cells [38], among other

primary cells. Even though PC derivatives reduce immune responses, concerns remain related to the possibility of blood-derived virus transmission [36,37].

Additionally, the use of platelet material formulations in regenerative medicine and tissue engineering has been suggested. For instance, the application of a gelatin scaffold impregnated with expired PC-derived HPL to a murine wound healing model promotes healing effects due to PDGF and TGF-β released from the scaffold [40,41]. However, a possible shortcoming is the insufficient release of GF that may not sustain tissue regeneration [42].

Even though expired PC have proven to be a valuable source of GF, their use raises other concerns including, (1) GF instability and short half-life time *in vivo* due to an elevated proteolytic activity, (2) rapid diffusion from the delivery site and, (3) adverse effects associated with the application of supraphysiological doses to achieve a therapeutic dose [43]. Thus, new strategies to circumvent these limitations are needed.

1.1.3.2. Extracellular vesicles-based applications

In 1967, for the first time, experiments performed by Peter Wolf described the progressive release of phospholipid enriched particles from platelets. This was observed by electron microscopy, which suggested that particles were originated from platelet granules during their storage [44]. Nowadays, these particles with a rich lipid content are known as platelet-derived extracellular vesicles (pEV).

pEV are the most prevalent EV in the human blood of healthy individuals, with percentages between 70-90% of total EV in the bloodstream [45]. The mechanism of pEV release was described in 1971 by Warren and Vales when studying the ultrastructure of platelets adhered to the vessel walls of human coronary arteries *in vitro*. The results indicated that during platelet activation (i.e., after interaction between platelets and vessel wall collagen), its structure changes and pEV were released from multivesicular membranous sacs of platelet pseudopods. In addition to collagen, other agonists are responsible for platelets activation and subsequently for pEV release [46]. Examples of different physiological agonists that bind to platelet adhesion receptors include ADP, thrombin, fibrinogen, fibronectin, serotonin, and platelet-activating factors [47]. Moreover, platelet activation can also occur in response to contact with surfaces and during platelets storage period, as indicated by a comparative study performed in 1991. In this report, the addition of platelet activation inhibitors combined with a decrease in the surface area of the storage container caused a reduction of almost 40% in pEV released [48]. Furthermore, it was found that the process of high shear stress in atherosclerotic arteries leads to platelet aggregation and the generation of microparticles [49]. Additionally, another study demonstrates that fluid shear stress at low temperatures increased platelet aggregation and induced the pEV release [50].

To evaluate the potential of pEV, it is useful to consider their biochemical characteristics. EV are defined as membrane vesicles delimited by a lipid bilayer and biochemically composed of proteins, lipids, and acid nucleic content [47,51] . EV seem to be produced and released by almost all cell types and are classified into three main subgroups based on their biogenesis and size: exosomes, microvesicles (MV), and apoptotic bodies (AB). Among these three EV subtypes, exosomes are the smallest vesicles with a typical diameter that comprises 40-120 nm. Exosomes have an endosomal

origin, meaning that they are generated from the invagination of endosomes membranes [52,53]. MV typically have a diameter that ranges between 50-1000 nm, so attend to be larger than exosomes. Conversely to exosomes, MV are released through outward budding from the plasma membrane (PM). For this process, cytoskeleton components are involved in the PM remodeling, including the phospholipid redistribution and the contraction of actin-myosin system [52,53]. Lastly, the AB represent the largest class of EV, with a diameter range of 500-2000 nm. AB are secreted during programmed cell death (apoptosis) through blebbing of PM into extracellular space [52]. Hence, AB include intact organelles and nuclear components, in contrast to exosomes and MV content. Although there are different subclasses of EV, it has been challenging to distinguish them due to common protein markers, including tetraspanins (CD9, CD63, CD81, and CD82) and cytosolic proteins (tumor susceptibility gene 101 and Alix) [54], and biophysical properties overlapping all different subtypes. Generally, EV share the same composition with their parent cells. Therefore, platelet-specific proteins - CD31, CD41, CD42a, and CD62p - and GF - such as PDGF, FGF, and TGF-β - have been detected in both platelets and pEV [55,56].

1.2. Therapeutic applications of pEV

PC represent an unexplored source of therapeutic pEV. However, platelets show several advantages as a cellular source of EV, such as (1) their collection is performed under well-defined and regulatory procedures; (2) their recognized clinical value; (3) their production in a concentrated form and, (4) the high production capacity of pEV directly from the collected PC [57]. This section reviews the main therapeutic applications of pEV in regenerative medicine field, and its use as a drug-delivery vehicle, especially in cancer treatment.

1.2.1. pEV in regenerative medicine

To accomplish the rapid longevity of the world population, it is extremely important to develop safe and effective therapies to treat the main aging-related diseases (e.g., heart disease, neurodegenerative diseases, or cancer) [58]. Therefore, regenerative medicine is essential, as it aims to develop approaches to restore damaged, nonfunctional, or missing tissues [59]. Recently, pEV have been gained an important position in regenerative medicine as a good alternative to cell-based therapies [57,59]. Mainly because great challenges have been reported for cell-based therapies, such as (1) loss of therapeutic potency due to long-term *in vitro* cells expansion and (2) potential side effects of exogenous cells after their clinical administration [57].

Given the nature of pEV cargo, its use in tissue regeneration and wound healing processes has been demonstrated. In fact, provided evidence showed that pEV enhanced the vasoregenerative potential of cells after arterial injury [60]. The mechanisms responsible for these effects involve the supply of angiogenic growth factors, promotion of cells differentiation, and increased recruitment and migration of cells to the site of tissue damage [60]. Further, the pro-healing role of pEV has been associated to i*n vitro wound* models using human keratinocytes [61] and human umbilical vein endothelial cells (HUVEC) [62]. *In vivo* experiments have also confirmed the regenerative potential of pEV to treat chronic wounds.

Treatment with pEV induced proliferation and migration of endothelial cells and fibroblasts, enhancing the cutaneous re-epithelialization in a diabetic rat model to a greater extent than PRP. These effects may have been mediated by the release of PDGF, VEGF, FGF, and TGF-β from pEV, which were greater than from PRP [63]. Additionally, pEV have been also involved in the neuroregenerative response. Neural stem cells treated with pEV promoted cell differentiation, proliferation, survival, and an increase in the number of newborn neurons. These effects were associated with VEGF, FGF, and PDGF, as individual blocking of these GF reduces the regenerative effects [64].

1.2.2. pEV as drug-delivery vehicles

Platelets and pEV express several membrane integrins and receptors, namely GPIIb/IIIa, GPIaIIa, GPIba, P-selectin (CD62p), PECAM-1 (Platelet-endothelial cell adhesion molecule-1, CD31) and CD63 [57]. These surface receptors are the scientific rationale behind the interaction of pEV with other cells, and consequently their use as targeted drug-delivery systems [57,65]. Studies with pEV to deliver anti-viral drugs [66] and anti-inflammatory drugs in a model for severe pneumonia [67], have demonstrated the broad therapeutic applicability of pEV. However, its primary use is for cancer treatment [57]. The well-described appealing interaction between tumor cells and platelets/pEV, and the capacity of cancer cells to internalize pEV, represents the principle behind the applicability of pEV as drug delivery vehicles in cancer field [57].

Platelets directly interact with tumor cells through a vast range of surface receptors and glycoproteins, such as platelet P-selectin and GPIIb/IIIa. Indirectly, platelet GF are essential to regulate tumor growth and spread [68]. The tumor vascular environment and its high permeability attract platelets and activate them through the process of tumor cell-induced platelet aggregation. Therefore, platelet granule content is released, promoting the activation of more platelets through P2Y1 and P2Y12 receptors and concomitantly the release of pro-angiogenic factors (e.g., VEGF, FGF, epidermal growth factors (EGF) and, TGF-β) and cytokines (interleukin-1β and interleukin-8), favoring angiogenesis, tumor growth, and metastasis [68,69]. TGF-β is an important GF released from α-granules, acting as an immunomodulator that suppresses the activity of cells from the immune system (e.g., natural killer cells) and alters the T-cell response. pEV share most of the biochemical composition with their parental cells and so, they also express an important role in tumor regulation. Therefore, platelets and pEV contribute to tumor cell dissemination since angiogenesis is a critical factor in cancer progression [68]. During the circulation of tumor cells, their interaction with platelets and pEV-form-heteroaggregates (containing tumor cells, platelet/pEV, and leukocytes) protects tumors cells from immune elimination and supports their attachment to the endothelium, contributing to the establishment of secondary invasions – metastasis [69].

1.2.2.1. pEV and breast tumor microenvironment

Breast cancer is one of the most prevalent cancers worldwide, a leading cause of death from cancer in less developed countries, and affects mainly women [70]. Breast cancer has been considered high heterogeneous in terms of histology, molecular and genetic profiles [71]. For this reason, breast tumors are classified into different subtypes to help clinicians with treatment strategies and prognostic

information. Molecular pathology methods are the most used to divide breast cancer into four main subtypes: luminal A, luminal B, HER2 overexpression, and triple-negative. This distinction is founded on estrogen receptor (ER) and progesterone receptor (PR) expression levels and on human epidermal growth factor receptor 2 (HER2) analysis [71,72]. Luminal breast cancers represent most of all diagnosed breast cancers and usually are associated with a better prognosis than non-luminal breast cancers [HER2 overexpressed and triple-negative breast cancers (TNBC)] [73]. An adverse prognostic factor in breast cancer progression is the physiological process, angiogenesis. Angiogenesis is the mechanism by which new blood vessels (composed of endothelial cells) are developed from preexisting capillaries. In healthy tissues, this process is regulated by the balance between angiogenesis inducers and inhibitors, however, tumors activate the angiogenic switch by dysregulation of this balance. New capillaries formation allows a constant oxygen and nutrients supply, necessaries for tumor growth and to increase their metastatic dissemination rate. Although several studies have been proposed anti-angiogenic treatment in breast cancer as a promising strategy, drug resistance remains a challenging problem in breast cancer therapy [74].

Discovered in 1963 following a plant screening for anticancer activity, paclitaxel (PTX, commercially known as Taxol) was posteriorly approved for clinical trials and used in cancer therapies as the first-line therapeutic agent in breast or ovarian cancer [75]. Its mechanism of action involves microtubule stabilization and dysfunctionality, unlike other anti-microtubule drugs that promote microtubules destabilization. Microtubules are tube-shaped proteins of the cytoskeleton of all eukaryotic cells, with key functions in the maintenance of cell shape, cell division and mitosis, cell signaling transmission, intracellular movement of material, and cellular motility [75,76]. Similarly to other anticancer agents, the PTX mechanisms of cellular resistance have been characterized for certain types of cancer. A mechanism of acquired resistance that has been described involves the multiple drug resistance phenotype. Cells that express this form of resistance have been characterized to display concomitantly resistance to drugs with different molecular structures and functionalities; reduced drug accumulation drug; overexpressed P-glycoproteins (P-gp) and genetic alterations (e.g., gene amplification). Among these characteristics, the one widely mentioned is the overexpression of membrane glycoproteins since P-gp reduces drugs' efficacy due to its role as drug efflux pumps [75,77].

The use of pEV and platelets has been purposed as a possible solution to the posterior challenging problems in breast cancer therapy field, due to their targeting abilities [57], camouflage to the immune system [68], and potential mechanism to overcome drug resistance [78] . Firstly, studies have shown that EV carrying anti-tumor drugs increase the treatment effectiveness, overcoming drug resistance. *Kim et al* [79] reported increased cytotoxicity in multidrug-resistant cancer cells treated with PTX-loaded exosomes compared to those treated with free PTX. Further, *Quiao et al* [80], described that Doxil (chemotherapy drug) loaded exosomes enhanced therapeutic retention in tumors compared to free Doxil. EV carrying anti-tumor drugs are pivotal to increasing therapeutic efficacy, delivering a drug into tumors in a selective manner, and consequently showing an interesting strategy to overcome drug resistance. Secondly, engineered nanocarriers have been developed through the functionalization of platelet and pEV membrane receptors aiming to enhance targeting ability to tumor cells and simultaneously protect them against the immune system [81]. Synthetic nanocarriers functionalized with

whole platelet membrane [82–84] or with a few platelet membrane proteins [85,86] and encapsulated with anti-breast cancer drugs have been showing excellent targeting performance, able to escape of immune clearance and inhibiting drug-resistant, tumor growth and metastasis (Table 1.1).

Table 1.1: Summary of selected studies on anti-cancer delivery strategies development via platelet membrane-functionalized synthetic nanocarriers.

Nanovehicle	Drug	Functionalization	Target cells	Effect	Ref.
Synthetic silica particles	Tumor-killing cytokine (TRAIL)	Membrane-derived vesicles from activated platelets (with maintenance of whole platelet membrane features)	Circulating breast cancer cells, MDA-MB-231 and prostate cancer cells, PC3 (CTC)	• Reduction of particle phagocytosis • Induction of apoptosis • Co-localization with CTC • Decrease in lung metastasis in a mouse breast cancer metastasis model	[82]
Liposomes	DOX	Few platelet membrane receptors (P-selectin and GPIIb-IIIa – like receptors)	MDA-MB-231 (high metastatic) and MCF-7 (low-metastatic) human breast cancer cells	• Enhanced drug binding and delivery to MDA-MB-231, suggesting a promising approach for metastasis-targeted drug delivery	[86]
Nanostructured lipid carrier	PTX	Platelet membrane proteins (platelet membrane integrity confirmed by CD41 expression)	SK-OV-3 cells (ovarian cancer cell line)	• Avoid an immune response • Cytotoxic effects on cells • Targeting appetency verified through presence of CD41 on SK-OV-3 cells surface	[85]
Melanin nanoparticles	DOX	RGD peptides modified platelet vesicles	Raw 264.7 (murine macrophages, immune cells), HUVEC, MDA-MB-231 and MDA-MB-231/ADR	• Inhibit the growth and metastasis of drug-resistant breast cancer • Inhibition of VEGF (promotes tumor growth) and MMP2 and MMP9 (metastasis-relevant gene) expression • Showing *in vitro* immune evasion potential	[84]
PLGA nanoparticles	DOX	Platelet vesicles obtained by repeated freeze and thaw cycles of PRP	Raw 264.7 and 4T1 mouse breast cancer cells	• Actively target to 4T1 cells and showing escape ability from Raw 264.7 cells • High accumulation in tumor site • Good stability, retention time in blood and with reduced side effects	[83]

TRAIL, Tumor necrosis factor – related apoptosis inducing ligand; PTX, Paclitaxel; DOX, Doxorubicin; CTC, Circulating tumor cells; RGD, tripeptide Arg-Gly-Asp acid; MMP2, Matrix metalloproteinases 2; MMP9, Matrix metalloproteinases 9; VEGF, Vascular endothelial growth factor; HUVEC, Human Umbilical Vein Endothelial Cells; PLGA, Poly (lactic-co-glycolic acid); PRP, platelet-rich plasma

Despite the promising effects of drug-loaded nanocarriers coated with platelet membranes, reinforcing the capacity of pEV as carriers of drugs against breast cancer, several limitations arise. Initially, the isolation of platelet membranes and their functionalization into synthetic nanocarriers reveals to be a difficult procedure. Then, during platelet membrane isolation, modifications on membrane could alter the physiological clues of platelets for cell targeting and immune system clearance [81]. Moreover, the ability of interaction between platelets and tumor cells could not be fully present when synthetic nanocarriers are involved [81]. For these reasons, the use of platelets/pEV themselves has been purposed. Nonetheless, due to their smaller size, pEV show a higher ability to penetrate the tumor microenvironment than platelets. Additionally, pEV exhibit a higher stability in freezing-thawing cycles than platelets, enabling its storage and processing [57]. In conclusion, pEV have received a lot of attention in the breast cancer treatment field due to their interaction with cancer cells, their camouflage for the immune system, and their potential to overcome drug resistance (Figure 1.2), as well as, exploiting advantages over synthetic nanocarriers.

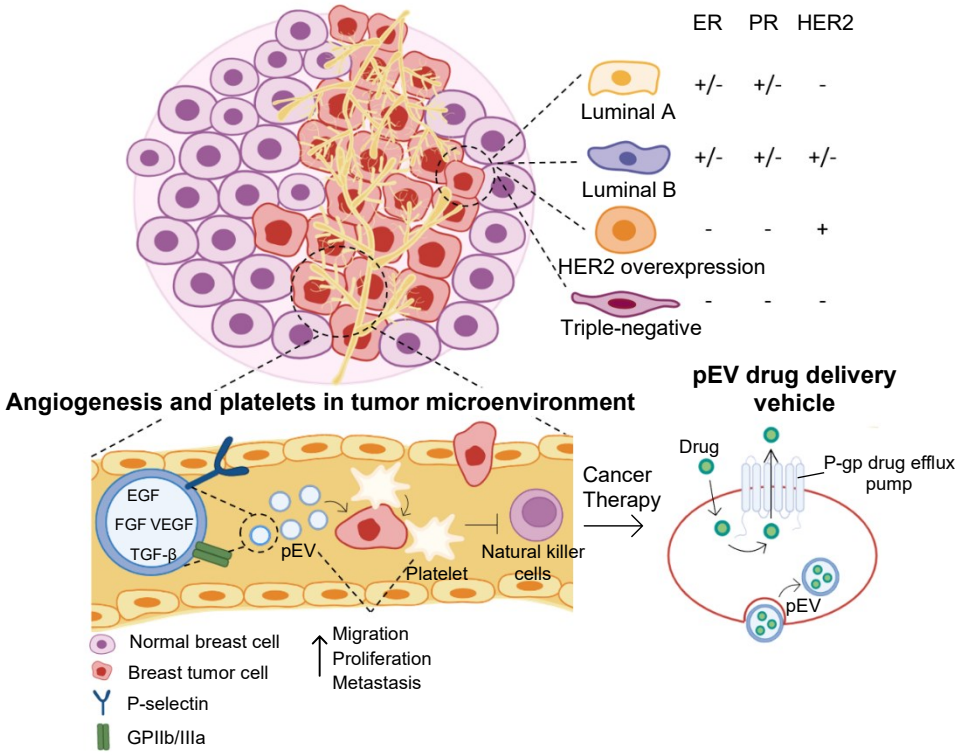

Figure 1.2: Role of platelets and pEV in the microenvironment and treatment of breast cancer. Breast cancer is a highly heterogeneous disease, mainly distinguished into four subtypes (Luminal A, Luminal B, HER2 overexpression, and triple-negative), with different expression patterns of ER/PR and HER2. Along with the vascularization that accompanies breast cancer growth and progression, challenges in clinical therapeutic management are raised. With the formation of new capillaries, circulating tumor cells can interact with platelets and pEV through membrane receptors such as P-selectin and GbIIb/IIIa. During this interaction, GF and cytokines content is released, favoring tumor migration, proliferation, and metastasis. Interaction with platelets and pEV further allows a camouflage formation that will protect breast tumor cells from immune system recognition (e.g., natural killer cells). Combining pEV's natural targeting abilities, protection from the immune system, and capacity to overcome drug resistance (e.g., bypassing P-gp drug efflux pump), makes them a promising therapeutic approach in breast cancer treatment as drug-delivery vehicles. ER, estrogen receptor; PR, progesterone receptor; HER2, human epidermal growth factor receptor 2; EGF, epidermal growth factor; VEGF, vascular endothelial growth factor; TGF-β, transforming growth factor- β; FGF, fibroblast growth factor; pEV, platelet-derived extracellular vesicles.

1.3. Factors affecting the efficacy of EV as drug delivery platforms

EV have been recognized as promising drug delivery platforms due to their intrinsic features, which offer them advantages compared to synthetic nanocarriers, such as cell targeting abilities, innate biocompatibility, non-immunogenic and non-cytotoxic properties [87]. As previously reviewed, pEV display receptors that interact with cancer cells and, consequently, are promising vehicles to deliver anti-cancer agents [81], although their use in clinical applications can be affected by different preconditions as summarized below.

1.3.1. Uptake of EV into the recipient cells

The underlying mechanism involved in the interaction between EV and cells is undoubtedly important to understand the efficacy of therapeutic agent delivery. Despite challenges in clearly understanding how EV can interact with recipient cells, distinct pathways have been suggested. The mechanisms of EV uptake may involve the direct fusion of EV with PM or EV internalization via endocytic routes. A large number of studies suggest the endocytic mechanism as the predominant one. This is responsible for the generation of membrane vesicles that transport the EV to the cytoplasm. Different types of endocytic pathways have been presented, such as clathrin-mediated endocytosis, caveolin-dependent endocytosis, phagocytosis, macropinocytosis, and lipid-raft mediated internalization [88], which are described below and represented in Figure 1.3.

Clathrin-mediated endocytosis begins with the recruitment of endocytic proteins (e.g., clathrin, clathrin adaptor proteins, and scaffold proteins) from the cytosol to the inner face of PM and subsequently their attachment to specific binding sites/ligands on EV, generating clathrin-coated endocytic vesicles. During this process, the polymerization of clathrin induces membrane curvature and, for this reason, the clathrin coating appears to be the key component of membrane bending. In addition, a network of actin filaments and scission proteins [e.g., BAR proteins (Bin, Amphiphysin and, Rvs)] are formed at the endocytic site and participate in the membrane curvature to complement the force needed to bend the membrane. Besides, BAR proteins participate in the recruitment of dynamin and other fission proteins. These proteins (BAR and dynamin) are essential to separate the clathrin-coated vesicle from PM, with vesicle scission mediated by GTPase dynamin 2 [89]. Lastly, the disassembly of the vesicle coat occurs and the EV is free to fuse with an early endosome, where its contents are deposited [89,88]. Treatments affecting the clathrin-mediated endocytosis process can be used to inhibit EV entry, such as dynasore, a specific GTPase dynamin 2 inhibitor [88].

Caveolin-dependent endocytosis is initially mediated by the assembly of integral membrane caveolin proteins, which are cholesterol-rich structures with lipid-binding activity, at the PM. The insertion of these proteins into PM leads to lipid enrichment and recruitment of cytoplasmic cavin proteins (e.g., Cavin1), which generates PM invaginations that can be internalized by the cell, known as caveolae [90]. The caveolae disassembled is mediated by the application of mechanical stress (membrane tension) or

nonmechanical stress (e.g., UV). Caveolin-1 (CAV-1) seems to be a fundamental player in caveolae formation, regulating the EV uptake by recipient cells [91]. Its role in EV internalization was documented when considerable inhibition of EV uptake by CAV-1 knockout HeLa cells was found [92].

Phagocytosis is defined as a cellular process of ingesting large solid particles (≥0.5 μm) into phagosomes, which result from the fusion of PM pseudopods [93]. Phagocytosis is well characterized for the engulfment of AB and cellular debris, however, exosomes and MV can also be internalized [88,94]. Initially, a recognition between specific receptors on the cell membrane and ligands on the target EV needs to arise. During receptor-ligand binding [e.g., TIM (T-cell immunoglobulin mucin)-PS (phosphatidylserine) binding], dynamic membrane extensions composed of phagocytic receptors and polymerized actin curves around the EV to create a cup-shaped form. In the receptor-mediated event, coordinated tyrosine kinases (e.g., SFKs, Src-family kinases) activation leads to lipid-modifying enzymes (e.g., PI3K, phosphatidylinositol 3-kinase) activity and GTPases stimulation, resulting in actin remodeling. Following this, sequential reactions occur to dissociate the phagosome from the surface membrane. Phagosomes undergo maturation stages, involving the fusion with early endosomes, late endosomes, and lysosomes. Antagonists of PI3K and PS have been described as capable to block or decrease EV phagocytosis [93,94].

Macropinocytosis is a cellular process that begins with the formation of the macropinosome, an endocytic organelle responsible for uptake of extracellular fluid and material. Primarily, the macropinosome formation mechanism involves the actin polymerization bordering on the PM, causing waving extensions recognized as ruffles. The following stage is macropinosome maturation, which is mainly represented by enrichment in phosphoinositide 3-phosphate (PI3P), a PI3K enzymatic product. PI3P plays an important role in macropinosome maturation since recruits sorting nexins (SNX). The SNX family is responsible for intracellularly trafficking the macropinosome through the endocytic pathway [95]. Treatment with PI3K inhibitors has been effective in inhibiting macropinocytosis by blocking the cytoskeleton remodeling. Another treatment already described is the incubating of cells with a Na^+/H^+ exchanger pump inhibitor, because a functional PM is required for the actin polymerization and, consequent macropinosomes formation [96].

Lipid raft-mediated pathway is a cholesterol-dependent and clathrin-independent pathway that begins with the formation of lipid rafts. Lipid rafts have been defined as microdomains in the PM with a highly organized structure, enriched in sterols, cholesterol, and sphingolipids [97]. Thereby, EV binding sites interact with the PM lipid domains through lipid-lipid or lipid-proteins interactions, leading to lipid rafts formation [98]. The accumulation of lipid domains with a different composition from the PM induces surface tension in the membrane, and ultimately promotes PM deformation (invagination). The gradual induction of membrane curvature by the attached EV leads to EV internalization and recruitment of scission machinery to generate endocytic vesicles that will end in the endocytic pathway [99]. As mentioned for the other endocytic pathways, the scission of vesicles is often catalyzed by dynamin, although it may be independent of this GTPase [99]. To understand the position of lipid rafts in EV uptake, a variety of cholesterol inhibitors (e.g., Methyl-β-cyclodextrin, filipin) have been tested, since

lipid raft-endocytosis is sensitive to cholesterol perturbation. However, perturbing the membrane cholesterol affects the membrane properties and, as a result, may affect other EV uptake pathways [98].

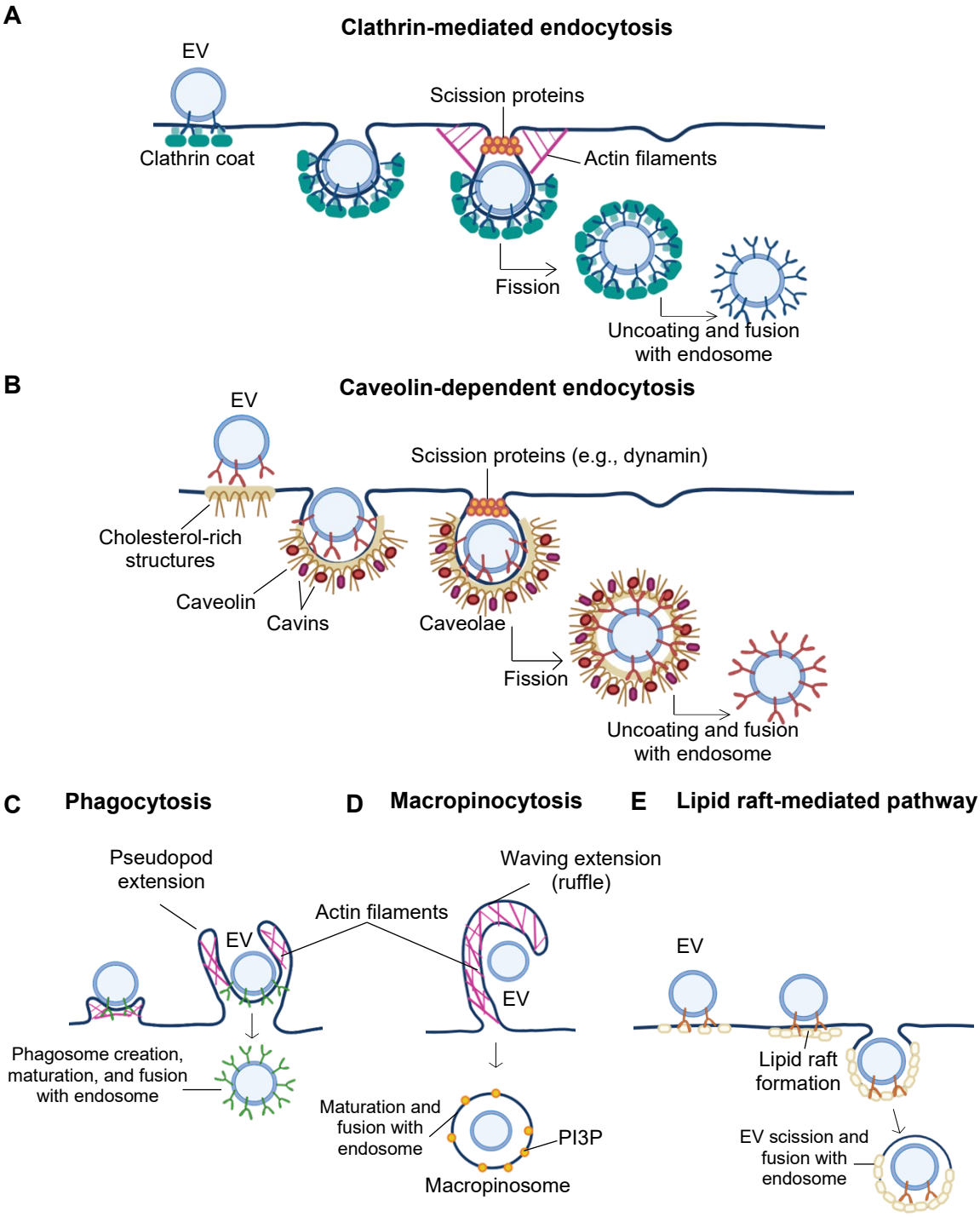

Figure 1.3: Endocytic pathways that participate in EV uptake by recipient cells. EV have been demonstrated to be internalized via (A) clathrin-mediated endocytosis, (B) caveolin-dependent endocytosis, (C) phagocytosis, (D) macropinocytosis, or (E) lipid raft-mediated pathway. Internalized EV usually fuses with endosomal compartments. EV, extracellular vesicles; PI3P; phosphoinositide 3-phosphate.

Although endocytosis seems to be the most common route of entry, direct binding and fusion of EV with PM appears to be another way of EV uptake. Here, the EV lipid bilayer merges with the lipid bilayer of PM. The initial contact requires the affinity between the EV transmembrane glycoproteins syncytins (syncytin-1 and syncytin-2) and their cognate receptors [ASCT-2 (Human alanine serine cysteine transporter 2), and MFSD2a (Major facilitator superfamily domain containing 2a), respectively] at the PM surface. The ligand-receptor interaction leads to membrane reorganization and consequently, the hemi-fusion of membranes occurs. As follows, a continuous membrane connects the EV with the cell, a fusion pore opens, and the EV content is released into the cytosol [100].

Summing up, to accurately understand the mechanism of EV uptake, some aspects must be considered. Firstly, the exact role of each pathway listed depends on the cell type and EV source. With that in mind, it is noticeable that the capability and potency of EV uptake inhibitors vary according to the recipient cells. Secondly, certain EV uptake processes have some overlapping biochemical or functional features, and therefore, some EV uptake inhibitors are not specific only for one pathway. Additionally, EV can enter into a cell through more than one pathway and, for this reason, more than one inhibitor must be tested [88].

1.3.2. Techniques for EV isolation

EV isolation methods available in the literature can affect EV integrity, functionality and, biodistribution, so, for therapeutic applications, it is critical to evaluate the optimal separation methodology. In particular, EV yield and purity are important parameters to consider for clinical application of EV as drug-delivery systems, in order to accurately interpret treatment findings. The common techniques used for EV isolation and the main advantages and limitations of each method are described below and summarized in table 1.2.

Differential Centrifugation. Differential centrifugation enables EV separation based on size and density through successive centrifugation steps with consecutive increase in centrifugal force and duration. Initially, larger particles are sedimented (e.g., AB and cell debris) and as the centrifuge steps advance, smaller particles (e.g., EV) are isolated. However, co-isolation is a common limitation since not all EV are equally distanced to the pellet, and not all EV show equal mass and density in relation to the medium, being distinctively sedimented. Hence, to achieve good levels of EV purity, this method should be selected if the sedimentation rates between particles are significantly different [101,102].

Density gradient Ultracentrifugation. There are two protocols available for density gradient ultracentrifugation (DGUC): top-down gradient and bottom-up gradient. These share the capability to separate EV according to their buoyant density, which implies the EV migration until reaching the position of the gradient solution with the same density as EV. Thus, in this technique, the starting position of particles in the gradient does not matter, because all EV will be positioned at the same band (1.1-1.19 g/mL is the typical density of EV). There are two methods to carry out the gradient, specifically, continuous and discontinuous gradients. Concisely, discontinuous gradient involves layer solutions with

different densities, starting with the densest solution, and finishing with the lowest density solution on top. A continuous gradient can be produced from a discontinuous gradient, waiting at RT to the diffusion of molecules across the interface until reaching a linear gradient. Nevertheless, automated methods are also available [103]. Iodixanol and sucrose are the most recurrently used density media to prepare density solutions, although iodixanol has been described with more benefits (e.g., iodixanol is inert, less viscous and, nontoxic) [102].

Size-exclusion chromatography. In size exclusion chromatography (SEC), EV are separated from other particles following physical size. The heterogenous solution passes through a chromatographic column packed with a porous stationary phase matrix and analytes higher than pore size are eluted first. On the other side, smaller molecules enter the pores and stay entrapped longer, eluting later. The column size cut-off is an important choice as, based on this, different chromatographic selectivity and resolution are achieved [104].

Ultrafiltration. Ultrafiltration separates EV using an ultrafine nano-membrane with an adequate molecular weight cut-off. Two ultrafiltration devices are available based on different configurations: tandem-configurated microfilter and sequential ultrafiltration. Succinctly, in tandem-configuration microfilter, two filters with different size-exclusion limits (20 nm and 200 nm) are placed sequentially. Particles are separated as they pass through filters, with large particles (e.g., cell debris and AB) entrapped in the 200 nm membrane, and EV with 20-200 nm remaining between the two filters. In sequential ultrafiltration, the sample passes through three filters (1000 nm, 500 kDa cut-off and, 200 nm). The first is to eliminate large particles (e.g., cell debris and AB), the second to remove small particles (e.g., free protein), and lastly, the 200 nm filter to collect EV [105].

Precipitation. Precipitation usually is induced with hydrophilic polymers, with polyethylene glycol (PEG) being the most used. Starting material is incubated with PEG overnight and during this incubation period, hydrophilic polymer interacts with water molecules surrounding EV, remodeling its water solubility. To collect the precipitated EV, low-speed centrifugation is performed. Although precipitation methods do not involve advanced equipment and achieve high EV yield, limitations arise. The use of hydrophilic polymers can promote co-isolation with other water-soluble particles, such as lipoproteins or proteins [105].

Immunoaffinity capture. Immunoaffinity capture appropriates the presence of characteristic surface EV molecules to specifically capture them through interaction with ligands immobilized on a surface. Targeted molecules usually explored are EV-specific proteins (e.g., CD63, CD81, CD9, CD82, annexin) and ligands are the corresponding antibodies [104].

Table 1.2: Commonly methods for EV Isolation. Adapted from [105].

Method	Advantage	Limitations	Concerns and/or Suggestions	Ref.
Differential centrifugation	Most used method; process large volume samples	Loss of EV integrity and EV clump; low EV yields and purity; time-consuming and laborious	Centrifugation duration and rotation speed vary between rotors, so optimizing them for the specific rotor used can be helpful to improve EV isolation; To enhance EV yield in viscous samples, rotation speed and time can be increased	[101,102, 105]
Density gradient ultracentrifugation	High purity; allows separation of different EV subpopulations	Time consuming, challenges in scale up due to limited sample volume; EV structure may be affected due to prolonged centrifugation time	To understand whether EV fractions have reached their buoyant density, measure the densities of collected fractions and, confirm if EV are present in the same fraction between experiments	[102,105]
Size exclusion chromatography	Fast and no specialized equipment is required; high purity	Low yield of recovery and limited processing volume result in low scalability	SEC column choice is a key factor to an optimized EV isolation, as the pore size of columns resin and the quality of the column stack are critical factors	[104,105]
Ultrafiltration	Fast, simple procedure and no specialized equipment	Moderate purity; low separation yields due to vesicle clogging; co-isolation with particles at the same size as EV; potential loss of EV function due to fragmentation	Tangential flow filtration technique can minimize vesicle clogging since a parallel flow force is applied to the membrane	[105]
Precipitation	Simple procedure; no sophisticated equipment; high efficiency; scalable to large preparation volumes	EV-specific biomarkers detection is unfeasible; co-precipitation of water-soluble identities; additional isolation methods are required to improve EV purity	To improve EV purity, EV must be isolated prior to the precipitation step, since this method is predominantly a concentration approach	[102,105]
Immunoaffinity capture	Ability to discriminate EV subpopulations isolation; Scalable	Low EV purity due to non-specific binding; stability and quality of antibodies may be compromised; EV integrity can be affected, as generally binding interactions are not readily reversible	A deep understanding of antibody chosen is an added advantage to an optimal EV isolation performance	[102,104]

1.3.3. Drug Loading Approaches

Analogous to the EV isolation method, drug loading protocol can also affect EV integrity and, consequently, EV function. The EV loading methods have been distinguished into two main categories. One is known as endogenous, passive, or pre-loading and the other as exogenous, active, or post-loading (e.g., direct incubation, electroporation, freeze-thaw cycle, sonication, surfactant treatment, and extrusion). In the endogenous method, the cells responsible for the EV source (so-called parental cells) are biologically modified and so during the EV biogenesis, the modification is acquired. In the case of exogenous technique, the loading is performed directly on the EV after isolation [106–108].

Endogenous methods have been described as the treatment of parental cells with drugs or the engineering of parental cells [108]. Distinct studies have been conducted as a resource of drug treatment, revealing the limitations and benefits of this approach. Pascucci *et al*. investigate whether PTX incorporated by MSC (mesenchymal stem/stromal cells) was also present in secreted EV. The group showed that EV morphology was substantially conserved, and strong anti-cancer activity *in vitro* and *in vivo* was demonstrated [109]. Although this method is relatively simple, the drug loading efficiency is impossible to control [108]. To engineer the parental cells, transfection with nucleic acids polymers (e.g., to enhance EV targeting to recipient cells) or therapeutic proteins is the most common technique employed [108].

Direct incubation is one of the less time-consuming and simpler exogenous loading methods. EV and drug are co-incubated, and the different drug concentration gradients inside and outside the EV represent the propulsion for loading [108]. PTX is one of the drugs that have been efficiently loaded into EV by direct incubation. Saari *et al* showed the incubation of 10^8-10^9 prostate cancer-cell derived EV with 5 μM of PTX solution at 22 °C for 1 h. The present study revealed that 9.2 ± 4.5 % of the drug was loaded into the EV and that PTX loaded EV were able to increase the cytotoxic effect of PTX [110]. Another incubation protocol has been described for platelet microparticles used to deliver anti-viral drugs. Herewith, EV were incubated with the drugs at 37 °C for a period of 2 h, leading to an encapsulation efficiency of 25 to 68%, depending on the drug. The authors justify this difference in drug retention due to differences in hydrophobicity [66].

Electroporation is a biophysical phenomenon that allows an increase in membrane permeability due to the application of a pulse electric field [111,112]. Hence, with this approach, lipid systems can be modeled because EV membrane structural changes occur with the creation of small pores, mainly hydrophobic pores (energetically more favorable). After the application of electrical pulses, the EV membrane undergoes rapid structural rearrangements, and the small pores disappear [112]. Kim *et al* evaluated the PTX loading capacity of exosomes released by macrophages, employing the electroporation method. Electroporation was performed at 1000 kV for 5 ms, following that, exosomes were placed at 37 °C to enhance the recovery of membrane integrity [79].

Freeze-thaw cycle is an active-loading method mediated by thermal energy. Different protocols can be used, enabling a fast (e.g., -80 °C) or slow (e.g., -20 °C) freezing followed by a fast (e.g., 60 °C) or slow (e.g., RT) thawing [97]. In this physical treatment, likewise temperature, number of cycles, and cycle duration, must be controlled to optimize the drug loading efficiency and decrease the induction of EV aggregation [108,113].

Sonication is an exogenous drug loading method that consists of the application of ultrasounds to EV. Sonication promote the agitation of EV particles, so, the integrity of EV membranes can be compromised [107]. The internalization of PTX into exosomes via the sonication method has also been described, particularly in macrophages-derived exosomes. In this study, an ultrasonic probe (sonicator) was used to apply 6 cycles with 20% of amplitude to exosomes and after an intermediate period for cooling down and a subsequent incubation of 1h at 37 °C, the amount of drug loading achieved was 28.29±1.38% [79].

Surfactant treatment is another approach to EV loading due to its capacity to disrupt EV lipid membrane architecture [107]. Surfactants are active agents that contain a hydrophilic head group and a hydrophobic tail (amphiphilic molecule). Thus, the surfactants interact with the phospholipid content and the lipid bilayer is penetrated and solubilized. The solubilization occurs due to the formation of hybrid micelles (surfactant and phospholipids), leading to the creation of bilayer pores. The type of surfactant and its concentrations must be selected carefully because specific surfactants can inactivate or degrade the drug cargo and at high concentrations, surfactants can irreversibly rearrange the lipidic membrane [114,115].

Extrusion is a mechanical technique that involves a forced passage of EV through membranes with pores and, depending on pores size, different profiles of EV membrane disruption are obtained. It is a simple method that does not disrupt the phospholipids of the EV membrane and allows a homogeneity in the formed membrane pores [116]. The drug loading efficiency and the integrity of the membrane can vary depending on the flow rate that the solution passes through the membrane pores and the temperature at which the method is performed [117].

CHAPTER 2

2. Thesis Aims

Due to their short shelf-life and the financial costs involved in their processing, alternative strategies have been studied to outdated clinical PC. PC have been recognized as a new source of pEV with therapeutic applicability in the regenerative medicine and drug delivery fields. Still, the therapeutic potential of pEV as natural drug delivery vehicles remains largely unexplored.

The main goal of this thesis was to evaluate the natural suitability of expired platelet donations as enriched sources of EV and the natural interactivity between pEV and cells (Figure 2.1), aiming to deepen the understanding of the therapeutic application of pEV.

The first specific objective was to identify the most efficient physical-based methodology to isolate pEV from expired PC. Then, to assess the therapeutic potential of pEV as PTX delivery systems in different *in vitro* models (HUVEC and two breast cancer cell lines, MDA-MB-231 and BT474). We hope that this new therapeutic value given to an expired blood product can motivate others to the potential of these biological entities for cancer treatment.

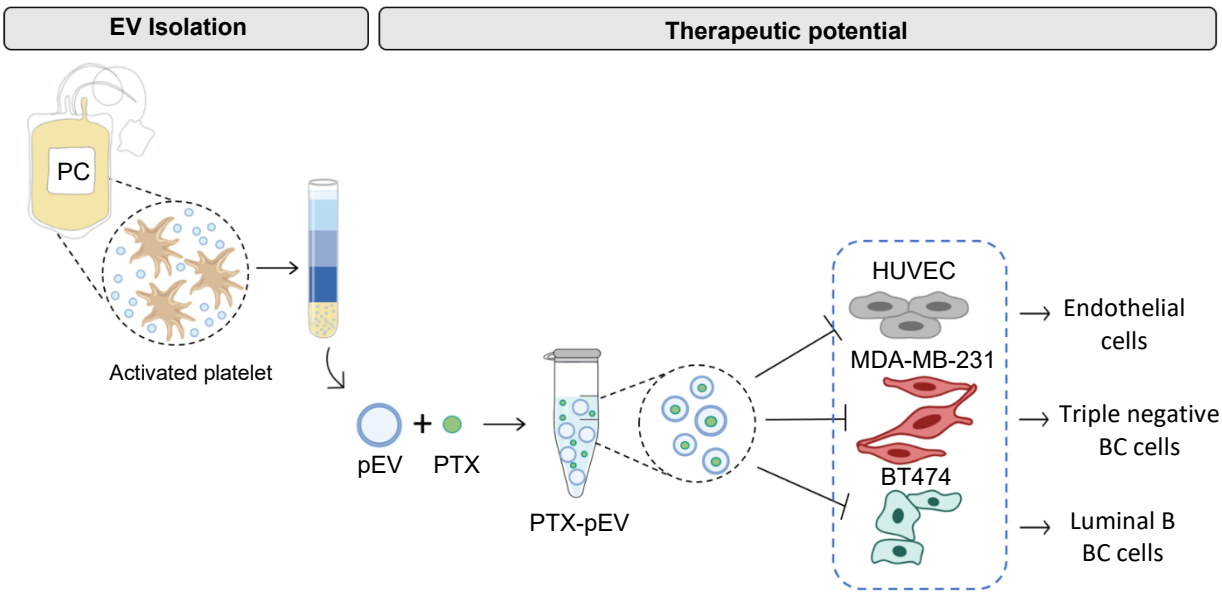

Figure 2.1: Schematic overview of the present thesis aims. Under the scope of developing new alternative applicability to expired PC, their derived EV were used as PTX delivery vehicles. To this purpose, will be evaluated: the most suitable EV isolation methodology and the therapeutic potential of PTX-EV into different cells present in the breast cancer microenvironment, such as HUVEC and two breast cancer cell lines: a triple negative and luminal B (MDA-MB-231 and BT474, respectively). PC, platelet concentrate; pEV, platelet-derived extracellular vesicles; PTX, paclitaxel; PTX-pEV, paclitaxel loaded pEV; HUVEC, human umbilical vein endothelial cell; BC, breast cancer.

CHAPTER 3

3. Materials and Methods

3.1. Isolation of pEV

3.1.1. PC collection and processing

PC derived from healthy volunteer donors were obtained from the Portuguese Institute for Blood and Transplantation (IPST, Lisbon, Portugal), 1-2 days after the expiration date. Blood donations were obtained according to the Portuguese and European regulatory legislation [19,118]. All donations were regularly tested for ABO group, RhD (Rhesus D) type and, infectious disease markers [(human immunodeficiency virus (HIV), hepatitis C virus (HCV) and, hepatitis B virus (HBV)]. Briefly, whole-blood-derived PC were prepared by pooling 4 units obtained by BC or PRP methods. The BC and PRP polled units were blood group-compatible, and PC were re-suspended with 300-450 mL of a medium containing 30% (v/v) of plasma and 70% (v/v) of PAS (InterSol, 280 mL), to a minimum final content of 2.0×10^{11} platelets per PC unit. PC were stored at 22 °C ($\pm$ 2 °C), under constant agitation. After their expiration date, PC were centrifuged for 10 min at 1000 × g (5010R centrifuge, Eppendorf) at RT. The supernatants were stored at - 20 °C until further use.

3.1.2. Methodologies for pEV isolation

PC supernatants stored at -20 °C were thawing overnight at 4 °C and centrifuged at 2000 × g (5010R centrifuge, Eppendorf) for 10 min at RT and filtered through a 0.45 μM filter (Nalgene™ Rapid-Flow™, Thermo Fisher Scientific) to remove residual platelets, debris, and pEV aggregates. Filtered samples were transferred to conical polypropylene tubes (Beckman Coulter) and ultracentrifuged, using a SW28 rotor, at 25.000 rpm for 2h45 at 4 °C (Ultracentrifuge Optima™ LE-80K, Beckman Coulter). pEV pellets were resuspended in Dulbecco's phosphate-buffered saline (DPBS, Gibco) and used as starting material for the pEV isolation protocols. Three different pEV isolation strategies were evaluated, as indicated below.

3.1.2.1. Isolation of pEV by iodixanol discontinuous density gradient ultracentrifugation (DGUC)

pEV pellets were layered on a discontinuous 40-5% iodixanol gradient prepared from OptiPrep™ density gradient medium [60% (w/v) aqueous iodixanol solution, BioVision], as previously described [119] with minor modifications. OptiPrep™ stock solution (60% (w/v)) was diluted in sucrose buffer [60 mM

Tromethamine-hydrochloride acid (Tris-HCl), 6 mM ethylenediamine tetraacetic acid (EDTA), 0.25 M sucrose, pH 7.4] to obtain a 50% (w/v) iodixanol solution (working solution). Consequently, the 50% (w/v) working solution was mixed with a homogenization solution (10 mM Tris-HCl, 1 mM EDTA, and 0.25 M sucrose, pH 7.4) to prepare iodixanol 5, 10 and 20% (w/v) gradient solutions. Lastly, the 40% (w/v) iodixanol solution was prepared by mixing the pEV pellet with 50% (w/v) working solution. The obtained gradient solutions were layered in open-top polypropylene tubes (Beckman Coulter): 4 mL layers of 10, 20 and 40% (w/v), 3.5 mL of 5% (w/v) and 1 mL of DPBS, as represented in Figure 3.1. Then, tubes were ultracentrifuged using a SW28 rotor, at 25.000 rpm, for 18 h at 4 °C (Ultracentrifuge Optima™ LE-80K, Beckman Coulter). After centrifugation, 1 mL of gradient fractions were carefully collected from top to bottom of the tube (Figure 3.1). Fractions were pooled according to the subsequent ranges: 1-4, 5-7, 8-9, 10-12, 13-16, and concentrated using Amicon® Ultra-2 mL 10 KDa filter units (Merk Millipore). Negative control gradient was performed with DPBS (Gibco) (DPBS gradient), instead of pEV pellet.

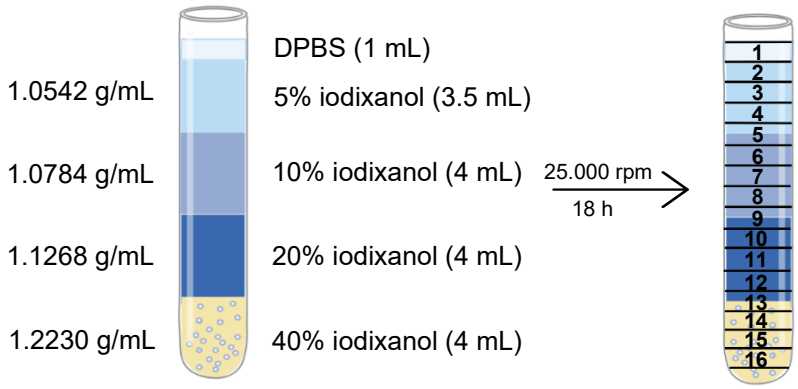

Figure 3.1: Schematic representation of pEV Isolation by DGUC. pEV pellet was placed onto 40-5% iodixanol gradient layers [respective density (left side) and volume (right side) of each layer]. Then, the tube was ultracentrifuged at 25.000 rpm for 18 h and 16 fractions were collected from top to bottom of the gradient.

3.1.2.2. Isolation of pEV by size exclusion chromatography (SEC)

pEV pellet was resuspended in DPBS to a final volume of 500 μL and was loaded on top of a qEV/70nm column packed with a polysaccharide resin (Izon Science), equilibrated with DPBS (according to manufacturer's instructions). A total of 17 sample fractions of 500 μL volume each were collected immediately after sample loading. The fractions 1-5, 6-7, 8-9, 10-13, and 14-17 were pooled and concentrated using Amicon® Ultra-2 mL 10 KDa filter units (Merk Millipore).

3.1.2.3. Isolation of pEV by DGUC followed by SEC (DGUC-SEC)

The pEV enriched fractions obtained by DGUC (see 3.1.2.1) were applied to a qEV/70 nm column and processed as explained above (section 3.1.2.2).

3.2. pEV drug loading by direct incubation

pEV were loaded with paclitaxel (PTX-pEV, Invitrogen) and PTX-conjugated dye (PTX488-pEV, Oregon Green™ 488 Taxol, Flutax-2, Invitrogen), as previously reported in the literature with slight modifications [79]. Briefly, 20 μM (25 μg/mL, Loading A), 50 μM (64 μg/mL, Loading B) of PTX (5 mM stock solution) or DMSO vehicle (Dimethyl sulfoxide, CryoSure-DMSO, WAK-Chemie Medical GmbH) were mixed with 5×10^{10} pEV, in DPBS (volume = 800 μL). All samples were incubated at 37 °C for 1 h under continuous agitation at 350 rpm (ThermoMixer® C Eppendorf). The free drug was removed by DGUC as described in 3.1.2.1.

A calibration curve for indirect quantification of PTX was prepared as previously published [120,121] (Figure 3.2). The stock solution of PTX was diluted with 30% (v/v) methanol in DPBS, to achieve a range of concentrations between 2.0-20.0 μg/mL. The calibration values were measured by UV at 230 nm wavelength (Shimadzu UV-1603 spectrophotometer), with a correction for the blank. Once PTX was dissolved in DMSO the absorbance values were corrected against the corresponding values for DMSO.

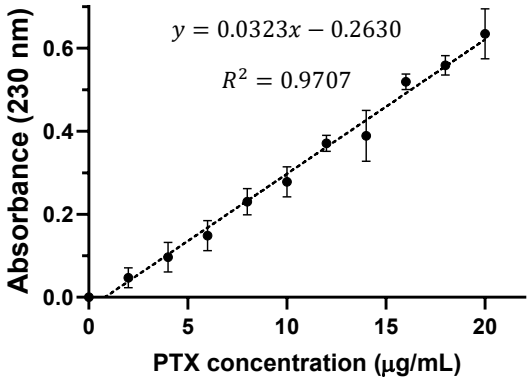

Figure 3.2: Paclitaxel calibration curve used to estimate PTX concentration into pEV. *n*=3, *n* represents independent experiments carried out inter-days.

To measure the PTX concentration into pEV, approximately 2×10^9 PTX-pEV were treated with 100 μL of 1 × RIPA buffer (Sigma) and placed on a thermomixer (ThermoMixer® C Eppendorf) for 30 min, at 4 °C with shaking (650 rpm), as previously described [122]. Subsequently, the absorbance was acquired as explained above. Drug entrapment efficiency (%) analysis was assessed in triplicate and calculated using equation Eq 3.1:

$$Entrapment\ efficiency\ (\%) = \frac{Amount\ of\ drug\ in\ EV}{Initial\ amount\ of\ drug} \times 100\% \qquad \text{(Eq 3.1)}$$

3.3. pEV Characterization

3.3.1. pEV protein extraction and quantification

pEV samples isolated by DGUC, SEC and, DGUC-SEC were lysed 1:1 in 1 × RIPA (Radioimmunoprecipitation assay, Sigma) buffer containing EDTA-free protease inhibitor cocktail

[Roche, 1:25 (v/v)], for preparing protein extracts. Total protein quantification of pEV protein extracts was determined with a bicinchoninic acid (BCA, Thermo Fisher Scientific) protein assay, following the manufacturer's instructions. Absorbances were measured at 562 nm in the microplate reader Infinite® 200 PRO NanoQuant (Life Sciences, Tecan).

3.3.2. Western blot (WB) analysis of pEV

Platelet lysates and pEV lysates with an equal amount of protein (20 μg) or equal sample volume were mixed with 4 × NuPAGE® LDS sample buffer (Novex® ThermoFisher Scientific) supplemented with a reducing agent (10 × NuPAGE® reducing agent, Novex® ThermoFisher Scientific) for antibodies under reducing conditions (RC, Table 3.1). All samples were then denatured at 95 °C (ThermoMixer® C Eppendorf) for 5 min.

Samples were loaded (20 μL per well) into a NuPAGE® 4-12 % Bis-Tris Mini-protein gel polyacrylamide 1.0 mm (Novex® ThermoFisher Scientific), as well as 8 μL of molecular weight marker SeeBlue™ Plus2 Pre-Stained Protein Standard (Invitrogen). Electrophoresis was performed at 200 V for one hour in the 1 × NuPAGE MOPS SDS Running buffer (Novex® ThermoFisher Scientific). Proteins were transferred to polyvinylidene fluoride membranes (PVDF, iBlot 2 Transfer Ministack, Invitrogen) via dry electroblotting at 15 V for 7 min, using iBlot™ 2 Dry Blotting System (Invitrogen). Membranes were washed with Tris-buffered saline powder (Sigma, pH 8.0) dissolved in water and containing 0.1% (v/v) of Tween-20 (Merck) (TBST solution). Membranes were blocked with 5% (w/v) of nonfat dry milk (PanReac AppliChem) dissolved in TBST (blocking solution) for 1 h at RT. Subsequently, membranes were incubated with primary antibodies (Table 3.1) diluted in blocking solution, overnight at 4 °C. The following day, membranes were washed three times with TBST solution and incubated for 1 h at RT with a secondary antibody (see Table 3.1) diluted in blocking solution. Chemiluminescent signal was detected using the WesternBright® ECL (enhanced chemiluminescence detection, Advansta) using ChemiDoc XRS+ System (Bio-Rad Laboratories, Hercules). Primary and secondary antibodies are listed in Table 3.1.

3.3.3. Nanoparticle tracking analysis (NTA)

pEV size distribution and concentration were assessed by NTA using the NanoSight NS300 system (Malvern), equipped with a 405 nm blue laser light source and a high sensitivity sCMOS camera. pEV samples were diluted 1:2000 in DPBS 0.2 μm filtered, to get a recommended concentration range of particles/mL, according to the manufacturer's indications. Particle measurements were obtained by the analysis of 3 videos of 60 seconds each acquired at 25 °C, using the NanoSight NTA 3.3 software.

3.3.4. Transmission electron microscopy (TEM)

For morphological and structural studies, pEV isolated by the three different procedures (DGUC, SEC, DGUC-SEC) and PTX-pEV were observed by TEM. First, 100 mesh formvar-carbon coated copper grids were pre-treated by glow discharge to increase the hydrophilicity of the film surface. EV samples were mixed (1:1) with 4% (w/v) formaldehyde in 0.1 M phosphate buffer saline (pH 7.4), incubated during

5 min at RT, and adsorbed to the grid for 5 min. The grid was washed with 10 drops of distilled H_2O and negative stained with 2 drops of 2% (w/v) uranyl acetate for 5 min at RT in dark. Grids were imaged with a Tecnai™ G² Spirit BioTWIN (FEI Company, Hillsboro, OR) transmission electron microscope at 120 kV. The images were acquired with a digital charge-coupled device camera (Olympus-SIS Veleta, Germany). This procedure was performed by the Electron Microscopy Facility at the Instituto Gulbenkian de Ciência (IGC,Oeiras).

3.3.5. pEV labeling with a lipophilic membrane dye (PKH26)

pEV and PTX488-pEV were fluorescently labeled with the PKH26 (PKH26-pEV and PKH26-PTX488-pEV, respectively) lipophilic membrane dye (Red Fluorescent Cell Linker for General Cell Membrane Labeling Mini kit, Sigma-Aldrich) as described in the literature, with minor modifications [123]. Briefly, a stock solution of 0.1% (v/v) bovine serum albumin (BSA) in DPBS was prepared, transferred to open-top polypropylene tubes (Beckman Coulter), and ultracentrifuged in a SW28 rotor at 25.000 rpm, for 20 h at 4 °C (Ultracentrifuge Optima™ LE-80K, Beckman Coulter). Following centrifugation, the supernatant was collected, filtered through a 0.22 μm filter, and stored at 4 °C. For the labeling of pEV with PKH26 dye, 50 μL of diluent C (component provided by manufacture's kit) was added to 50 μL of pEV stock and gently mixed. Then, 1.5 μL of PKH26 were diluted in 100 μL of diluent C and pEV were added to the diluted PKH26. The mixture was incubated for 5 min at RT and the labeling reaction was interrupted by adding 100 μL of ultracentrifuged 0.1% (v/v) BSA. The protocol was executed in the dark and was repeated for the negative control, i.e., with DPBS. In order to separate labeled pEV and unbound dye, a DGUC was performed as described in 3.1.2.1.

3.4. Functional assays using cell culture

3.4.1. HUVEC culture

Human umbilical vein endothelial cell (HUVEC) line (CC-2517A, Lonza) were thawed as recommended by the manufacturer and cultured in EBM™-2 Basal Medium (Lonza) supplemented with EGM™-2 Endothelial SingleQuots™ Kit [FBS, hydrocortisone, hFGF-B (human Fibroblastic Growth Factor B), VEGF, R3-IGF-1 (R3-Insulin-like Growth Factor-1), ascorbic acid, hEGF (human Epidermal Growth Factor), GA-1000 (Gentamicin/Amphotericin-B) and heparin] in T-175 tissue-culture flasks. Cells were maintained at 37 °C in a saturated humidified atmosphere with 5% (v/v) CO_2, and the culture medium was exchanged every 2-3 days. When cell confluency was reached, cells were harvested with TrypLE™ Select (Gibco™) and subcultured according to the subsequent assays. Cells until passage P5 were used for the experiments.

3.4.2. Breast cancer cells (MDA-MB-231 and BT474) culture

Luminal B BT474 (ATCC HTB-20) (ER^+, PR^+, $HER2^+$) and triple-negative MDA-MB-231 (ATCC HTB-26) (ER^-, PR^-, $HER2^-$) breast cancer cell lines were grown at 37 °C in a humidified atmosphere with 5% (v/v) CO_2. Cells were cultured in phenol red-free Roswell Park Memorial Institute culture medium

(RPMI,1640 Medium, no phenol red, Gibco™ Invitrogen) with 10% (v/v) FBS in T-225 tissue-culture flasks. The medium was replaced every 2-3 days until they reached confluency. Cells were harvested with TrypLE™ Select (Gibco™) and subcultured according to the functional assays.

3.4.3. Immunocytochemistry (IC)

Sterilized glass coverslips were placed into each well of a 24-well plate and coated with 500 μL of 0.1% (w/v) gelatin (from porcine skin, Type A) for 30 min at 37 °C. At the end of the experiment, cells were washed in DPBS, fixed in 4% (w/v) paraformaldehyde (PFA) for 15 min at RT and then blocked with 0.2% (w/v) of FSG (Fish Skin Gelatin) in DPBS for 30 min at RT. Cells were incubated with primary antibodies (Table 3.1) diluted in 0.125% (w/v) of FSG in DPBS, overnight at 4 °C. Following this, cells were washed three times with DPBS (+/+) (Gibco) and incubated with secondary antibody (Table 3.1) diluted in 0.125% (w/v) of FSG in DPBS, for 1 h at RT. Then, the cells were washed three times with DPBS (+/+) and incubated for 5 min with DAPI (4′,6-diamidino-2-phenylindole, dihydrochloride) diluted in DPBS (1:2000). Three extra DPBS (+/+) washes were performed and finally, coverslips were mounted onto slides using ProLong™ Gold Antifade Kit (Molecular Probes, Invitrogen). Slides were stored at 4 °C in the dark, until visualized in an inverted fluorescence microscope (DMI6000, Leica). Primary and secondary antibodies are listed in Table 3.1.

Table 3.1: List of primary and secondary antibodies used for western blot under non-reducing conditions (WB, NC) or, under reducing conditions (WB, RC) and for immunocytochemistry analysis (IC).

Primary Antibodies	Host/type	Manufacturer (Catalog number)	Dilution
anti-CD9 (WB, NC)	mouse, monoclonal	Invitrogen (10626D)	1:1000
anti-CD41 (WB, NC)	rabbit, polyclonal	Abcam (ab134131)	1:1000
anti-CD63 (WB, NC)	mouse, monoclonal	Abcam (ab59479)	1:1000
anti-Flotillin-2 (WB, RC)	mouse, monoclonal	BD Biosciences (610383)	1:1000
anti-Argonaute-2 (WB, RC)	rabbit, polyclonal	Abcam (ab32381)	1:1000
anti-APOA1 (WB, RC)	rabbit, polyclonal	Abcam (ab20453)	1:1000
anti-EGF Receptor (IC)	rabbit, monoclonal	Cell Signaling Technology (D38B1)	1:100
anti-HER2 (IC)	rabbit, monoclonal	Abcam (ab134182)	1:100
Secondary Antibodies	**Host**	**Manufacturer (Catalog number)**	**Dilution**
HRP-conjugated anti-rabbit (WB)	Goat	System Biosciences (EXOAB-KIT-1)	1:10000
HRP-conjugated anti-mouse (WB)	Donkey	(Amersham)	1:5000
Alexa 488-conjugated anti-rabbit (IC)	Goat	Molecular probes (A11008)	1:200

3.4.4. pEV internalization

HUVEC, MDA-MB-231 and, BT474 cells were seeded in 24-well plates containing a pre-coated glass coverslip (section 3.4.3) at a density of 2.5×10^4, 3.8×10^4 and 4.7×10^4 cell/well, respectively. After 24 h of culture, fresh EBM™-2 fully supplemented medium (see 3.4.1) and 10% (v/v) FBS RPMI medium (see 3.4.2) containing 6000 PKH26-pEV/cell or an equal volume of PKH26-DPBS (negative control) were added to HUVEC and to MDA-MB-231 or BT474, respectively.

To confirm that PTX488 was internalized into pEV, HUVEC were also incubated with PKH26-PTX488-pEV (see section 3.3.5) for 24 h.

To elucidate the pEV uptake pathway in breast cancer lines, MDA-MB-231 and BT474 were simultaneously incubated with PKH26-pEV and EV uptake inhibitors: 100 μM dynasore (Dynasore hydrate Sigma-Aldrich, D7693) or 500 μg/mL heparin (STEMCELL™ Tecnhologies). Following 24 and 48 h of incubation with or without EV uptake inhibitors cells were gently rinsed with DPBS and fixed for 15 min at RT with 4% (w/v) PFA. Fixed cells were washed three times with DPBS and cell nuclei were stained with DAPI (as described above, section 3.4.3). The slides were mounted with ProLong™ Gold Antifade Kit (Molecular Probes, Invitrogen). Fluorescence images were acquired using an inverted fluorescence microscope (DMI6000, Leica), and signal intensity was quantified using ImageJ software.

For flow cytometry analysis, HUVEC, MDA-MB-231 and, BT474 cells were seeded at a density of 5×10^5 cell/well (6-well plate). The following day, HUVEC were incubated with PKH26-pEV or PKH26-DPBS and breast cancer cells with PKH26-pEV or PKH26-DPBS, simultaneously with the EV uptake inhibitors. After 24 or 48 h of incubation at 37 °C in an atmosphere containing 5% (v/v) CO_2, cells were washed twice with DPBS, dissociated with Tryple™ Select at RT for 5 min, then centrifuged at 300 × g for 5 min and the pellet was resuspended in DPBS (this step was performed twice). The final cell pellet was resuspended in 1 mL of flow cytometry buffer [FC buffer, 2% (v/v) FBS in DPBS]. Samples were analyzed with the BD FACSCelesta™ (BD Biosciences) flow cytometer, with at least 20.000 events recorded per sample. Data was acquired using the BD FACS DIVA software and pEV uptake analysis was performed using FlowJo software (TreeStar).

3.4.5. Scratch wound assay

HUVEC, MDA-MB-231, and BT474 were plated at a density of 3×10^4 (HUVEC), 4×10^4 (MDA-MB-231), and 5×10^4 (BT474) cell/well in 96-well ImageLock™ microplates (Essen Bioscience) and cultured as described above (Sections 3.4.1 and 3.4.2) until reaching a 95-100% confluent monolayer. Cell monolayers were serum-starved with 0.1% (v/v) FBS EBM™-2 basal medium (Lonza) and breast cancer cells with 0.5% (v/v) FBS exosome-depleted (Gibco) RPMI for 24 h. In parallel, cells were pre-treated with pEV or PTX-pEV and vehicle condition (DMSO-pEV). After 24 h, cell monolayers were scratched using a 96-pin mechanical wound making device (WoundMaker™ Essen Bioscience), washed with DPBS and incubated with positive control (fully supplemented EBM™-2 and RPMI) or the following conditions: pEV, 8-9 fractions of DPBS gradient (negative control), PTX-pEV, DMSO-pEV and PTX as free drug and respective carrier's conditions, diluted in starvation media. Plates were placed in the

IncuCyte ZOOM® (Essen Bioscience) and automatically scanned every two hours until wounds closed. The scratch area was determined with the aid of a wound healing size plugin [124] for ImageJ software (NIH,Bethesda,MD). The percentage of wound closure was estimated according to the following equation:

$$Wound\ Closure\ (\%) = \left(\frac{A_0 - A_t}{A_t}\right) \times 100\% \qquad \text{(Eq. 3.2)}$$

where A_0 is the initial wound area and A_t is the wound area after a period of time t of the initial scratch.

3.4.6. Tube formation assay

HUVEC were seeded onto a 6-well plate at a density of 2×10^4 cell/well. One day after, cells were serum-starved with 0.1% (v/v) FBS EGM™-2 basal medium with pEV, PTX-pEV, and vehicle condition (DMSO-pEV) for 24 h. HUVEC were detached with TrypLE™ Select (Gibco™) and 1.2×10^4 cell/well were seeded on 96 well-plates previously coated with 40 μL/well of growth factor-reduced Matrigel (Corning® Matrigel® Growth Factor Reduced Basement Membrane Matrix, Phenol red-free, 356231). After 30 min of incubation at 37 °C, cells were treated with positive control (fully supplemented EBM™-2) and the subsequent conditions properly diluted in starvation media: pEV, 8-9 fractions of DPBS gradient (negative control), PTX-pEV and DMSO-pEV. Plates were placed in IncuCyte ZOOM® (Essen Bioscience) for up to 8 h and images were captured every two hours (5 images per well were acquired). The segments length, number of nodes, junctions, and branches were determined using Angiogenesis Analyzer plugin of ImageJ software [125]. Figure 3.3 demonstrates a representative image of the constitutive elements of the tube network formation:

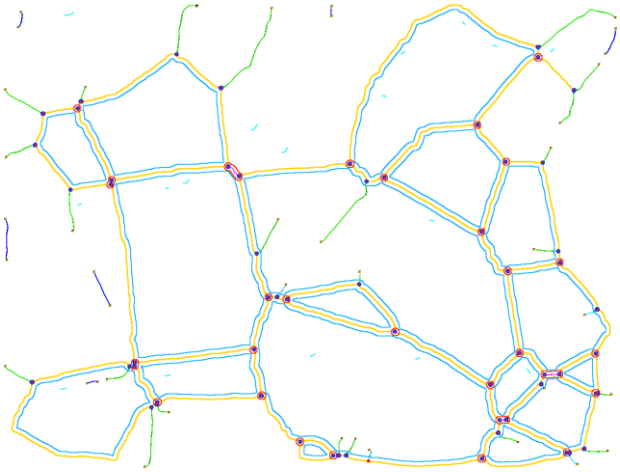

Figure 3.3: Representation of constitutive elements of the tube network. Segments (elements linked by two junctions) are represented in yellow, nodes (dots with at least three neighbors) in blue dark dots, branches (elements linked by a junction and an extremity) in green and junctions (groups of nodes creating a bifurcation) in pink [125,126].

3.4.7. Cytotoxicity assay

Cell death induced by PTX treatment was assessed in MDA-MB-231 and BT474 cells by measuring changes in membrane integrity using the CellTox™ Green Cytotoxicity Assay (Promega). MDA-MB-231 and BT474 cells were seeded in 96-well plates at a density of 6.8×10^3 cell/well and 8.5×10^3 cell/well, respectively, and allowed to adhere the well. To formulate the conditions groups, CellTox™ Green Dye was added to 10% (v/v) FBS RPMI medium (0.1 μL/mL) with free PTX (0.01 μM and 0.5 μM), PTX-pEV (15000 PTX-pEV/cell), or negative controls (DMSO and DMSO-pEV). Plates were placed on the IncuCyte ZOOM® (Essen Bioscience), and the imaging was coursed after 24 h. After 24 h of treatment, cells were lysed with 0.5% (v/v) Triton X-100 (Sigma-Aldrich) to attain 100% cell death. Phase and fluorescence images were acquired after 24 h using IncuCyte™ Zoom (Essen BioScience). The number of dead cells was achieved by using IncuCyte™Zoom basic analyzer and green color (green object count/mm^2). Percentage of cell death was calculated for each sample relative to the total number of cells (after treatment with Triton X-100).

3.4.8. Cell proliferation assay

MDA-MB-231 and BT474 cells were seeded in a 24-well plate with coated coverslips at a density of 3.8×10^4 and 4.7×10^4 cell/well, respectively. After cell adhesion, cells were treated for 48 h with free PTX conditions (0.01 μM and 0.5 μM), PTX-pEV (15000 PTX-pEV/cell), DMSO and, DMSO-pEV, in a humidified incubator [37 °C, 5% (v/v) CO_2]. EdU (5-ethynyl-2'-deoxyuridine) solution (Component A of Click-it™ EdU Cell Proliferation Kit for Imaging, Alexa Fluor™ 488 dye, Thermo Fisher Scientific) was added to each well at a dilution of 1:1000, for the lasted 24 h. At the end, cells were fixed with 4% (w/v) PFA for 15 min at RT and washed twice with 3% (v/v) BSA in DPBS. To permeabilize the cell membrane, cells were incubated with 0.5% (v/v) Triton X-100 (Sigma-Aldrich) in DPBS for 20 min at RT. After two washing steps with 3% (v/v) BSA in DPBS, Click-iT™ Plus reaction cocktail (prepared according to the manufacturer instructions) was added for 30 min at RT in the dark, followed by 3% (v/v) BSA in DPBS washes. Nuclei were stained with DAPI, and coverslips were mounted, as described above (3.4.3). Fluorescence images were acquired using an inverted fluorescence microscope (DMI6000, Leica). Images were further analyzed using ImageJ software to count the EdU- and DAPI-positive nucleus. The percentage of proliferative cells was calculated for each sample relative to the total number of DAPI-positive nuclei.

3.5. Statistical analysis

Data are shown as mean $\pm$ standard deviation, where *n* represents the number of independent experiments performed (indicated in figure legends). Statistical significance was determined by Student's T test, by two-way or by one-way analysis of variance (ANOVA) with Tukey's multiple comparison test or Bonferroni's post hoc test using the GraphPad Prism 8 software. * $p<0.05$, ** $p<0.01$, *** $p<0.001$, **** $p<0.0001$ were considered significant.

CHAPTER 4

4. Results and discussion

4.1. Establishment of an efficient pEV isolation protocol, pEV characterization and pEV bioactivity

4.1.1. Assessment of pEV yield and purity

Since blood is the most complex body fluid and PC is a blood-derived product, the presence of co-isolated non-EV components during pEV isolation is expected [127,128]. Therefore, the choice of isolation method is a determinant factor using PC as starting material. However, there is no consensus on the ideal EV isolation and purification method [129]. In this study, three pEV separation methods exploring different physiochemical properties of EV were compared, namely DGUC, SEC, and DGUC-SEC (Figure 4.1 A).

To select the ideal pooled pEV fractions obtained by DGUC and SEC methods, pEV yield and purity were investigated. As such, particle concentration was evaluated by NTA, and the level of contaminating protein was quantified by BCA assay. As shown in Figure 4.1 B and C, a similar profile between DGUC and SEC protocols was observed. More specifically, protein concentration peaks occurred mostly in later fractions, whereas the highest pEV yield was detected in fractions 8 and 9 (1.3×10^{11} particles/100 mL PC, Figure 4.1 B and 8.6×10^{10} particles/100 mL of PC, Figure 4.1 C). Furthermore, when compared to fractions 8-9, an increase in particles to protein ratio of ~75% and ~80% was observed for fractions 10-12 from DGUC and fractions 10-13 from SEC, respectively. This evidences an increase in non-vesicular nature particles. Therefore, fractions 8-9 represented the best balance between yield and purity in both methodologies, so they were selected to further analysis. In fact, fractions 8-9 from DGUC (Fr.8-9 interfacing 1.08 g/mL - 1.13 g/mL densities) encompass the density range of the EV preponderance (1.10 g/mL) usually reported [130] and SEC fractions 8-9 comprise the typical EV enriched fractions eluted from a qEV column. The qEV column manufacturer's instructions [131], indicate that typical EV elution occurs 1 mL $\pm$ 0.5 mL after the column void volume (3 mL, i.e., 6 fractions) and the elution of proteins occurs 2.5-7.0 mL after the void volume (later fractions). Given that the bulk of lipoproteins and soluble proteins present in blood-derived products, generally have a size distribution between 8-40 nm [132], they are capable to penetrate within the pores of the column resin (pore size of 70 nm), showing a longer retention time.

However, a slight co-isolation with proteins was visible in fractions 8-9 (Figure 4.1 B and C). Since single methods evidenced a light co-purification of proteins, and the combination of multiple isolation methods was purposed as a solution to obtain higher purity levels [106,133], DGUC-SEC protocol was evaluated (Figure 4.1 A).

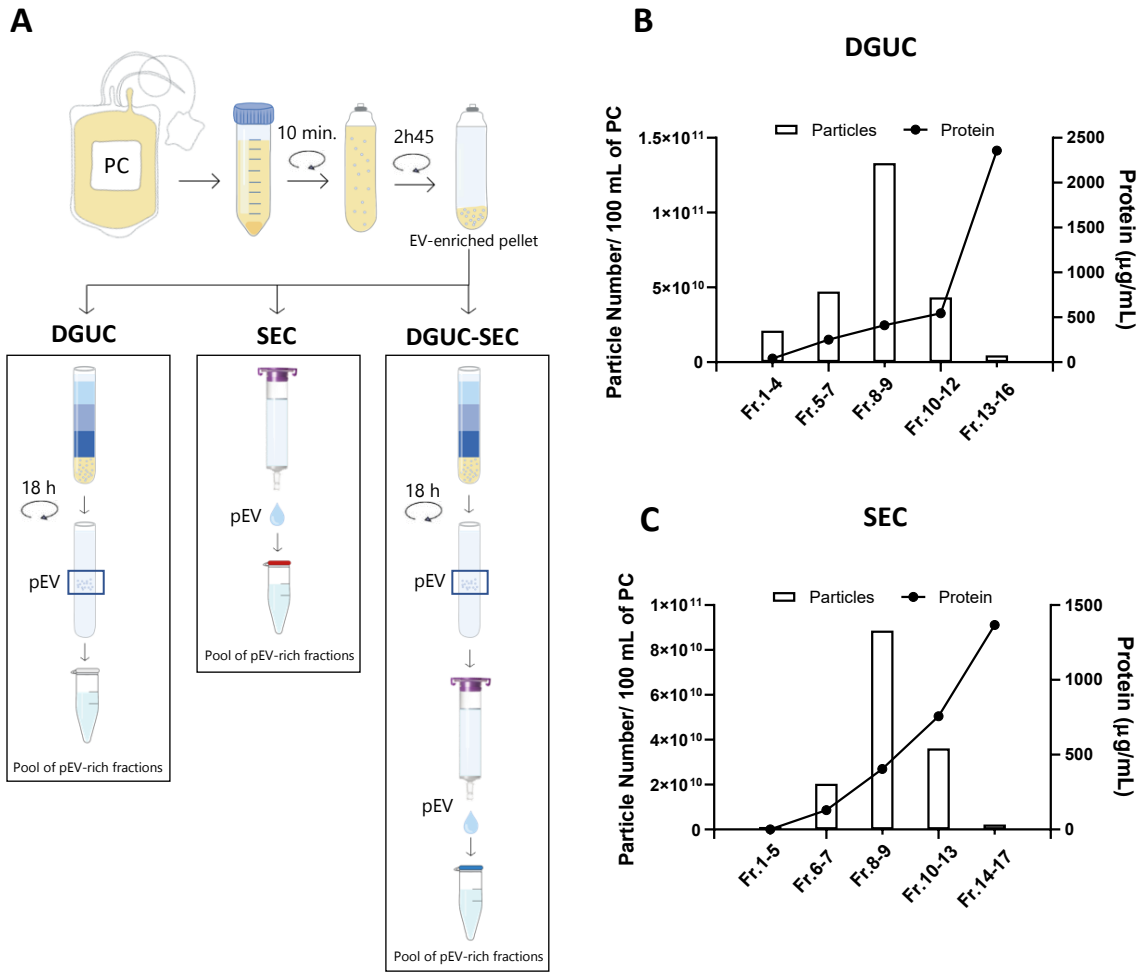

Figure 4.1: Characterization of isolated fractions in terms of yield and purity to identify optimal pooled pEV fractions. (A) Schematic overview of the pEV isolation methods used: DGUC, SEC and, DGUC-SEC. (B) pEV yield, measured as isolated particle number normalized per 100 mL of platelet concentrate (bars) and pEV purity measured as contaminating protein (line) concentration from pooled DGUC and (C) SEC fractions. Fractions 8 and 9 were considered pEV-enriched; Data are represented as mean.

According to some studies, the ratio of particle to protein content has been purposed as an insufficient approach for measuring the purity of plasma EV preparations, as BCA assay assesses total protein concentrations [133,134]. Consequently, western blot assay was performed to identify the expression of specific EV and non-EV markers (Figure 4.2 A). Both isolation techniques confirmed the previously established pEV recovery profile (Figure 4.1 A and B), with the highest expression levels of tetraspanins CD63 and CD9 and cytosolic protein flotillin-2 (FLOT2) in fractions 8 and 9 (Figure 4.2 A). Overall, DGUC revealed the highest expression of EV markers, in contrast to DGUC-SEC, where only the presence of CD63 and CD9 was observed, although CD9 was scarcely detected. This lower expression in DGUC-SEC reveals a clear decrease in pEV yield, which is reliable with previous results

[127,135,136], indicating that more labor-consuming protocols (i.e., with more processing steps) negatively impact the EV yield [137]. The presence of platelet-specific surface marker CD41 [55] in all pEV-enriched fractions, confirmed the cellular origin of isolated EV. The non-EV markers apolipoprotein A1 (ApoA1) and argonaute-2 (Ago2) were detected to identify the presence of HDL and RNA-binding proteins contaminations, respectively. Of note, residual amounts of Ago2 in EV have been previously described, however, other studies indicate that Ago2 can be considered as a marker to estimate contamination levels on EV preparations [119,138].

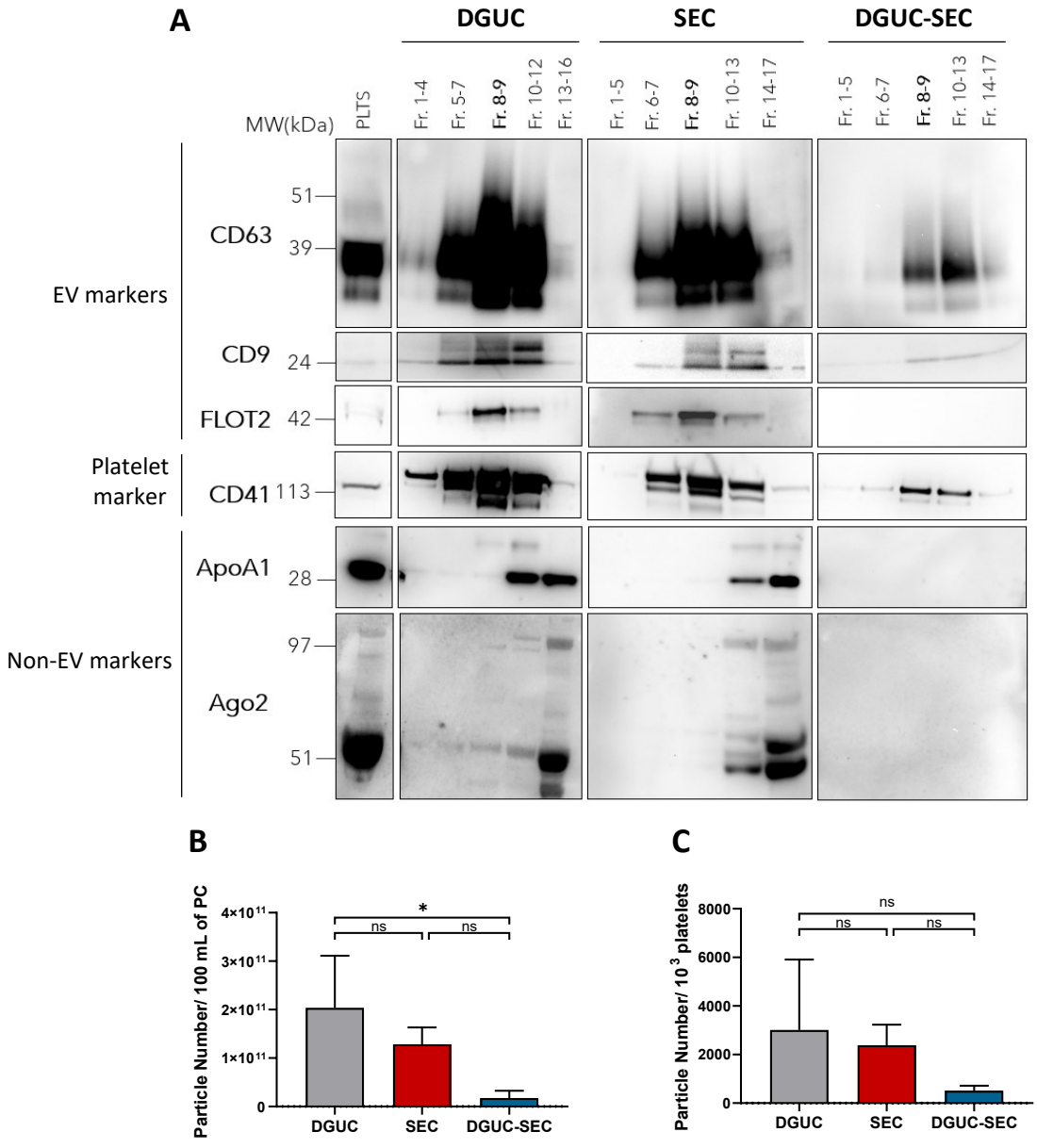

Figure 4.2: Characterization of pEV fractions isolated by DGUC, SEC, and DGUC-SEC, in terms of purity and yield. (A) Western blot analysis of specific EV markers (tetraspanins CD63 and CD9, and cytosolic protein flotillin-2), platelet-specific marker (CD41), and non-EV markers [apolipoprotein A1 (ApoA1) and argonaute 2 (Ago2)] of pooled fractions and platelet lysate (PLTS). (B) pEV-enriched samples (fractions 8 and 9) were analyzed using nanoparticle tracking analysis. Particle number was normalized to platelet concentrate (PC) volume (100 mL) and (C) to platelet count (10^3 platelets). *n*=3, *n* represents biologically independent replicates. Data are represented as mean ± S.D. **p* < 0.05, n.s. not significant, determined by one-way ANOVA followed by Tukey's multiple comparison test.

Non-EV contaminants were undetectable for DGUC-SEC and mainly detected in DGUC and SEC later fractions, as previously described [119,135,138]. In fact, small particles such as HDL (8-16 nm) [132], reach their buoyant equilibrium position later [139,140], and are lastly eluted from qEV column. These findings also suggested that 18 hours of ultracentrifugation was an ideal time, consistent with a previous study, indicating that HDL required 65 h of centrifugation time until reach its equilibrium density [139]. The high degree of purity of DGUC-SEC pEV preparations could be justified by the fact that this method separates pEV by exploiting two different physical properties of EV: size and density. Considering this, particles overlapping in diameter with EV but with different density (e.g., chylomicrons; $\rho < 0.930$ g/mL and 75-1200 nm) or overlapping in density with distinct size (e.g., HDL; $\rho = 1.063\text{-}1.210$ g/mL and 8-16 nm) were expected to be removed [128,132].

The nanoparticle recovery was compared between fractions 8-9 isolated by each method. DGUC-SEC showed the lowest pEV yield and DGUC revealed a trend toward higher pEV yield with $2.03 \times 10^{11} \pm 1.08\text{x}10^{11}$ particles/100 mL of PC (Figure 4.2 B) and $3.01 \times 10^{3} \pm 2.89 \times 10^{3}$ particles/10^{3} platelets (Figure 4.2 C), and as previously suggested by western blot analysis. Although vesicle's concentration difference was not statistically significant between DGUC- and SEC-isolated pEV ($1.29 \times 10^{11} \pm 3.46 \times 10^{10}$ particles/100 mL of PC and $2.38 \times 10^{3} \pm 8.46 \times 10^{2}$ particles/10^{3}platelets, Figures 4.2 B and C, respectively), the lowest pEV concentration was attained using SEC methodology. These differences may be associated with pEV losses due to non-specific binding to SEC column resin. This could be avoided if columns were equilibrated with DPBS containing BSA, to block the non-specific binding sites. However, with this treatment, the protein contamination profile could not be evaluated [139].

4.1.2. pEV size and morphology characterization

According to minimal requirements reported by International Society for Extracellular Vesicles (ISEV) to characterize EV, morphology and size distribution are two critical parameters recommended to monitor the impact of each isolation method on EV preparations [4,102].

For DGUC and SEC, the representative size distribution profiles were similar, with a bimodal distribution ranging between 100-300 nm, as previously described [141]. Particularly, the main peak was at 148 nm and 128 nm, and the lower peak was at 202 nm and 223 nm, for DGUC and SEC, respectively (Figure 4.3 A). Thus, two pEV populations appear to be isolated, with the largest pEV population ranging between 100-200 nm, as the expansion of the peak around the main mode was broader than that around the smaller mode. In contrast, the combined method (DGUC-SEC) showed a more heterogeneous profile with numerous peaks (Figure 4.3 A). This result can be related to the higher variability associated with this protocol, requiring longer processing times and multiple steps [133]. Although several peaks were observed, the two pEV populations seen in DGUC and SEC can also be identified in the combined method. The apparent presence of two pEV populations seems to be justified by other studies that evidence the existence of two major pEV populations, small and large [142,143].

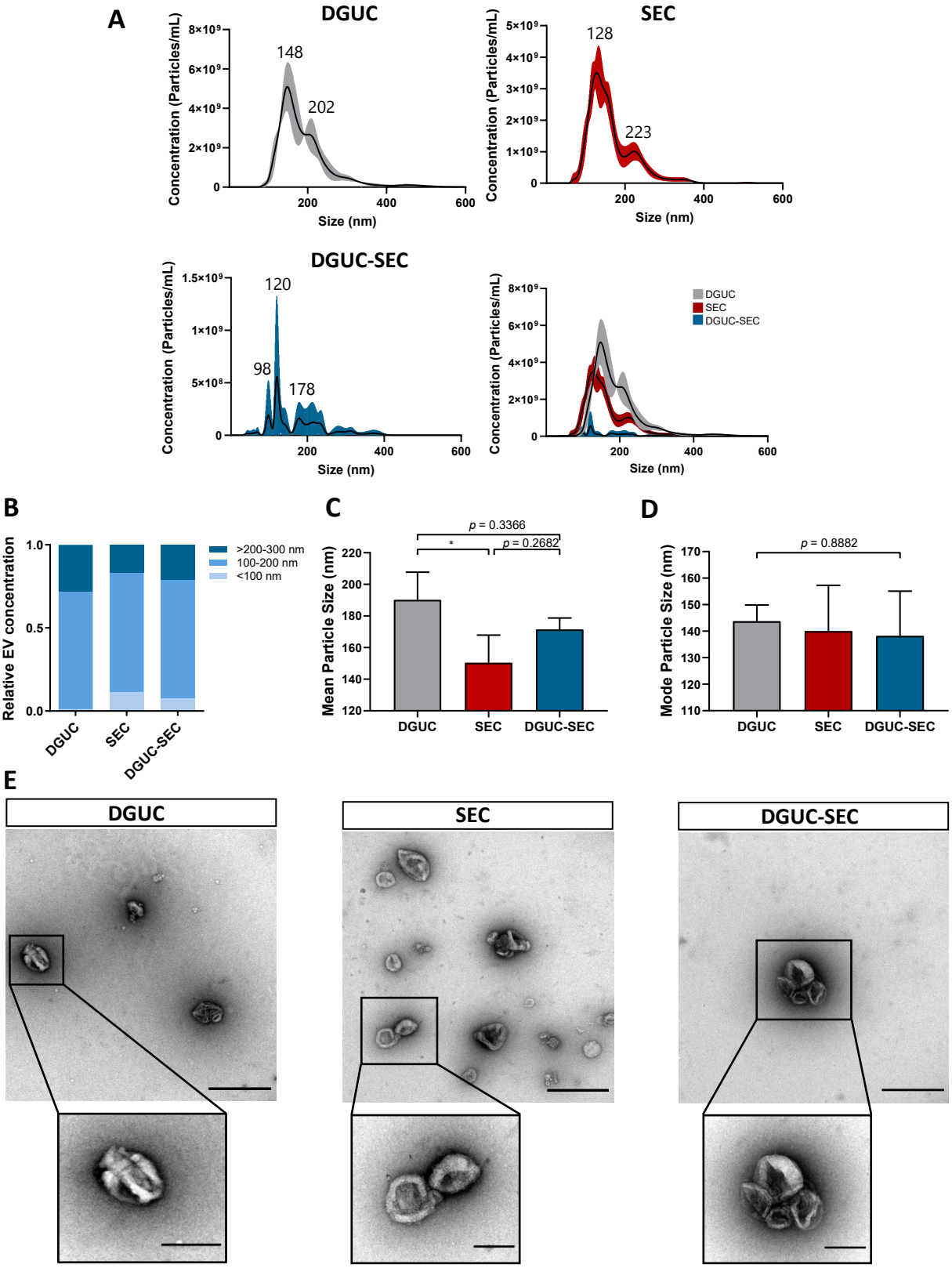

Figure 4.3: Size distribution and morphological characterization of pEV isolated by DGUC, SEC and DGUC-SEC. (A) Representative size distribution profiles of pEV preparations analyzed by nanoparticle tracking analysis. Size distribution is represented as a mean (black line) ± S.D. (colored shaded area). (B) Relative pEV distribution ranged into three different size classes: <100 nm, 100-200 nm and >200-300 nm; *n*=3 (C) Mean and (D) mode particle size (nm) of pEV samples; *n*=3 (E) Representative negative staining transmission electron microscopy (TEM) images. Higher magnification images detailing the morphology of pEV. Scale bars: 500 nm, 200 nm (high magnification). *n* represents biologically independent replicates. Data are represented as mean ± S.D. **p* < 0.05, n.s. not significant, determined by one-way ANOVA followed by Tukey's multiple comparison test.

Of the applied methods, SEC was the one with the largest portion of particles in the <100 nm range (11.08%) and DGUC was the one that isolated the largest particles, with 27.08% of particles in the >200-300 nm range (Figure 4.3 B). The same trend is observed for mean particle size, with the pEV isolated by SEC the ones with the lowest mean particle size (150.33 ± 17.54 nm, Figure 4.3 C), which is consistent with previous findings isolating pEV with a sepharose column [144]. Contrarily, pEV isolated by DGUC showed the highest mean size value of 190.23 ± 17.45 nm (Figure 4.3 C), since a possible constraint of centrifugation-based isolation methods is potential vesicle aggregation due to centrifugation at high forces for long-lasting periods [102,145]. Comparing the three methodologies, we observed that the modal size was similar between methods, as the most common pEV size range (100-200 nm, Figure 4.3 B) intersected all methods (142.16 ± 21.22 nm, 141.87 ± 17.27 nm, and 138.20 nm $\pm$ 16.85 for DGUC, SEC, and DGUC-SEC, Figure 4.3 D).

TEM characterization of fractions 8-9 isolated by each method confirmed the typical EV morphology [144,146] with their preserved structural integrity, as shown by the presence of a heterogeneous sphere or cup-shaped EV (Figure 4.3 E) [147]. For DGUC-SEC, only a few particles could be identified in pEV enriched sample, supporting the low yield observed for this isolation protocol (Figure 4.2) [148]. For all pEV isolation methodologies, a background without granularity was observed and this may be another indication of low co-isolation in proteins. In fact, in TEM images, white ragged structures and white spheres are not present, which are commonly representative of lipoproteins and proteins [144].

Taken together, the results presented above, especially considering the EV yield obtained, the DGUC method was selected for EV isolation in the following studies.

4.1.3. pEV cellular uptake by endothelial cells

To investigate the functionality of pEV upon uptake on HUVEC and its specificity to these recipient cells, a cellular uptake assay was performed. One of the broadest defining features of EV is their lipid membrane, thus, a lipophilic membrane dye (PKH26) was used to label and track them. Previous studies showed that steps such as simple washing by sedimentation through ultracentrifugation were ineffective in removing dye aggregates, whereas sucrose density gradient ultracentrifugation showed its effectiveness [149]. Hence, excess of unbound or aggregated dye was removed through a DGUC step to avoid non-specific fluorescence signals. In addition, to ensure that the observed results were from the PKH26 labeled pEV (PKH26-pEV), in parallel, a PKH26-DPBS control was used. In pEV samples, the presence of two dye bands on the density gradient was observed, one at the level of fractions 8-9, indicating PKH26-pEV, and a second band on denser fractions, representing the unbound dye (Supplementary information Figure 7.1). For PKH26-DPBS control, only the band on denser fractions was detected, indicating the absence of nanoparticles formation from fluorescent dye.

After 24 and 48 h of incubation with PKH26-pEV, fluorescent PKH26-pEV were imaged in these cells using fluorescence microscopy and measured quantitatively by flow cytometry. PKH26-pEV uptake was evident in cells incubated with labeled pEV, being located in cell periphery and perinuclear regions (Figure 4.4 A), as previously reported [150]. This could be an indicator of endocytic internalization, as

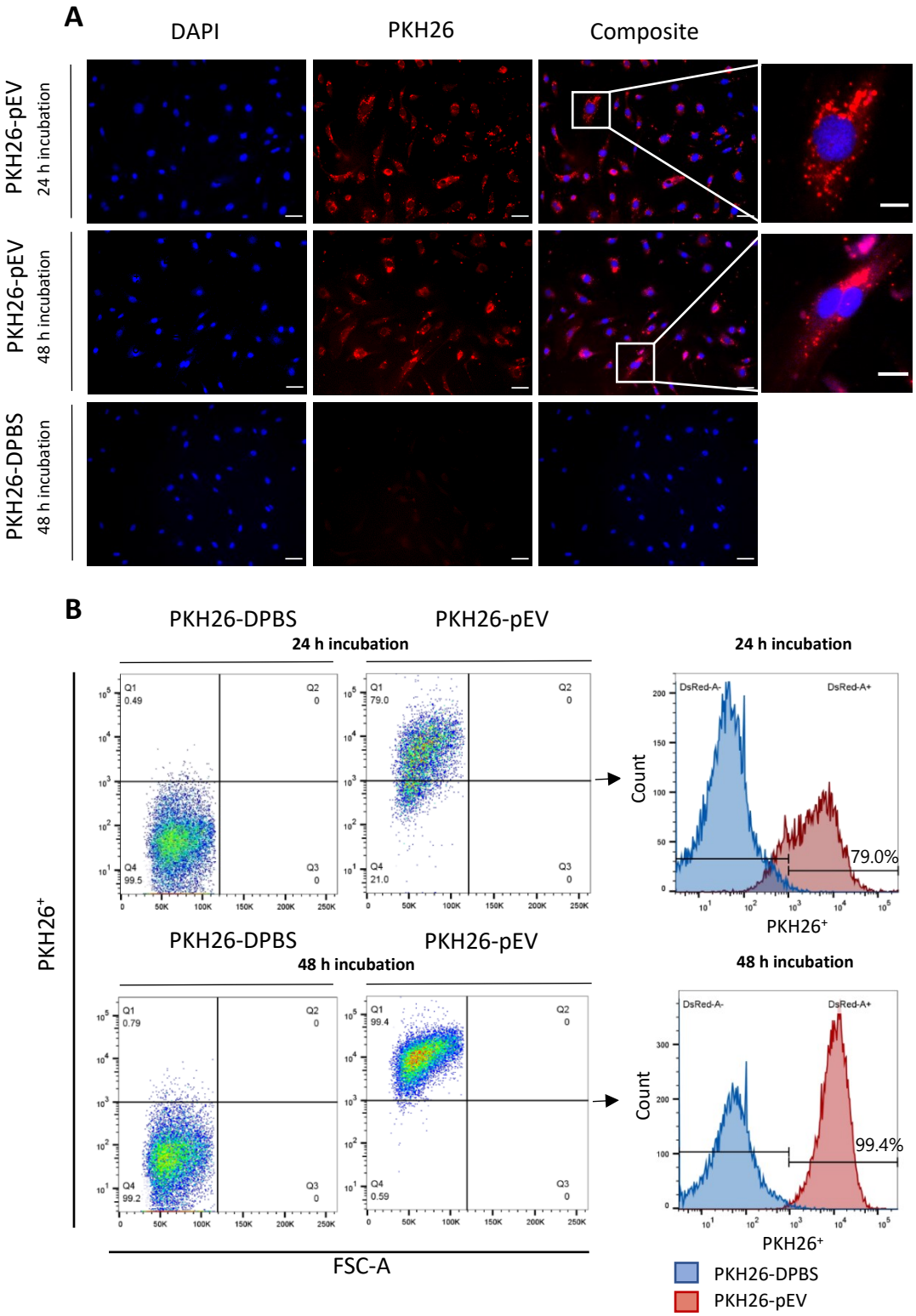

Figure 4.4: Cellular uptake of PKH26-pEV into HUVEC. (A) Representative immunofluorescence images of PKH26-pEV uptake. HUVEC were incubated with PKH26-pEV (Red, at a density of 6000 pEV/cell) for 24 and 48 h. As a negative control, HUVEC were incubated with PKH26-labelled DPBS (PKH26-DPBS). Cell nuclei were stained with DAPI (blue), and cells were analyzed by fluorescence microscopy. Scale bars: 50 μm, 20 μm (high magnification). (B) Flow cytometry analysis of pEV-internalized HUVEC after 24 and 48 h. PKH26-positive cells were measured quantitatively by flow cytometry, using the same gating strategy for each sample. HUVEC were incubated with PKH26-pEV (at a density of 6000 pEV/cell) for 24 h (upper graphs) or 48 h (lower graphs). PKH26-DPBS was used as a negative control for both time points. Corresponding histograms showing the PKH26-DPBS control (blue) and PKH26-pEV population (red) after an incubation period of 24 h (upper graph) or 48 h (lower graph). The x-axis represents the detection by the DsRed-A filter and y-axis represents pEV counts.

pEV appears to pass through the periphery, rich in early endosomes towards the perinuclear region, enriched in late endosomes [151]. Even so, to confirm the intracellular trafficking and internalization pathway of pEV, live-cell microscopy and the use of EV uptake inhibitors will be necessary to elucidate these processes, correspondingly. On the other side, the absence of fluorescence in cells incubated with PKH26 labeled DPBS (PKH26-DPBS, Figure 4.4. A, B), proved a specific pEV internalization by HUVEC due to an efficient remotion of unbound PKH26. Our results also showed that HUVEC internalized pEV in a time-dependent manner, with 99.4% of cells showing internalization with PKH26-pEV after 48 h of incubation (Figure 4.4 B).

4.1.4. Migration and angiogenic potential of pEV

To investigate the effect of pEV on the angiogenesis process, more precisely, on endothelial cells migration and tube-like structures network formation, a wound healing assay and a tube formation assay were performed with HUVEC, respectively. To reduce the influence of cell proliferation interfering with the observed effects and to ensure that results were due to pEV presence, serum starvation media was used during these assays. We performed the scratch assay for 16 h since we noticed that HUVEC needed approximately that time to close the scratch wound. For tube formation assay, we determined that 8 h was the optimal time point, since after this period a regression in the tubular structures was identified. This regression in a time-dependent manner is a common phenomenon in tube formation [152], since during angiogenesis three key steps are involved: endothelial cell proliferation and migration, sprouting of vessels and capillaries, and vasculature regression [153].

The cells' ability to migrate into the scratch wound was enhanced after pEV treatment (Figure 4.5 A-C). Overall, wound closure percentage reveals that pEV promotes a dose-dependent enhancing effect on cell migration compared to CTL- cells (Figure 4.5 B), with the highest wound closure effect achieved at 6000 pEV/cell (1.91 ± 0.55; p= 0.5419; Figure 4.5 C). Still, during the initial 6 hours of the assay, slight differences in the percentage of wound closure between CTL- and pEV conditions were observed. This may be due to an incomplete internalization of pEV by HUVEC, since a complete uptake is only achieved after 48 h of incubation (Figure 4.4 A, B).

Data on the angiogenic potential of pEV are in line with the migration results, with a tubule formation promotion *in vitro* in the presence of 6000 pEV/cell (Figure 4.5 D-G). The number of junctions increased from 261.66 in the CTL- (or 284.75 for CTL+) up to 400.66 at 6000 pEV/cell (Figure 4.5 D), and from 908.33 for CTL- (or 1076.33 for CTL+) up to 1358 number of nodes at 6000 pEV/cell (Figure 4.5 E). The total segments length increased to 27735 μm at 6000 pEV/cell (18699 μm for CTL- and 20757 μm for CTL+, Figure 4.5 F).

Angiogenic potential of EV has been mainly attributed to the EV ability to transfer GF and other bioactive molecules that stimulate phenotypical and functional changes of recipient cells, like signal transduction pathways, promoting cell-to-cell communication involved in modulation of the angiogenic process [154]. Previous studies have reported the release of VEGF, TGF-β, and PDGF present in pEV as the essential GF to promote angiogenesis [55,62,154,155]. VEGF binds to tyrosine kinase receptors

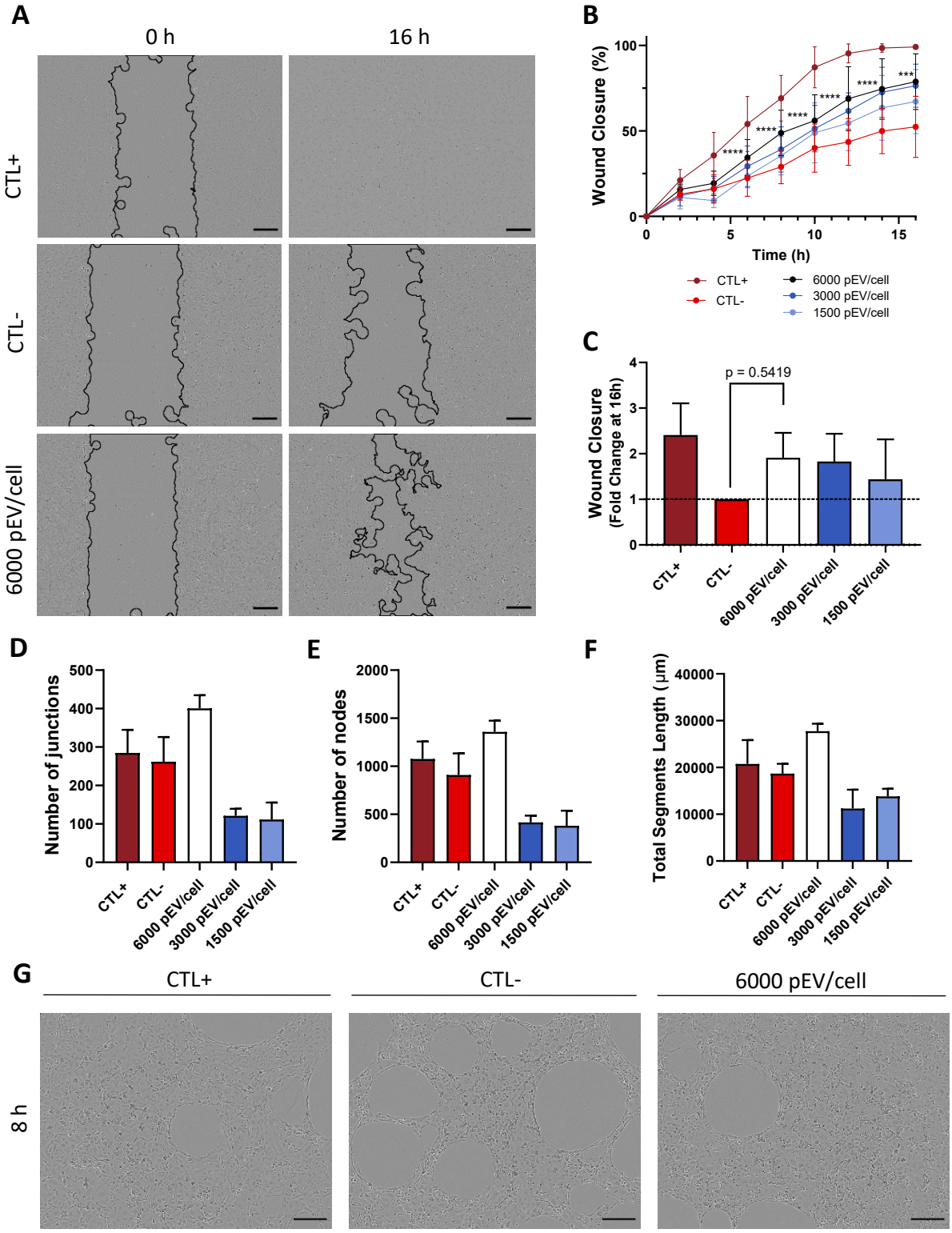

Figure 4.5: Effect of pEV on HUVEC angiogenesis (A) Representative images of cell migration at the initial time (0 h) and 16 h of wound healing assay of pEV-treated HUVEC (1500,3000 and 6000 pEV/cell) or with controls, CTL+ (cells cultured in supplemented media) and CTL- (8-9 fractions of DPBS gradient). Scale bars: 200 μm. (B) Quantitative analysis of the wound closure percentage throughout culture time; *n*=3. (C) Fold change of wound closure at 16 h (relative to CTL-) in the presence of distinct pEV concentrations; *n*=3. (D) Number of junctions, (E) nodes and (F) total segments length (μm) of HUVEC incubated with pEV or with controls, CTL- and CTL+. (G) Representative images from tube formation assay of HUVEC cultured on growth-factor reduced matrigel with CTL+, CTL-, and pEV (6000 pEV/cell) for 8 h. *n* represents biologically independent replicates. Data are represented as mean ± S.D. ***p < 0.001, ****p < 0.0001, determined by two-way ANOVA followed by Bonferroni's post hoc test (B) 6000 pEV/cell versus CTL-. n.s. not significant, determined by one-way ANOVA followed by Tukey's multiple comparison test (C).

on the surface of HUVEC and promotes their recruitment, initiating the angiogenesis process. TGF-β is capable to induce PDGF expression and PDGF induces cell migration [155,156]. Additionally, a study demonstrated that the inhibition or neutralization of these stimulators in separate eliminated the pro-angiogenic effect of platelet-derived microparticles, evidencing the dependence of the mutual action of these factors in angiogenesis induction [157]. Thus, we can propose that these GF were the main drivers of the pro-migratory effect of pEV on HUVEC. To confirm this, further experiments will be required, such as the use of enzyme-linked immunosorbent assay (ELISA) kits to determine the release kinetics of these GF.

4.2. Development of pEV as drug delivery vehicles for breast cancer therapy

The potential of pEV as drug-delivery vehicles to block cancer progression has been evidenced [57]. The reason behind that is the biochemical lipid membrane composition of this EV type, which enhances their interaction with cancer cells [57]. Although pEV has been demonstrated to infiltrate solid tumors and transfer its content to tumor cells [158], the delivery of drugs loaded into pEV to tumor cells has been understudied [57]. Therefore, in this second part of this thesis project, we were particularly interested in evaluating, for the first time to our knowledge, the potential of pEV as a paclitaxel-delivery system.

4.2.1. Loading of PTX into pEV and PTX-pEV characterization

The choice of drug loading protocol plays a critical role in the development of EV as drug delivery systems. The available drug loading protocols are known to differently influence the entrapment efficiency, structural integrity of EV, and the functional properties of the therapeutic drug [159].

For this work, the incorporation of PTX into pEV (PTX-pEV) was done by direct incubation, exploring the high hydrophobicity of PTX [160], and PTX-pEV were further characterized. Briefly, pEV (5×10^{10} pEV) were incubated with two different concentrations of PTX [25 μg/mL (20 μM) and 64 μg/mL (50 μM), hereafter named as loading A (lA) and loading B (lB), respectively], for 1 hour at 37 °C (Figure 4.6 A). In parallel, the same approach was adopted for pEV incubated with DMSO, to ensure that results obtained were not a consequence of the vehicle solution.

The quantification of entrapped PTX, was performed using UV-VIS spectrophotometry, as described in other works [161]. Data showed that similar values (without statistical differences) of PTX entrapment efficiency were observed for both loading conditions (10.12 $\pm$ 1.90% for loading A and 5.92 $\pm$ 0.01% for loading B; p=0.0616, Figure 4.6 B), therefore, loading B had a higher PTX concentration (3.79 μg/mL $\pm$ 0.04; Figure 4.6 C) than loading A (2.53 $\pm$ 0.47 μg/mL; p=0.0436; Figure 4.6 C). The amount of PTX loaded within pEV increased with the enhancement of the initial PTX concentration used for incubation, and this dependence has been reported in other studies [161,162]. With respect to entrapment efficiency, similar values have previously been reported using the passive diffusion technique to load PTX into EV [110].

Drug loading into EV could have broad consequences on the vesicles' size and morphology. Although direct incubation is not the most aggressive method (i.e., contrary to transfection, electroporation, ultrasound, extrusion, or freeze-thaw cycle [163]), the integrity of vesicles needs to be ensured after drug loading. TEM results confirmed that there were no changes in morphology between samples obtained after drug loading A and B, and pEV incubated with vehicle solution (DMSO-pEV) (Figure 4.6 D). Besides, PTX-pEV morphology was similar to pEV before drug loading (as seen in Figure 4.3 E). Additionally, no substantial differences were observed in mean particle size (177.20 $\pm$ 8.28 nm, 167.63 $\pm$ 8.15 nm, 158.76 $\pm$ 8.69 nm and 157.13 $\pm$ 4.05 nm for pEV, DMSO-pEV, PTX-pEV, and PTX-EV, respectively; Figure 4.6 E) or in mode particle size (136.20 $\pm$ 18.91 nm, 125.33 $\pm$ 5.51 nm,

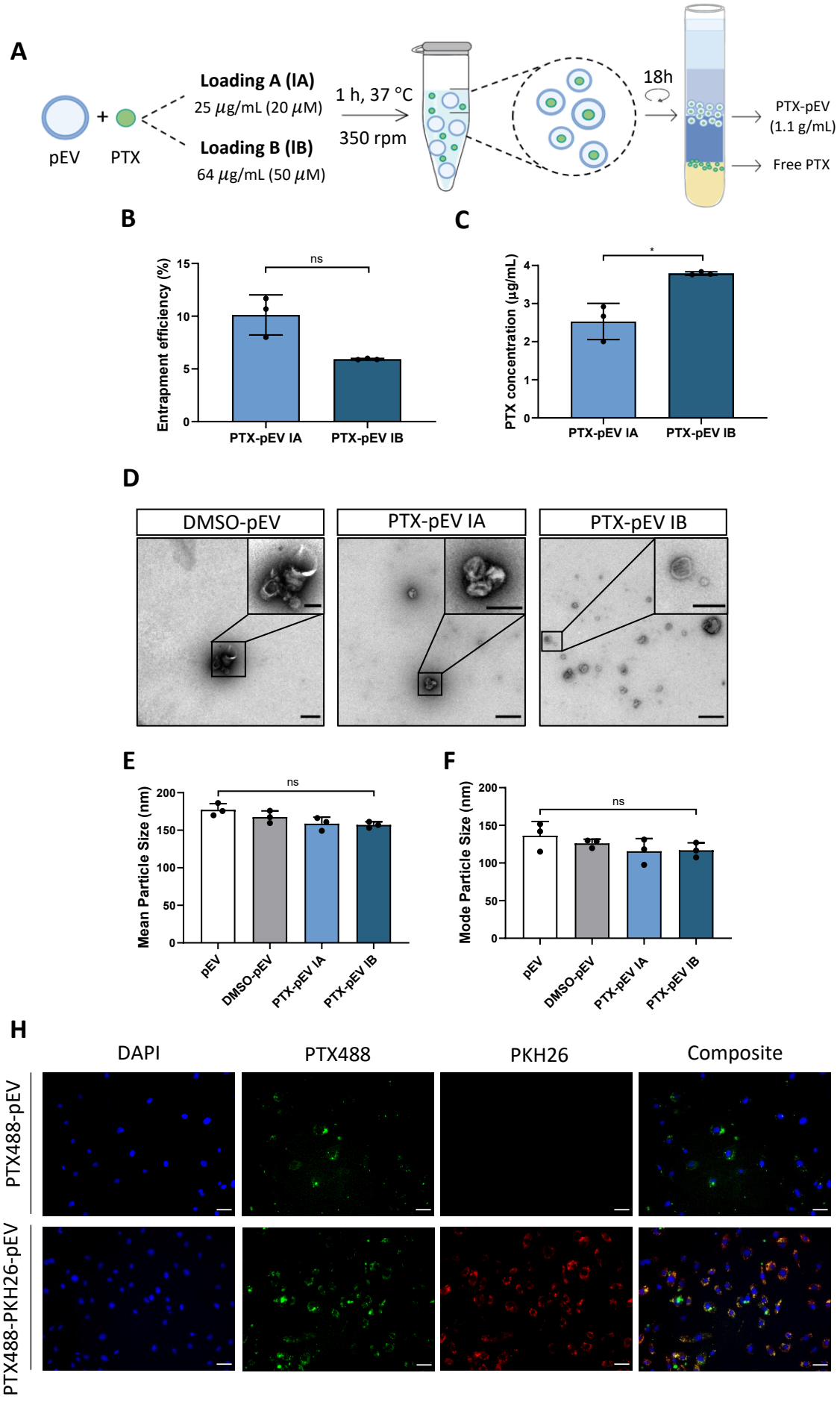
A
pEV
PTX
Loading A (IA)
25 μg/mL (20 μM)
Loading B (IB)
64 μg/mL (50 μM)
1 h, 37 °C
350 rpm
18h
PTX-pEV
(1.1 g/mL)
Free PTX
B
Entrapment efficiency (%)
ns
PTX-pEV IA
PTX-pEV IB
C
PTX concentration (μg/mL)
*
PTX-pEV IA
PTX-pEV IB
D
DMSO-pEV
PTX-pEV IA
PTX-pEV IB
E
Mean Particle Size (nm)
ns
pEV
DMSO-pEV
PTX-pEV IA
PTX-pEV IB
F
Mode Particle Size (nm)
ns
pEV
DMSO-pEV
PTX-pEV IA
PTX-pEV IB
H
DAPI
PTX488
PKH26
Composite
PTX488-pEV
PTX488-PKH26-pEV

Figure 4.6: Loading of paclitaxel into pEV and characterization of PTX-pEV. (A) Schematic representation of PTX-loaded pEV by direct incubation via loading A (lA) or loading B (lB). (B) Entrapment efficiency of PTX in pEV by lA and lB; *n*=3 (C) PTX concentration encapsulated by $2x10^9$ pEV for lA (20 μM or 25 μg/mL) and lB (50 μM or 64 μg/mL); *n*=3 (D) Representative negative staining transmission electron microscopy (TEM) images of DMSO-pEV, PTX-pEV lA and PTX-pEV lB. Scale bars: 500 nm, 200 nm (high magnification). (E) Mean and (F) mode particle size (nm) of pEV, DMSO-pEV, PTX-pEV lA and PTX-pEV lB measured by NTA; *n*=3. (H) HUVEC were treated with pEV-loaded fluorescence-labeled PTX488 (green, PTX488-pEV) and PTX488-pEV labeled with PKH26 (red) (PTX488-PKH26-pEV), for 24 h. Cell nuclei were stained with DAPI (blue), and cells were analyzed by fluorescence microscopy. Scale bars: 50 μm. *n* represents biologically independent replicates. Data are represented as mean $\pm$ S.D. $*p < 0.05$, n.s. not significant, determined by one-way ANOVA followed by Tukey's multiple comparison test.

115.63 $\pm$ 16.85 nm and 116.96 $\pm$ 9.75 nm for pEV, DMSO-pEV, PTX-pEV lA and PTX-EV lB, respectively; Figure 4.6 F), before and after drug loading.

Taking into consideration the previous results, loading B was selected to prepare PTX-pEV for the following studies. Since no significant differences were observed in the entrapment efficiency and PTX-pEV integrity between loading A and loading B, our choice was based on the amount of therapeutic cargo that best fit the doses required for the functional assays.

Having verified that drug loading did not affect pEV integrity, to certify PTX entrapment into pEV and PTX-pEV uptake by cells, labeled pEV and PTX were used. As shown in figure 4.6 H, a high co-localization between pEV (red) and PTX488 (green) in cells was observed, confirming that PTX was effectively entrapped into pEV.

4.2.2. PTX-pEV effect on endothelial cells angiogenic potential

Considering that tumor growth and progression are favored by angiogenesis and PTX has been described as an angiogenic inhibitor [164,165], the effect of PTX-pEV on angiogenesis was evaluated. To investigate the PTX-pEV functionality, the effect of PTX-pEV on HUVEC migration capacity was quantified by the wound healing assay. Moreover, the capacity of free PTX to inhibit HUVEC migration has been established [164,165]. The tube formation capacity of HUVEC upon PTX-pEV treatment was also evaluated. In this study, to ensure that observations from PTX-pEV were caused by the PTX presence, two control conditions were included: DMSO-pEV and pEV.

As seen in Figure 4.7 A-C, a clear inhibition in wound closure capacity of HUVEC after 16 h of PTX-pEV treatment was obtained, validating the efficacy of the drug loading approach. On the contrary, DMSO-pEV and pEV conditions promote a similar effect, (72.51% and 60.62% for pEV and DMSO-pEV, respectively, at 16 h; Figure 4.7 B) evidencing the pro-migratory effect of pEV, as noted above (section 4.1.4). Additionally, the effect of PTX-pEV showed a higher anti-migratory effect, i.e., lower wound closure, when compared to free PTX (Figure 4.7 C). In effect, the theoretical drug entrapped concentration in PTX-pEV for 1.8×10^8 pEV added to cells was lower than 0.5 μM, approximately 0.4 μM (20.83 $\pm$ 8.96 for PTX-pEV and 22.87 $\pm$ 3.15 for 0.5 μM PTX; Figure 4.7 C). The use of EV as drug delivery carriers has been presented to be more advantageous compared to free drug applications, due to their higher safety, stability in circulation or high biocompatibility, mainly due to its endogenous origin [87].

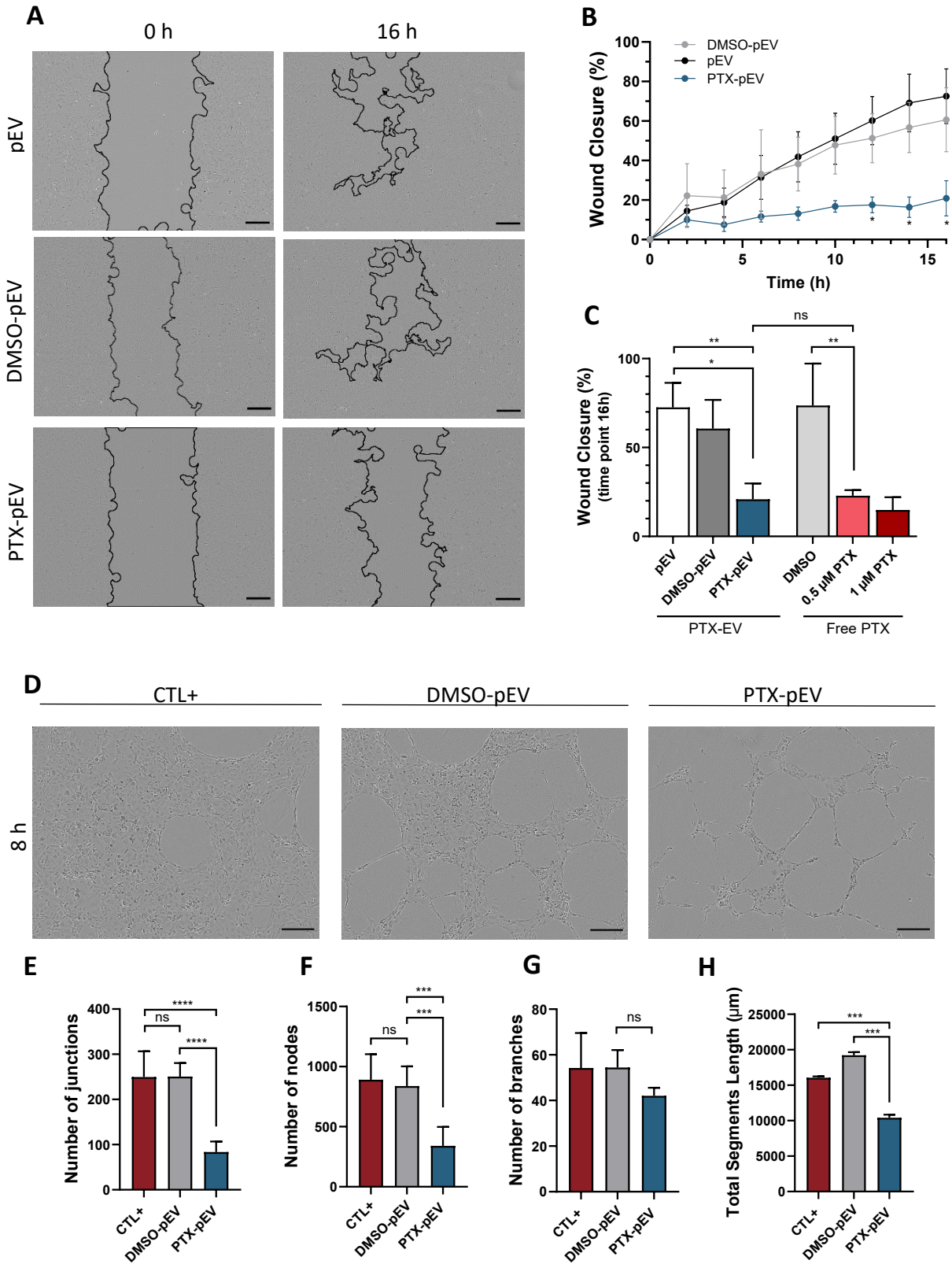
A
0 h
16 h
pEV
DMSO-pEV
PTX-pEV
B
DMSO-pEV
pEV
PTX-pEV
Wound Closure (%)
Time (h)
C
Wound Closure (%)
(time point 16h)
pEV
DMSO-pEV
PTX-pEV
DMSO
0.5 µM PTX
1 µM PTX
PTX-EV
Free PTX
ns
D
CTL+
DMSO-pEV
PTX-pEV
8 h
E
Number of junctions
F
Number of nodes
G
Number of branches
H
Total Segments Length (µm)
CTL+
DMSO-pEV
PTX-pEV

Figure 4.7: Effect of PTX-pEV on HUVEC angiogenesis (A) Representative images of cell migration at the initial time (0 h) and 16 h of wound healing assay of HUVEC treated with pEV, DMSO-pEV and PTX-pEV at a density of 6000 pEV/cell. Scale bars: 200 μm. (B) Quantitative analysis of the wound closure percentage throughout culture time; *n*=3. (C) Bar graph illustrating percentage of wound closure at 16 h for cells treated without PTX, with PTX-pEV and, free PTX (0.5 μM or 0.6 μg/mL and 1 μM or 1.3 μg/mL); *n*=3. (D) Representative images of tube formation assay of HUVEC cultured on growth-factor reduced matrigel in CTL+ (cells cultured in supplemented media), DMSO-pEV and PTX-pEV at a density of 6000 pEV/cell for 8 h. Scale bars: 200 μm. (E) Number of junctions, (F) nodes (G) branches and (H) total segments length (μm), after 8 h of treatment; *n*=2. *n* represents biologically independent replicates. Data are represented as mean ± S.D. Two-way ANOVA followed by Bonferroni's post hoc test (B) PTX-pEV/cell versus pEV. One-way ANOVA followed by Tukey's multiple comparison test (C, E-H) *p < 0.05, **p < 0.01, ***p < 0.001, ****p < 0.0001, n.s. not significant.

The improved effect of PTX-pEV compared to free drug can be explained by the ability of pEV to carry more drug into HUVEC, compared to the ability of cells to uptake conventional therapeutic drugs from the medium, as previously shown [166]. Another hypothesis could be related to differences in the uptake pathway, resulting in possible different subcellular locations of drug. It is described that the endocytic pathway is the most effective site for drug delivery, maximizing its therapeutic activity [167]. In fact, data from section 4.1.3 suggest the internalization of pEV into HUVEC via endocytic pathways, although further studies are required to elucidate this assumption.

The different angiogenic parameters (junctions, nodes, branches, and segments length) showed that the formation of tridimensional vessels *in vitro* was also compromised after 8 h of HUVEC incubation with PTX-pEV, compared to DMSO-pEV control group (Figure 4.7 D-H). Accordingly, PTX-pEV caused irregular and broken tubes (Figure 4.7 D), confirming their anti-angiogenic effect.

4.2.3. Pathways involved on pEV uptake by breast cancer cells

The effect of PTX-pEV was also evaluated in two breast cancer cell lines: the triple-negative MDA-MB-231 (ER^-, PR^-, $HER2^-$), and the luminal B BT474 (ER^+, PR^+, $HER2^+$).

EV seem to be more powerfully internalized by recipient cells than synthetic therapeutics and this advantage should be given to the endogenous mechanisms that are involved in their cellular uptake [168]. Furthermore, it has been shown that EV from the same cellular source can express different intercellular communications and traffic to different types of recipient cells [88,168]. Therefore, to better understand possible variations in the therapeutic potential of PTX-pEV between MDA-MB-231 and BT474, it is important to elucidate the mechanisms of EV uptake. For the purpose of this work, two different chemical inhibitors of EV uptake were investigated to characterize the pathways responsible for pEV internalization by MDA-MB-231 and BT474, namely dynasore [88] and heparin [169], previously described to be able to impair EV uptake. Dynasore is a dynamin 2 inhibitor that blocks the activity of this GTPase, thereby, stopping the vesicle scission from PM during clathrin or caveolin mediated endocytosis [116]. Heparin targets are heparan sulphate proteoglycans (HSP), which are predominant receptors of the cell membrane-EV surface cluster and are directly involved in EV uptake by recipient cells [169], especially in cancer cells [170]. Both inhibitors have been defined as endocytosis inhibitors and so we chose them because EV are generally internalized by this mechanism [88].

Cells were simultaneously incubated with PKH26-pEV and the inhibitors to analyze cellular uptake blockage. Immunofluorescence images and flow cytometry analysis showed that pEV internalization pathway was different between MDA-MB-231 and BT474 (Figure 4.8 A and B).

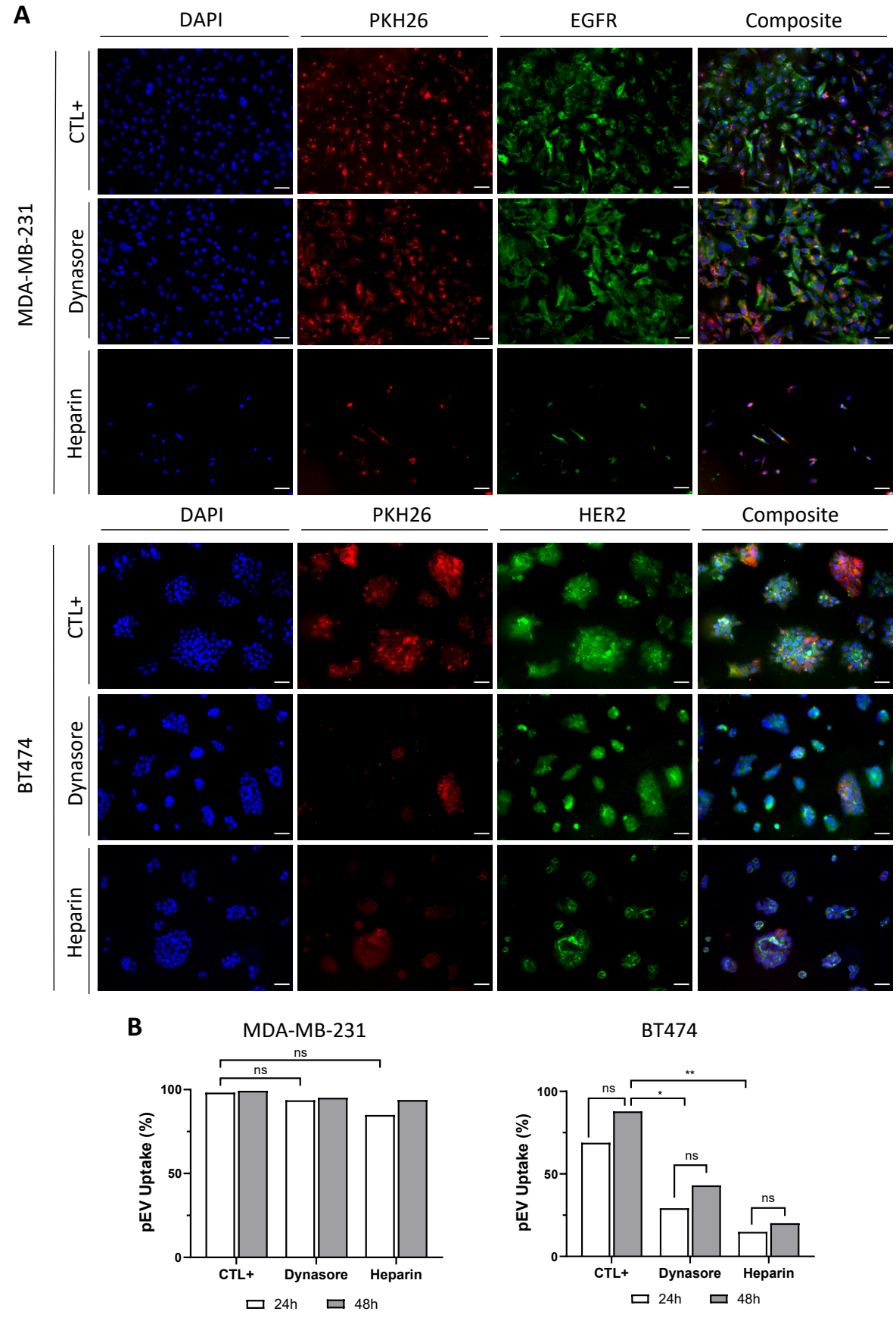

Figure 4.8: Assessment of chemical inhibitors in pEV uptake blockage in breast cancer cells. (A and B) MDA-MB-231 and BT474 cells were incubated only with PKH26-pEV (CTL+, at a density of 6000 pEV/cell) or simultaneously with PKH26-pEV (6000 pEV/cell) and dynasore (100 μM) or heparin (500 μg/mL). (A) Representative images of PKH26-pEV uptake (red) were acquired by fluorescence microscopy 24 h post-treatment. MDA-MB-231 and BT474 were stained for EGFR and HER2 (green), respectively, and for nuclei (DAPI, blue). Scale bars: 50 μm. (B) PKH26-pEV positive cells were quantitatively measured by flow cytometry, 24 and 48 h post-treatment. (A and B) Cells completely untreated were used as a negative control. Data are represented as mean $\pm$ S.D. *$p < 0.05$, **$p < 0.01$, n.s. not significant, determined by two-way ANOVA followed by Tukey's multiple comparison test.

More specifically, pEV uptake by MDA-MB-231 was neither inhibited by dynasore nor significantly affected by heparin, whereas in BT474 a noted decrease in pEV uptake was observed in cells treated with both inhibitors (MDA-MB-231: 98.2%, 93.6% and 84.9% for CTL+, Dynasore and heparin conditions, respectively; and, BT474: 68.9%, 29.2% and 14.9% for CTL+, Dynasore and heparin conditions, respectively, at 24 h; Figure 4.8 B and Supplementary information Figures 7.2 and 7.3). These data suggest that pEV may be entering in BT474 cells via clathrin or caveolin mediated endocytosis and HSP-dependent mechanism, while in MDA-MB-231 cells these pathways seem not to be involved in pEV internalization.

Still, we cannot assume with complete certainty that pEV do not enter MDA-MB-231 by clathrin or caveolin mediated endocytosis, since dynamin has been involved in other biochemical pathways and processes, so it has been considered an unspecific target for these pathways [171]. Furthermore, to ensure that HSP-dependent mechanism was not a crucial process for pEV uptake by MDA-MB-231, further investigations should be taken. Indeed, for MDA-MB-231, heparin at the doses and incubation times employed in this assay seems to be cytotoxic, as corroborated by the cell loss observed in these cells (Figure 4.8 A). We considered that a possible explanation for this cell loss observed only in MDA-MB-231 could be related to the disruption of CXCL12/CXCR4 interaction, caused by heparin. CXCL12/CXCR4 signaling plays a critical role on metastatic breast cancer cells (e.g., MDA-MB-231), and its disruption is known for the loss of metastatic potential, cell migration, proliferation, and survival [172]. To examine the effect of heparin on CXCL12/CXCR4 disruption between the two cell lines, quantitative reverse transcription polymerase chain reaction (qRT-PCR) and WB of downstream target genes should be performed, as well as test the effect of heparin on CXCL12 and CXCR4 knockout or knockdown MDA-MB-231.

4.2.4. PTX-pEV effect on breast cells migration

The effect of PTX-pEV treatment on MDA-MB-231 and BT474 migration ability was evaluated by wound healing assay.

For BT474, 48 h of incubation with PTX-pEV was performed, whereas 24 h was established for the MDA-MB-231 (Figure 4.9 A and D). The rationale behind the selection of incubation times is in line with the metastatic potential of MDA-MB-231 due to its higher migratory capacity when compared to other breast cancer cell lines [173]. For both cell lines, the migration ability of PTX-pEV treated cells was significantly decreased compared to those treated with control conditions (pEV and DMSO-pEV; Figure 4.9 A and D). In fact, at the end of the assay, the results indicate that PTX-pEV was able to markedly

inhibit MDA-MB-231 and BT474 migration by ~50%, compared to pEV control (44.39 ± 11.35 for PTX-pEV and 96.38 ± 2.01 for pEV, Figure 4.9 B and 40.84 ± 10.02 for PTX-pEV and 88.54 ± 2.50 for pEV, Figure E).

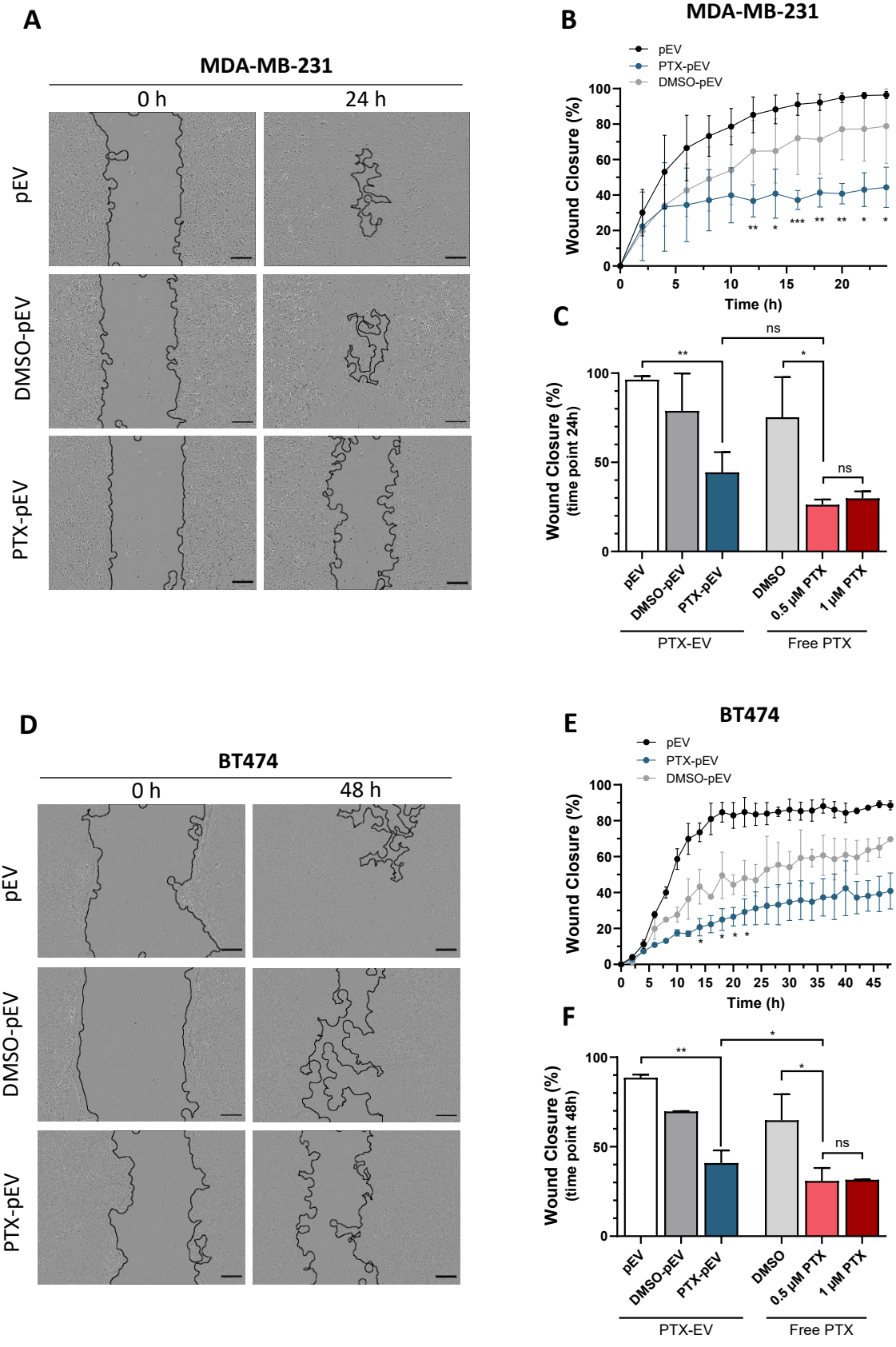

Figure 4.9: Effects of PTX-pEV on breast cancer cell migration. (A and D) Representative images at the initial time (0 h) and wound healing of 24 h for MDA-MB-231 and 48 h for BT474 cells incubated with PTX-pEV (6000 pEV/cell). As controls, pEV and DMSO-pEV (treatment vehicle) were used at a density of 6000 pEV/cell. Scale bars: 200 μm. (B and E) Quantitative analysis of the wound closure percentage throughout culture treatment with PTX-pEV, or with controls, DMSO-pEV and pEV for (B) MDA-MB-231 and (E) BT474. (C and F) Bar graph illustrating percentage of wound closure for cells treated without PTX, with PTX-pEV, and free PTX (0.5 μM or 0.6 μg/mL and 1 μM or 1.3 μg/mL), (C) MDA-MB-231 at 24 h and (F) BT474 at 48 h. *n* represents biologically independent replicates. Data are represented as mean $\pm$ S.D. *n*=3 (B and C) and *n*=2 (E and F). Two-way ANOVA followed by Bonferroni's post hoc test (B and E), 6000 pEV/cell versus PTX-pEV; One-way ANOVA followed by Tukey's multiple comparison test (C and F). **p* < 0.05, ***p* < 0.01, ****p* < 0.001, n.s. not significant.

For the free PTX experiment, two doses of PTX were evaluated, with our special interest in 0.5 μM PTX, because the concentration of drug entrapped into pEV was close to this value. As estimated, treatment with free PTX reduced the ability of MDA-MB-231 and BT474 cells to regenerate the monolayer scratch compared to DMSO control (26.24 $\pm$ 2.90% for 0.5 μM PTX, and 75.30 $\pm$ 22.46% for DMSO; Figure 4.9 C and 30.85 $\pm$ 7.27% for 0.5 μM PTX, and 64.76 $\pm$ 14.56% for DMSO; Figure 4.9 F). In our data we could observe that the use of pEV in BT474 as a drug delivery system increases the anti-migratory effect of the free drug. However, no significant difference was observed for PTX-pEV when compared to 0.5 μM PTX in MDA-MB-231 cells.

4.2.5. PTX-pEV effect on breast cells viability and proliferation

PTX has been demonstrated not only to affect the cell migration and angiogenesis process, but also cell viability (through apoptosis induction) and cell proliferation [164,165]. To study the effect of PTX on cancer cell viability, MDA-MB-231 and BT474 cells were incubated with PTX-pEV and free PTX for 24 h. Cell death was measured through the binding of CellTox™ Green dye to the DNA of cells with a compromised membrane.

Comparing death cell values between cell lines, a higher effect was observed in BT474 cells incubated with PTX-pEV (Figure 4.10 A). Particularly, cytotoxicity values for BT474 were 78.95% $\pm$ 27.36 for 15000 pEV/cell whereas for MDA-MB-231 only 10.68% $\pm$ 2.03 for 15000 pEV/cell was observed.

These findings are in accordance with those reported in the literature, which demonstrated a significant increase in cytotoxicity in drug resistant P-gp positive cells incubated with PTX-loaded exosomes [79]. Furthermore, it has been described that most patients with HER2-positive breast cancer cells (e.g., BT474) expressed drug resistance due to high levels of P-gp (drug transporter) once it reduces drug intake [75,77] distribution and toxicity [174]. In fact, exosomes have been proposed as interesting drug carriers to reverse drug resistance [175]. Thus, in BT474, pEV could deliver its cargo mainly bypassing P-gp drug efflux pump, through interaction with bilayer membrane phospholipids, avoiding drug sequestration in lysosomes and consequently, PTX elimination. To confirm the hypothesis of bypassing the drug efflux system, cells should be treated with a P-qp inhibitor to understand whether the effect of PTX-pEV is maintained in the presence of P-gp inhibitor [75,79,176].

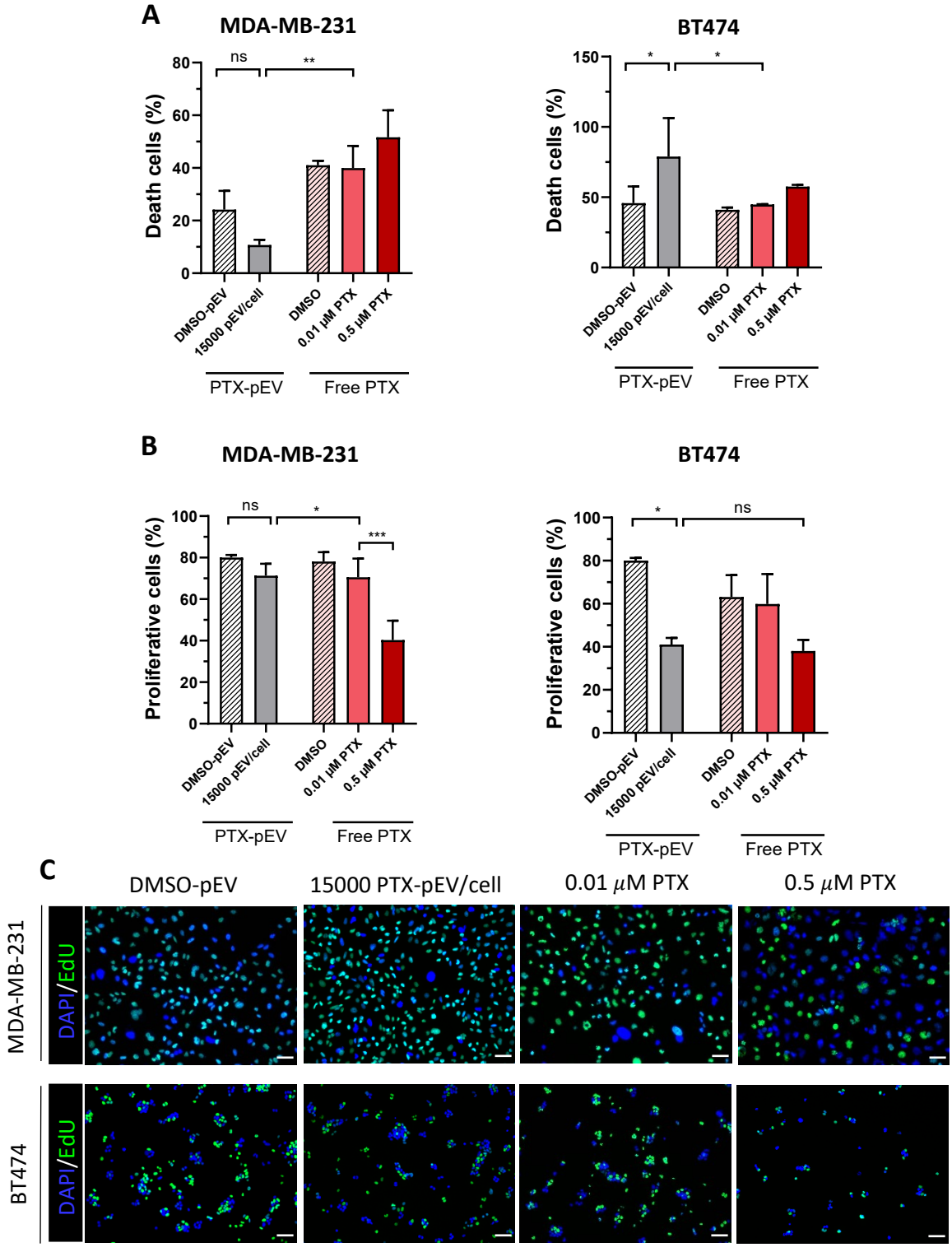

Figure 4.10: *In vitro* cytotoxicity and proliferation of breast cancer cells treated with PTX-pEV. (A and B) MDA-MB-231 an BT474 cells were treated with PTX-pEV (15000 pEV/cell) and free PTX (0.01 and 0.5 μM) for (A) 24h and (B) 48 h. (A) Cell death was measured using CellTox Green Dye; n=3, and (B) cell proliferation by EdU dye staining; n=2. (C) Representative images of EdU (green) immunofluorescence staining of breast cancer cells after 48 h of incubation. Nuclei were stained with DAPI (blue). Scale bars: 50 μm. n represents biologically independent replicates. Data are represented as mean ± S.D.*p < 0.05, **p<0.01, ns. not significant, determined by one-way ANOVA followed by Tukey's multiple comparison test.

The effect of free drug was similar for MDA-MB-231 (39.97 ± 8.38 for 0.01 μM PTX and 51.61 ± 10.31 for 0.5 μM) and BT474 (44.81 ± 0.19 for 0.01 μM PTX and 57.53 ± 1.33 for 0.5 μM). These results are in accordance with a previous study reporting that almost no difference in cytotoxicity was observed in drug-resistant and drug-sensitive cells treated with free taxol [75]. Still, in BT474, PTX-pEV appears to be more cytotoxic than the free drug, and we possibly attributed this result to differences in pEV uptake and synthetic drug uptake. Indeed, previous studies revealed that PTX alone enters cells without requiring ligand-receptor-mediated endocytosis pathway, so, less variability was expected in PTX free uptake between different recipient cells [177].

In order to complement the anti-cancer properties of PTX-pEV, we evaluated the cell proliferation rate using a thymidine analogue, specifically EdU, which is incorporated into the DNA of proliferating cells. Similar to the cytotoxic effect, a lower cell proliferation was observed for BT474 treated with PTX-pEV. Thus, an apparent higher sensitivity to PTX for BT474 (41.04 ± 3.06 for 15000 pEV/cell, Figure 4.10 B) relative to MDA-MB-231 (71.27 ± 5.80 for 15000 pEV/cell, Figure 4.10 B) was observed. The relationship between cell proliferation and susceptibility to cell death has been evidenced for a long time [178].

CHAPTER 5

5. Conclusion

5.1. Concluding Remarks

In this thesis, we evaluated a promising therapeutic application for expired PC by exploring the potential of pEV as PTX delivery vehicles to target breast cancer cells. pEV are key mediators in intercellular communication and exhibit a natural propensity to enhance their interaction and targeting ability to cancer cells.

pEV were efficiently isolated from expired PC using all the three methods (DGUC, SEC and, DGUC-SEC), as confirmed by the identification of pEV with a typical cup-shaped morphology in the expected size range and expressing specific EV markers (CD9, CD63, FLOT2). The combined methodology, DGUC-SEC, showed the purest pEV preparation although with a significant decrease in EV recovery whereas the DGUC protocol was selected as the most suitable approach as it allowed higher pEV yields. Furthermore, pEV isolated by DGUC showed bioactivity, as revealed by its successful internalization into recipient cells, as well as a pro-migratory and pro-angiogenic ability.

pEV were successfully loaded with PTX (PTX-pEV) by direct incubation and expected entrapment efficiencies were achieved. PTX-pEV integrity (size and morphology) was not compromised and its uptake capacity into recipient cells was maintained. The biological functionality of PTX-pEV was assessed in HUVEC, showing a higher wound healing inhibition than free PTX treatment and pEV. In addition, the formation of HUVEC tridimensional vessels *in vitro* was also compromised in the presence of PTX-pEV treatment. HUVEC are key cells in angiogenesis, favoring the tumor progression [74], and so affecting these cells in anticancer therapy reveals an important advantage.

The pEV uptake mechanism by BT474 and MDA-MB-231 seemed to be distinct, with different pathways responsible for pEV entering. Similar anti-migration effects between breast cancer cell lines were demonstrated, with a clear decrease in cell migration after PTX-pEV treatment. However, only BT474 showed sensitivity to PTX-pEV in terms of viability and proliferation and with promising effects, since better results were obtained in comparison to the free PTX incubation condition.

5.2. Future Prospects

Drug delivery vehicles in tumor treatment represent a flourishing research field. Nowadays, synthetic vehicles for delivering drugs entail several limitations that are overcome using natural carriers, including EV. The innate characteristics of EV offer them exciting opportunities for drug delivery, with targeting, safety and pharmacokinetic benefits over synthetic nanocarriers. Still, the translational applicability of

EV in the cancer field is scattered, and more efforts have been postulated to improve their innate advantages. Although the intrinsic targeting properties of pEV, their surface functionalization with targeting molecules (e.g., anti-HER2 or anti-EGFR antibody), might provide even a more efficient cancer cell interaction. Moreover, complementing our studies with other drug-resistance and drug-sensitive breast cell lines would be interesting to analyze whether similar trends in cell viability and proliferation would be obtained. In addition, since EV may enter cells through various pathways [88], it would be useful to test other potential chemical inhibitors of EV uptake, to better elucidate differences in the therapeutic effectiveness of PTX-pEV between cancer cell lines.

Furthermore, some studies have been demonstrated that distinct populations of EV (e.g., MV and exosomes) show differences in their effectiveness as drug carriers [110,179]. Therefore, it would be interesting to isolate the two populations of pEV separately in order to understand which one will be the best to further optimize for carrying PTX.

Additionally, to complement the interactions of PTX-pEV in biological environments, studies in more complex *in vitro* models, including advanced three-dimensional models (e.g., culture in spheroids that better recapitulate *in vivo* cell environments) [4], should be evaluated.

For the use of EV in drug delivery applications, the evaluation of its molecular composition and its interaction with cells is pivotal. Thus, omics technologies such as proteomics, lipidomics and transcriptomics [4] could be employed to identify the active substance on pEV, understanding whether co-delivery of unwanted species from EV lumen is a possibility. Besides, proteomic characterization of pEV must be addressed to elucidate potential differences in P-gp levels, possibly associated with the distinct results in cell viability and proliferation observed between the breast cancer cell lines evaluated in this work.

CHAPTER 6

6. Bibliography

[1] Alcaina, P. Platelet Transfusion: And Update on Challenges and Outcomes. *Journal of Blood Medicine* **11**, 19–26 (2020).

[2] Burnouf, T. Multifaceted regenerative lives of “expired” platelets. *ISBT Science Series* **13**, 323–330 (2018).

[3] Burnouf, T., Goubran, H. A., & Seghatchian, J. Multifaceted regenerative lives of expired platelets in the second decade of the 21st century. *Transfusion and Apheresis Science* **51**, 107–112 (2014).

[4] Herrmann, I. K., Wood, M. J. A., & Fuhrmann, G. Extracellular vesicles as a next-generation drug delivery platform. *Nature Nanotechnology* **16**, 748–759 (2021).

[5] Van der Meijden, P. E. J., & Heemskerk, J. W. M. Platelet biology and functions: new concepts and clinical perspectives. *Nature Reviews Cardiology* **16**, 166-179 (2019).

[6] Semple, J. W., Italiano, J. E., & Freedman, J. Platelets and the immune continuum. *Nature Reviews Immunology* **11**, 264–274 (2011).

[7] Twomey, L., G. Wallace, R., M. Cummins, P., Degryse, B., Sheridan, S., Harrison, M., … P. Murphy, R. Platelets: From Formation to Function. *Homeostasis - An Integrated Vision* **5**, 71-92 (2019).

[8] McFadyen, J. D., & Kaplan, Z. S. Platelets Are Not Just for Clots. *Transfusion Medicine Reviews* **29**, 110–119 (2015).

[9] Harrison, P., & Martin Cramer, E. Platelet α-granules. *Blood Reviews* **7**, 52–62 (1993).

[10] Sharda, A., & Flaumenhaft, R. The life cycle of platelet granules. *F1000Research* **7**, 1-12 (2018).

[11] Chen, Y., Yuan, Y., & Li, W. Sorting machineries: how platelet-dense granules differ from α-granules. *Bioscience reports **38***, BSR20180458 (2018).

[12] Rendu, F., & Brohard-Bohn, B. The platelet release reaction: granules’ constituents, secretion and functions. *Platelets **12**, 261–273* (2001).

[13] British Committee for Standards in Haematology, Blood Transfusion Task Force. Guidelines for the use of platelet transfusions. *British journal of haematology **122***, 10–23 (2003).

[14] Freireich, E. J. Origins of Platelet Transfusion Therapy. *Transfusion Medicine Reviews* **25**, 252–256 (2011).

[15] Vassallo, R. Scott Murphy, MD: Platelet Storage Pioneer. *Transfusion Medicine Reviews* **25**, 156–161(2011).

[16] T*ynngård, N.* Preparation, storage and quality control of platelet concentrates. *Transfusion and Apheresis Science* **41**, 97–104 (2009).

[17] WHO: WHO Model List of Essential Medicines: 20th List. Geneva: WHO; 2017.

[18] Estcourt L. J. Why has demand for platelet components increased? A review. *Transfusion medicine* **24**, 260–268 (2014).

[19] European Directorate for the Quality of Medicines & HealthCare (EDQM). The Guide to the Preparation, Use and Quality Assurance of Blood Components, 20th edition (2020)

[20] Levin, E., Culibrk, B., Gyöngyössy-Issa, M. I. C., Weiss, S., Scammell, K., LeFresne, W., … Devine, D. V. Implementation of buffy coat platelet component production: comparison to platelet-rich plasma platelet production. *Transfusion* **48**, 2331–2337 (2008).

[21] Vassallo, R. R., & Murphy, S. A critical comparison of platelet preparation methods. *Current Opinion in Hematology* **13***,* 323–330 (2006).

[22] Foster, T. E., Puskas, B. L., Mandelbaum, B. R., Gerhardt, M. B., & Rodeo, S. A. Platelet-Rich Plasma. *The American Journal of Sports Medicine* **37**, 2259–2272 (2009).

[23] Dhurat, R., and Sukesh, M., Principles and methods of preparation of platelet-rich plasma: A review and author's perspective. *J. Cutan. Aesthet. Surg.* **7**, 189-197 (2014).

[24] Marx R. E. Platelet-rich plasma (PRP): what is PRP and what is not PRP? *Implant Dentistry* **10**, 225-228 (2001).

[25] Lozano, M., and Cid, J. Recent advances in platelet processing and storage. *ISBT Science Series* **11**, 34–38 (2016).

[26] Benjamin, R. J., Katz, L. Gammon, R. R., Stramer, S. L., Quinley, E., & Consortium for Blood Availability The argument(s) for lowering the US minimum required content of apheresis platelet components. *Transfusion* **59**, 779–788 (2019).

[27] Hardwick,J. Blood processing and components. *ISBT Science Series* **15**, 207–231 (2020).

[28] Hofmann, A., Ozawa, S., & Shander, A. Activity-based cost of platelet transfusions in medical and surgical inpatients at a US hospital. *Vox sanguinis* **116**, 998–1004 (2021).

[29] Verma, A., & Agarwal, P. Platelet utilization in the developing world: Strategies to optimize platelet transfusion practices. *Transfusion and Apheresis Science* **41**, 145–149 (2009).

[30] Farrugia A. Platelet concentrates for transfusion-metabolic and storage aspects. *Platelets* **5**, 177–185 (1994).

[31] Lozano, M., & Cid, J. Platelet concentrates: Balancing between efficacy and safety? *La Presse medicale (Paris, France: 1983)* **45**, e289–e298 (2016).

[32] Védy, D., Robert, D., Canellini, G., Waldvogel, S., & Tissot, J.-D. Bacterial contamination of platelet concentrates: pathogen detection and inactivation methods. *Hematology Reports* **1**, 22-28 (2009).

[33] Palavecino, E. L., Yomtovian, R. A., & Jacobs, M. R. Bacterial contamination of platelets. *Transfusion and Apheresis Science* **42**, 71–82 (2010).

[34] Blair, P., & Flaumenhaft, R. Platelet α-granules: Basic biology and clinical correlates. *Blood Reviews* **23**, 177–189 (2009).

[35] Prakash, S., & Thakur, A. Platelet Concentrates: Past, Present and Future. *Journal of Maxillofacial and Oral Surgery* **10**, 45–49 (2011).

[36] Becherucci, V., Piccini, L., Casamassima, S., Bisin, S., Gori, V., Gentile, F., … Bambi, F. Human platelet lysate in mesenchymal stromal cell expansion according to a GMP grade protocol: a cell factory experience. *Stem Cell Research & Therapy* **9**, 124 (2018).

[37] Jonsdottir-Buch, S. M., Lieder, R., & Sigurjonsson, O. E. Platelet lysates produced from expired platelet concentrates support growth and osteogenic differentiation of mesenchymal stem cells. *PloS one* **8**, e68984 (2013).

[38] Dessels, C., Durandt, C., & Pepper, M. S. Comparison of human platelet lysate alternatives using expired and freshly isolated platelet concentrates for adipose-derived stromal cell expansion. *Platelets* **30**, 356-367 (2018).

[39] Hassan,M., Yap,Z., Tang, Y., Law, M. Expired Platelet Concentrate as a Source of Human Platelet Lysate for Xenogeneic Free Culture of Human Dermal Fibroblasts. *Sains Malaysiana* **50**, 2355-2365 (2021).

[40] Notodihardjo, S. C., Morimoto, N., Kakudo, N., Mitsui, T., Le, T. M., Tabata, Y., & Kusumoto, K. Efficacy of Gelatin Hydrogel Impregnated with Concentrated Platelet Lysate in Murine Wound Healing. *Journal of Surgical Research* **234**, 190–201 (2019).

[41] Ito, R., Morimoto, N., Pham, L. H., Taira, T., Kawai, K., & Suzuki, S. Efficacy of the Controlled Release of Concentrated Platelet Lysate from a Collagen/Gelatin Scaffold for Dermis-Like Tissue Regeneration. *Tissue Engineering Part A* **19**, 1398–1405 (2013).

[42] Ding, Z. Y., Tan, Y., Peng, Q., Zuo, J., & Li, N. Novel applications of platelet concentrates in tissue regeneration (Review). *Experimental and therapeutic medicine* **21**, 226 (2021).

[43] Ren, X., Zhao, M., Lash, B., Martino, M. M., & Julier, Z. Growth Factor Engineering Strategies for Regenerative Medicine Applications. *Frontiers in bioengineering and biotechnology* **7**, 469 (2020).

[44] Wolf, P. The Nature and Significance of Platelet Products in Human Plasma. *British Journal of Haematology* **13**, 269–288 (1967).

[45] Italiano, J. E., Jr, Mairuhu, A. T., & Flaumenhaft, R. Clinical relevance of microparticles from platelets and megakaryocytes. *Current opinion in hematology* **17**, 578–584 (2010).

[46] Warren, B. A., & Vales, O. The release of vesicles from platelets following adhesion to vessel walls in vitro. *British journal of experimental pathology* **53**, 206–215 (1972).

[47] Kerris, E., Hoptay, C., Calderon, T., & Freishtat, R. J. Platelets and platelet extracellular vesicles in

hemostasis and sepsis. *Journal of investigative medicine: the official publication of the American Federation for Clinical Research* **68**, 813–820 (2020).

[48] Bode, A. P., Orton, S. M., Frye, M. J., & Udis, B. J. Vesiculation of platelets during in vitro aging. *Blood* **77**, 887–895 (1991).

[49] Miyazaki, Y., Nomura, S., Miyake, T., Kagawa, H., Kitada, C., Taniguchi, H., Komiyama, Y., Fujimura, Y., Ikeda, Y., & Fukuhara, S. High shear stress can initiate both platelet aggregation and shedding of procoagulant containing microparticles. *Blood* **88**, 3456–3464 (1996).

[50] Zhang, J. N., Wood, J., Bergeron, A. L., McBride, L., Ball, C., Yu, Q., Pusiteri, A. E., Holcomb, J. B., & Dong, J. F. Effects of low temperature on shear-induced platelet aggregation and activation. *The Journal of trauma* **57**, 216–223 (2004).

[51] Woith, E., Fuhrmann, G., & Melzig, M. F. Extracellular Vesicles-Connecting Kingdoms. *International journal of molecular sciences* **20**, 5695 (2019).

[52] Akers, J. C., Gonda, D., Kim, R., Carter, B. S., & Chen, C. C. Biogenesis of extracellular vesicles (EV): exosomes, microvesicles, retrovirus-like vesicles, and apoptotic bodies. *Journal of neuro-oncology* **113**, 1–11 (2013).

[53] Jadli, A. S., Ballasy, N., Edalat, P., & Patel, V. B. Inside(sight) of tiny communicator: exosome biogenesis, secretion, and uptake. *Molecular and cellular biochemistry* **467**, 77–94 (2020).

[54] Yáñez-Mó, M., Siljander, P. R.-M., Andreu, Z., Bedina Zavec, A., Borràs, F. E., Buzas, E. I., … Carvalho, J. Biological properties of extracellular vesicles and their physiological functions. *Journal of Extracellular Vesicles* **4***,* 27066 (2015).

[55] Tao, S.-C., Guo, S.-C., & Zhang, C.-Q. Platelet-derived Extracellular Vesicles: An Emerging Therapeutic Approach. *International Journal of Biological Sciences* **13***,* 828–834 (2017).

[56] Antich-Rosselló, M., Forteza-Genestra, M. A., Monjo, M., & Ramis, J. M. Platelet-Derived Extracellular Vesicles for Regenerative Medicine. *International journal of molecular sciences* **22**, 8580 (2021).

[57] Johnson, J., Wu, Y.-W., Blyth, C., Lichtfuss, G., Goubran, H., & Burnouf, T. Prospective Therapeutic Applications of Platelet Extracellular Vesicles. *Trends in Biotechnology* **39**, 598–612 (2021).

[58] Stambler, I. Recognizing degenerative aging as a treatable medical condition: Methodology and policy. *Aging and Disease* **8**, 583–589 (2017).

[59] De Jong, O. G., Van Balkom, B. W., Schiffelers, R. M., Bouten, C. V., & Verhaar, M. C. Extracellular vesicles: potential roles in regenerative medicine. *Frontiers in immunology **5***, 608 (2014).

[60] Mause, S. F., Ritzel, E., Liehn, E. A., Hristov, M., Bidzhekov, K., Müller-Newen, G., Soehnlein, O., & Weber, C. Platelet microparticles enhance the vasoregenerative potential of angiogenic early outgrowth cells after vascular injury. *Circulation* **122**, 495–506 (2010).

[61] Lovisolo, F., Carton, F., Gino, S., Migliario, M., & Renò, F. Platelet rich plasma-derived microvesicles increased in vitro wound healing. *European review for medical and pharmacological sciences* **24**, 9658–9664 (2020).

[62] Kim, H. K., Song, K. S., Chung, J. H., Lee, K. R., & Lee, S. N. Platelet microparticles induce angiogenesis in vitro. *British journal of haematology* **124**, 376–384 (2004).

[63] Guo, S. C., Tao, S. C., Yin, W. J., Qi, X., Yuan, T., & Zhang, C. Q. Exosomes derived from platelet-rich plasma promote the re-epithelization of chronic cutaneous wounds via activation of YAP in a diabetic rat model. *Theranostics* **7**, 81–96 (2017).

[64] Hayon, Y., Dashevsky, O., Shai, E., Varon, D., & Leker, R. R. Platelet microparticles promote neural stem cell proliferation, survival and differentiation. *Journal of molecular neuroscience : MN* **47**, 659–665 (2012

[65] Horak, E. R., Leek, R., Klenk, N., LeJeune, S., Smith, K., Stuart, N., Greenall, M., Stepniewska, K., & Harris, A. L. Angiogenesis, assessed by platelet/endothelial cell adhesion molecule antibodies, as indicator of node metastases and survival in breast cancer. *Lancet (London, England)* **340**, 1120–1124 (1992).

[66] Soleymani, S., Yari, F., Bolhassani, A., & Bakhshandeh, H. Platelet microparticles: An effective delivery system for anti-viral drugs. *Journal of Drug Delivery Science and Technology* **51***,* 290-296 (2019).

[67] Ma, Q., Fan, Q., Xu, J., Bai, J., Han, X., Dong, Z., Zhou, X., Liu, Z., Gu, Z., & Wang, C. Calming Cytokine Storm in Pneumonia by Targeted Delivery of TPCA-1 Using Platelet-Derived Extracellular Vesicles. *Matter* **3**, 287–301 (2020).

[68] Goubran, H. A., Kotb, R. R., Stakiw, J., Emara, M. E., & Burnouf, T. Regulation of tumor growth and metastasis: the role of tumor microenvironment. *Cancer growth and metastasis* **7**, 9–18 (2014).

[69] Gay, L. J., & Felding-Habermann, B. Contribution of platelets to tumour metastasis. *Nature Reviews Cancer,* **11***, 123–134* (2011)*.*

[70] Harbeck, N., & Gnant, M. Breast cancer. The *Lancet* **389**, 1134–1150 (2017).

[71] Sims, A. H., Howell, A., Howell, S. J., & Clarke, R. B. Origins of breast cancer subtypes and therapeutic implications. *Nature clinical practice. Oncology* **4**, 516–525 (2007).

[72] Ye, J., Wang, W., Xu, L., Duan, X., Cheng, Y., Xin, L., Zhang, H., Zhang, S., Li, T., & Liu, Y. A retrospective prognostic evaluation analysis using the 8th edition of American Joint Committee on Cancer (AJCC) cancer staging system for luminal A breast cancer. *Chinese journal of cancer research* **29**, 351–360 (2017).

[73] Szostakowska, M., Trębińska-Stryjewska, A., Grzybowska, E. A., & Fabisiewicz, A. Resistance to endocrine therapy in breast cancer: molecular mechanisms and future goals. *Breast cancer research and treatment* **173**, 489–497 (2019).

[74] Madu, C. O., Wang, S., Madu, C. O., & Lu, Y. Angiogenesis in Breast Cancer Progression, Diagnosis, and Treatment. *Journal of Cancer* **11**, 4474–4494 (2020).

[75] Rowinsky, E. K., & Donehower, R. C. Paclitaxel (taxol). *The New England journal of medicine* **332**, 1004–1014 (1995).

[76] Jordan, M. A., & Wilson, L. Microtubules as a target for anticancer drugs. *Nature reviews. Cancer* **4**, 253–265 (2004).

[77] Casazza, A. M., & Fairchild, C. R. Paclitaxel (Taxol): mechanisms of Resistance. *Cancer treatment and research* **87**, 149–171 (1996).

[78] Ji, X., Lu, Y., Tian, H., Meng, X., Wei, M., & Cho, W. C. Chemoresistance mechanisms of breast cancer and their countermeasures. *Biomedicine & pharmacotherapy* **114**, 108800 (2019).

[79] Kim, M. S., Haney, M. J., Zhao, Y., Mahajan, V., Deygen, I., Klyachko, N. L., Inskoe, E., Piroyan, A., Sokolsky, M., Okolie, O., Hingtgen, S. D., Kabanov, A. V., & Batrakova, E. V. Development of exosome-encapsulated paclitaxel to overcome MDR in cancer cells. *Nanomedicine: nanotechnology, biology, and medicine* **12**, 655–664 (2016).

[80] Qiao, L., Hu, S., Huang, K., Su, T., Li, Z., Vandergriff, A., Cores, J., Dinh, P. U., Allen, T., Shen, D., Liang, H., Li, Y., & Cheng, K. Tumor cell-derived exosomes home to their cells of origin and can be used as Trojan horses to deliver cancer drugs. *Theranostics* **10**, 3474–3487 (2020).

[81] Wu, Y. W., Huang, C. C., Changou, C. A., Lu, L. S., Goubran, H., & Burnouf, T. Clinical-grade cryopreserved doxorubicin-loaded platelets: role of cancer cells and platelet extracellular vesicles activation loop. *Journal of biomedical science* **27**, 45 (2020).

[82] Li, J., Ai, Y., Wang, L., Bu, P., Sharkey, C. C., Wu, Q., … King, M. R. Targeted drug delivery to circulating tumor cells via platelet membrane-functionalized particles. *Biomaterials* **76**, 52–65 (2016).

[83] Pei, W., Huang, B., Chen, S., Wang, L., Xu, Y., & Niu, C. Platelet-Mimicking Drug Delivery Nanoparticles for Enhanced Chemo-Photothermal Therapy of Breast Cancer. *International Journal of Nanomedicine* **15**, 10151–10167 (2020).

[84] Jing, L., Qu, H., Wu, D., Zhu, C., Yang, Y., Jin, X., & Wang, Y. Platelet-camouflaged nanococktail: Simultaneous inhibition of drug-resistant tumor growth and metastasis via a cancer cells and tumor vasculature dual-targeting strategy. *Theranostics* **8**, 2683–2695 (2018).

[85] Bang, K. H., Na, Y. G., Huh, H. W., Hwang, S. J., Kim, M. S., Kim, M., Lee, H. K., & Cho, C. W. (2019). The Delivery Strategy of Paclitaxel Nanostructured Lipid Carrier Coated with Platelet Membrane. *Cancers* **11**, 807 (2019).

[86] Pan, V., Siva, P. N., Modery-Pawlowski, C. L., Singh Sekhon, U. D., & Gupta, A. S. Targeted killing of metastatic cells using a platelet-inspired drug delivery system. *RSC Advances* **5**, 46218–46228 (2015).

[87] Meng, W., He, C., Hao, Y., Wang, L., Li, L., & Zhu, G. Prospects and challenges of extracellular vesicle-based drug delivery system: considering cell source. *Drug Delivery* **27**, *585–598* (2020).

[88] Mulcahy, L. A., Pink, R. C., & Carter, D. R. Routes and mechanisms of extracellular vesicle uptake. *Journal of extracellular vesicles* **3**, 24641 (2014).

[89] Kaksonen, M., & Roux, A. Mechanisms of clathrin-mediated endocytosis. *Nature Reviews Molecular Cell Biology* **19**, *313–326* (2018).

[90] Parton, R. G., McMahon, K.-A., & Wu, Y. Caveolae: Formation, dynamics, and function. *Current Opinion in Cell Biology* **65**, 8–16 (2020).

[91] Ni, K., Wang, C., Carnino, J. M., & Jin, Y. The Evolving Role of Caveolin-1: A Critical Regulator of Extracellular Vesicles. *Medical sciences (Basel, Switzerland)* **8**, 46 (2020).

[92] Costa Verdera, H., Gitz-Francois, J. J., Schiffelers, R. M., & Vader, P. Cellular uptake of extracellular vesicles is mediated by clathrin-independent endocytosis and macropinocytosis. *Journal of Controlled*

Release **266**, 100–108 (2017).

[93] Botelho, R. J., & Grinstein, S. Phagocytosis. *Current Biology* **21**, R533–R538 (2011).

[94] Flannagan, R. S., Jaumouillé, V., & Grinstein, S. The Cell Biology of Phagocytosis. *Annual Review of Pathology: Mechanisms of Disease* **7***,* 61–98 (2012).

[95] Kerr, M. C., & Teasdale, R. D. Defining macropinocytosis. *Traffic (Copenhagen, Denmark)* **10**, 364–371 (2009).

[96] Ritter, M., Bresgen, N., & Kerschbaum, H. H. From Pinocytosis to Methuosis-Fluid Consumption as a Risk Factor for Cell Death. *Frontiers in cell and developmental biology* **9**, 651982 (2021).

[97] Lajoie, P., & Nabi, I. R. Lipid rafts, caveolae, and their endocytosis. *International review of cell and molecular biology* **282**, 135–163 (2010).

[98] Lajoie, P., & Nabi, I. R. Regulation of raft-dependent endocytosis. *Journal of cellular and molecular medicine* **11**, 644–653 (2007).

[99] Ewers, H., & Helenius, A. Lipid-Mediated Endocytosis. *Cold Spring Harbor Perspectives in Biology* **3**, *a004721* (2011).

[100] Prada, I., & Meldolesi, J. Binding and Fusion of Extracellular Vesicles to the Plasma Membrane of Their Cell Targets. *International journal of molecular sciences* **17**, 1296 (2016).

[101] Livshits, M. A., Khomyakova, E., Evtushenko, E. G., Lazarev, V. N., Kulemin, N. A., Semina, S. E., Generozov, E. V., & Govorun, V. M. Isolation of exosomes by differential centrifugation: Theoretical analysis of a commonly used protocol. *Scientific reports* **5**, 17319 (2015).

[102] Coumans, F., Brisson, A. R., Buzas, E. I., Dignat-George, F., Drees, E., El-Andaloussi, S., Emanueli, C., Gasecka, A., Hendrix, A., Hill, A. F., Lacroix, R., Lee, Y., van Leeuwen, T. G., Mackman, N., Mäger, I., Nolan, J. P., van der Pol, E., Pegtel, D. M., Sahoo, S., Siljander, P., … Nieuwland, R. Methodological Guidelines to Study Extracellular Vesicles. *Circulation research* **120**, 1632–1648 (2017).

[103] Axis-Shield Density Gradient Media. Types of centrifugal separations. URL: https://www.axis-shield-density-gradient-media.com/Types%20of%20centrrifugal%20separations-1.pdf

[104] Tengattini, S. Chromatographic Approaches for Purification and Analytical Characterization of Extracellular Vesicles: Recent Advancements. *Chromatographia* **82**, 415-424 (2019).

[105] Yang, D., Zhang, W., Zhang, H., Zhang, F., Chen, L., Ma, L., … Wang, T. Progress, opportunity, and perspective on exosome isolation - efforts for efficient exosome-based theranostics. *Theranostics* **10***,* 3684–3707 (2020).

[106] Villa, F., Quarto, R., & Tasso, R. *Extracellular Vesicles as Natural, Safe and Efficient Drug Delivery Systems. Pharmaceutics* **11**, 557 (2019).

[107] Villata, S., Canta, M., & Cauda, V. EVs and Bioengineering: From Cellular Products to Engineered Nanomachines. *International journal of molecular sciences* **21**, 6048 (2020).

[108] Antimisiaris, S. G., Mourtas, S., & Marazioti, A. Exosomes and Exosome-Inspired Vesicles for Targeted Drug Delivery. *Pharmaceutics* **10**, 218 (2018).

[109] Pascucci, L., Coccè, V., Bonomi, A., Ami, D., Ceccarelli, P., Ciusani, E., Viganò, L., Locatelli, A., Sisto, F., Doglia, S. M., Parati, E., Bernardo, M. E., Muraca, M., Alessandri, G., Bondiolotti, G., & Pessina, A. Paclitaxel is incorporated by mesenchymal stromal cells and released in exosomes that inhibit in vitro tumor growth: a new approach for drug delivery. *Journal of controlled release: official journal of the Controlled Release Society* **192**, 262–270 (2014).

[110] Saari, H., Lázaro-Ibáñez, E., Viitala, T., Vuorimaa-Laukkanen, E., Siljander, P., & Yliperttula, M. Microvesicle- and exosome-mediated drug delivery enhances the cytotoxicity of Paclitaxel in autologous prostate cancer cells. *Journal of controlled release: official journal of the Controlled Release Society* **220**, 727–737 (2015).

[111] Weaver, J. Electroporation in cells and tissues: A biophysical phenomenon due to electromagnetic fields *Radio Science* **30**, 205–221 (1995).

[112] Weaver, J. C., & Chizmadzhev, Y. A. Theory of electroporation: A review. *Bioelectrochemistry and Bioenergetics* **41***, 135–160* (1996).

[113] Zhao, Y.-Z., & Lu, C.-T. Increasing the Entrapment of Protein-Loaded Liposomes with a Modified Freeze–Thaw Technique: A Preliminary Experimental Study. Drug Development and Industrial Pharmacy **35**, 165–171 (2009).

[114] Parsi, K. Interaction of detergent sclerosants with cell membranes. *Phlebology: The Journal of Venous Disease* **30***, 306–315* (2014).

[115] Aguirre-Ramírez, M., Silva-Jiménez, H., Banat, I. M., & Díaz De Rienzo, M. A. Surfactants: physicochemical interactions with biological macromolecules. *Biotechnology Letters* **43**, 523–535 (2021).

[116] Olson, F., Hunt, C. A., Szoka, F. C., Vail, W. J., & Papahadjopoulos, D. Preparation of liposomes of defined size distribution by extrusion through polycarbonate membranes. *Biochimica et Biophysica Acta (BBA) - Biomembranes* **557**, 9–23 (1979).

[117] Ong, S. G., Chitneni, M., Lee, K. S., Ming, L. C., & Yuen, K. H. Evaluation of Extrusion Technique for Nanosizing Liposomes. *Pharmaceutics* **8**, 36 (2016).

[118] Direção Geral da Saúde, "Norma número 010/2012; 16/12/2012: Utilização Clínica de Concentrados Plaquetários no Adulto, (2012).

[119] Van Deun, J., Mestdagh, P., Sormunen, R., Cocquyt, V., Vermaelen, K., Vandesompele, J., Bracke, M., De Wever, O., & Hendrix, A. The impact of disparate isolation methods for extracellular vesicles on downstream RNA profiling. *Journal of extracellular vesicles* **3**, 24858 (2014).

[120] Kesarwani,P., Tekade, R., and Jain,N. Spectrophotometric estimation of paclitaxel. *International Journal of Advances in Pharmaceutical Sciences* **2**, 29-32 (2011).

[121] Sugo, K., & Ebara, M. A simple spectrophotometric evaluation method for the hydrophobic anticancer drug paclitaxel. *PeerJ Analytical Chemistry* **2**, e3 (2020).

[122] Subedi, P., Schneider, M., Philipp, J., Azimzadeh, O., Metzger, F., Moertl, S., Atkinson, M. J., & Tapio, S. Comparison of methods to isolate proteins from extracellular vesicles for mass spectrometry-based proteomic analyses. *Analytical biochemistry* **584**, 113390 (2019).

[123] Van der Vlist, E. J., Nolte-'t Hoen, E. N., Stoorvogel, W., Arkesteijn, G. J., & Wauben, M. H. Fluorescent labeling of nano-sized vesicles released by cells and subsequent quantitative and qualitative analysis by high-resolution flow cytometry. *Nature protocols*, **7**, 1311-1326 (2012).

[124] Suarez-Arnedo, A., Torres Figueroa, F., Clavijo, C., Arbeláez, P., Cruz, J. C., & Muñoz-Camargo, C. An image J plugin for the high throughput image analysis of in vitro scratch wound healing assays. *PloS one* **15**, e0232565 (2020).

[125] Carpentier, G. ImageJ contribution: Angiogenesis Analyzer. *ImageJ News*, (2012).

[126] Carpentier, G., Berndt, S., Ferratge, S., Rasband, W., Cuendet, M., Uzan, G., & Albanese, P. Angiogenesis Analyzer for ImageJ - A comparative morphometric analysis of "Endothelial Tube Formation Assay" and "Fibrin Bead Assay". *Scientific reports* **10**, 11568 (2020).

[127] Brennan, K., Martin, K., FitzGerald, S. P., O'Sullivan, J., Wu, Y., Blanco, A., Richardson, C., & Mc Gee, M. M. A comparison of methods for the isolation and separation of extracellular vesicles from protein and lipid particles in human serum. *Scientific reports* **10**, 1039 (2020).

[128] Karimi, N., Cvjetkovic, A., Jang, S. C., Crescitelli, R., Hosseinpour Feizi, M. A., Nieuwland, R., Lötvall, J., & Lässer, C. Detailed analysis of the plasma extracellular vesicle proteome after separation from lipoproteins. *Cellular and molecular life sciences: CMLS* **75**, 2873–2886 (2018).

[129] Gardiner, C., Di Vizio, D., Sahoo, S., Théry, C., Witwer, K. W., Wauben, M., & Hill, A. F. Techniques used for the isolation and characterization of extracellular vesicles: results of a worldwide survey. *Journal of extracellular vesicles* **5**, 32945 (2016).

[130] Deville, S., Berckmans, P., Van Hoof, R., Lambrichts, I., Salvati, A., & Nelissen, I. Comparison of extracellular vesicle isolation and storage methods using high-sensitivity flow cytometry. *PloS one* **16**, e0245835 (2021).

[131] Izon science. Specifications and operational guide for smart columns, rapid & reliable purification of extracellular vesicle, qEVoriginal User Manual, (2021).

[132] Phillips, W., Willms, E., & Hill, A. F. Understanding extracellular vesicle and nanoparticle heterogeneity: Novel methods and considerations. *Proteomics* **21**, e2000118 (2021).

[133] Takov, K., Yellon, D. M., & Davidson, S. M. Comparison of small extracellular vesicles isolated from plasma by ultracentrifugation or size-exclusion chromatography: yield, purity and functional potential. *Journal of extracellular vesicles* **8**, 1560809 (2018).

[134] Tian, Y., Gong, M., Hu, Y., Liu, H., Zhang, W., Zhang, M., Hu, X., Aubert, D., Zhu, S., Wu, L., & Yan, X. Quality and efficiency assessment of six extracellular vesicle isolation methods by nano-flow cytometry. *Journal of extracellular vesicles* **9**, 1697028 (2019).

[135] Onódi, Z., Pelyhe, C., Terézia Nagy, C., Brenner, G. B., Almási, L., Kittel, Á., Manček-Keber, M., Ferdinandy, P., Buzás, E. I., & Giricz, Z. Isolation of High-Purity Extracellular Vesicles by the Combination of Iodixanol Density Gradient Ultracentrifugation and Bind-Elute Chromatography From Blood Plasma. *Frontiers in physiology* **9**, 1479 (2018).

[136] Otahal, A., Kuten-Pella, O., Kramer, K., Neubauer, M., Lacza, Z., Nehrer, S., & De Luna, A. Functional repertoire of EV-associated miRNA profiles after lipoprotein depletion via ultracentrifugation and size exclusion chromatography from autologous blood products. *Scientific reports* **11**, 5823 (2021).

[137] Gudbergsson, J. M., Johnsen, K. B., Skov, M. N., & Duroux, M. Systematic review of factors influencing extracellular vesicle yield from cell cultures. *Cytotechnology* **68**, 579–592 (2015).

[138] Pavani, K. C., Lin, X., Hamacher, J., Broeck, W., Couck, L., Peelman, L., Hendrix, A., & Van Soom, A. The Separation and Characterization of Extracellular Vesicles from Medium Conditioned by Bovine Embryos. *International journal of molecular sciences* **21**, 2942 (2020).

[139] Zhang, X., Borg, E., Liaci, A. M., Vos, H. R., & Stoorvogel, W. A novel three step protocol to isolate extracellular vesicles from plasma or cell culture medium with both high yield and purity. *Journal of extracellular vesicles* **9**, 1791450 (2020).

[140] Price, C. A.1- Particle Abstraction in Biology—An Introduction. *Centrifugation in Density Gradients, Academic Press*, 1–11 (1982).

[141] Freitas, D., Balmaña, M., Poças, J., Campos, D., Osório, H., Konstantinidi, A., Vakhrushev, S. Y., Magalhães, A., & Reis, C. A. Different isolation approaches lead to diverse glycosylated extracellular vesicle populations. *Journal of extracellular vesicles* **8**, 1621131(2019).

[142] Aatonen, M. T., Ohman, T., Nyman, T. A., Laitinen, S., Grönholm, M., & Siljander, P. R. Isolation and characterization of platelet-derived extracellular vesicles. *Journal of extracellular vesicles* **3**, 24692 (2014).

[143] Kuravi, S. J., Harrison, P., Rainger, G. E., & Nash, G. B. Ability of Platelet-Derived Extracellular Vesicles to Promote Neutrophil-Endothelial Cell Interactions. *Inflammation* **42** 290–305 (2019).

[144] Böing, A. N., van der Pol, E., Grootemaat, A. E., Coumans, F. A., Sturk, A., & Nieuwland, R. Single-step isolation of extracellular vesicles by size-exclusion chromatography. *Journal of extracellular vesicles* **3**, 23430 (2014).

[145] Rosado, M., Silva, R., G Bexiga, M., G Jones, J., Manadas, B., & Anjo, S. I. Advances in biomarker detection: Alternative approaches for blood-based biomarker detection. *Advances in clinical chemistry* **92**, 141–199 (2019).

[146] Lobb, R. J., Becker, M., Wen, S. W., Wong, C. S., Wiegmans, A. P., Leimgruber, A., & Möller, A. Optimized exosome isolation protocol for cell culture supernatant and human plasma. *Journal of extracellular vesicles* **4**, 27031 (2015).

[147] Dong, L., Zieren, R. C., Horie, K., Kim, C. J., Mallick, E., Jing, Y., Feng, M., Kuczler, M. D., Green, J., Amend, S. R., Witwer, K. W., de Reijke, T. M., Cho, Y. K., Pienta, K. J., & Xue, W. Comprehensive evaluation of methods for small extracellular vesicles separation from human plasma, urine and cell culture medium. *Journal of extracellular vesicles* **10**, e12044 (2020).

[148] Veerman, R. E., Teeuwen, L., Czarnewski, P., Güclüler Akpinar, G., Sandberg, A., Cao, X., Pernemalm, M., Orre, L. M., Gabrielsson, S., & Eldh, M. Molecular evaluation of five different isolation methods for extracellular vesicles reveals different clinical applicability and subcellular origin. *Journal of extracellular vesicles* **10**, e12128 (2021).

[149] Nolte-'t Hoen, E. N., van der Vlist, E. J., Aalberts, M., Mertens, H. C., Bosch, B. J., Bartelink, W., Mastrobattista, E., van Gaal, E. V., Stoorvogel, W., Arkesteijn, G. J., & Wauben, M. H. Quantitative and qualitative flow cytometric analysis of nanosized cell-derived membrane vesicles. *Nanomedicine: nanotechnology, biology, and medicine* **8**, 712–720 (2012).

[150] Tian, T., Wang, Y., Wang, H., Zhu, Z., & Xiao, Z. Visualizing of the cellular uptake and intracellular trafficking of exosomes by live-cell microscopy. *Journal of cellular biochemistry* **111**, 488–496 (2010).

[151] Pedrioli, G., & Paganetti, P. Hijacking Endocytosis and Autophagy in Extracellular Vesicle Communication: Where the Inside Meets the Outside. *Frontiers in cell and developmental biology* **8**, 595515 (2021).

[152] Lee, H., & Kang, K. T. Advanced tube formation assay using human endothelial colony forming cells for *in vitro* evaluation of angiogenesis. *The Korean journal of physiology & pharmacology: official journal of the Korean Physiological Society and the Korean Society of Pharmacology* **22**, 705–712 (2018).

[153] Hock, S., Fan, Z., Buchfelder, M., Eyüpoglu, I., Savaskan, N. Brain Tumor-induced angiogenesis: approaches and bioassays. *Evolution of the Molecular Biology of Brain Tumors and the Therapeutic Implications **4***, 125-146 (2013)

[154] Reinmuth, N., Rensinghoff, S., Raedel, M., Fehrmann, N., Schwöppe, C., Kessler, T., … Mesters, R. Paracrine interactions of vascular endothelial growth factor and platelet-derived growth factor in endothelial and lung cancer cells. *International Journal of* Oncology **31**, 621-626 (2007).

[155] Bai, Y., Bai, L., Zhou, J., Chen, H., & Zhang, L. Sequential delivery of VEGF, FGF-2 and PDGF from the polymeric system enhance HUVECs angiogenesis in vitro and CAM angiogenesis. *Cellular Immunology*

323, 19–32 (2018).

[156] Gai, C., Carpanetto, A., Deregibus, M. C., & Camussi, G. Extracellular vesicle-mediated modulation of angiogenesis. *Histology and histopathology* **31**, 379–391 (2016).

[157] Brill, A., Dashevsky, O., Rivo, J., Gozal, Y., & Varon, D. Platelet-derived microparticles induce angiogenesis and stimulate post-ischemic revascularization. *Cardiovascular research* **67**, 30–38 (2005).

[158] Michael, J. V., Wurtzel, J., Mao, G. F., Rao, A. K., Kolpakov, M. A., Sabri, A., Hoffman, N. E., Rajan, S., Tomar, D., Madesh, M., Nieman, M. T., Yu, J., Edelstein, L. C., Rowley, J. W., Weyrich, A. S., & Goldfinger, L. E. Platelet microparticles infiltrating solid tumors transfer miRNAs that suppress tumor growth. *Blood* **130**, 567–580 (2017).

[159] Gaurav, I., Thakur, A., Iyaswamy, A., Wang, X., Chen, X., & Yang, Z. Factors Affecting Extracellular Vesicles Based Drug Delivery Systems. *Molecules (Basel, Switzerland)* **26**, 1544 (2021).

[160] Kingston D. G. Taxol: the chemistry and structure-activity relationships of a novel anticancer agent. *Trends in biotechnology* **12**, 222–227 (1994).

[161] Kalimuthu, S., Gangadaran, P., Rajendran, R. L., Zhu, L., Oh, J. M., Lee, H. W., Gopal, A., Baek, S. H., Jeong, S. Y., Lee, S. W., Lee, J., & Ahn, B. C. A New Approach for Loading Anticancer Drugs into Mesenchymal Stem Cell-Derived Exosome Mimetics for Cancer Therapy. *Frontiers in pharmacology* **9**, 1116 (2018).

[162] Jang, S. C., Kim, O. Y., Yoon, C. M., Choi, D.-S., Roh, T.-Y., Park, J., … Gho, Y. S. *Bioinspired Exosome-Mimetic Nanovesicles for Targeted Delivery of Chemotherapeutics to Malignant Tumors. ACS Nano* **7**, 7698–7710 (2013).

[163] Cao, X. H., Liang, M. X., Wu, Y., Yang, K., Tang, J. H., & Zhang, W. Extracellular vesicles as drug vectors for precise cancer treatment. *Nanomedicine (London, England)* **16**, 1519–1537 (2021).

[164] Belotti, D., Vergani, V., Drudis, T., Borsotti, P., Pitelli, M. R., Viale, G., Giavazzi, R., & Taraboletti, G. The microtubule-affecting drug paclitaxel has antiangiogenic activity. *Clinical cancer research: an official journal of the American Association for Cancer Research* **2**, 1843–1849 (1996).

[165] Bocci, G., Di Paolo, A., & Danesi, R. The pharmacological bases of the antiangiogenic activity of paclitaxel. *Angiogenesis* **16**, 481–492 (2013).

[166] Tang, K., Zhang, Y., Zhang, H., Xu, P., Liu, J., Ma, J., Lv, M., Li, D., Katirai, F., Shen, G. X., Zhang, G., Feng, Z. H., Ye, D., & Huang, B. Delivery of chemotherapeutic drugs in tumour cell-derived microparticles. *Nature communications* **3**, 1282 (2012).

[167] Kumar, A., Ahmad, A., Vyawahare, A., & Khan, R. Membrane Trafficking and Subcellular Drug Targeting Pathways. *Frontiers in pharmacology* **11**, 629 (2020).

[168] Elsharkasy, O. M., Nordin, J. Z., Hagey, D. W., de Jong, O. G., Schiffelers, R. M., Andaloussi, S. E., & Vader, P. Extracellular vesicles as drug delivery systems: Why and how?. *Advanced drug delivery reviews*, **159**, 332–343 (2020).

[169] Faria-Ramos, I., Poças, J., Marques, C., Santos-Antunes, J., Macedo, G., Reis, C. A., & Magalhães, A. Heparan Sulfate Glycosaminoglycans: (Un)Expected Allies in Cancer Clinical Management. *Biomolecules* **11**, 136 (2021).

[170] Cerezo-Magaña, M., Bång-Rudenstam, A., & Belting, M. The pleiotropic role of proteoglycans in extracellular vesicle mediated communication in the tumor microenvironment. *Seminars in cancer biology* **62**, 99–107 (2020).

[171] Preta, G., Cronin, J. G., & Sheldon, I. M. Dynasore - not just a dynamin inhibitor. *Cell communication Signal* **13**, 24 (2015).

[172] Mellor, P., Harvey, J. R., Murphy, K. J., Pye, D., O'Boyle, G., Lennard, T. W., Kirby, J. A., & Ali, S. Modulatory effects of heparin and short-length oligosaccharides of heparin on the metastasis and growth of LMD MDA-MB 231 breast cancer cells in vivo. *British journal of cancer* **97**, 761–768 (2007).

[173] Privat, M., Cavard, A., Zekri, Y., Ponelle-Chachuat, F., Molnar, I., Sonnier, N., & Bignon, Y. J. A high expression ratio of RhoA/RhoB is associated with the migratory and invasive properties of basal-like Breast Tumors. *International journal of medical sciences* **17**, 2799–2808 (2020).

[174] Tang, Y., Wang, Y., Deosarkar, S., Soroush, F., Kiani, M. F., & Wang, B. Fast, Stable Induction of P-Glycoprotein-mediated Drug Resistance in BT-474 Breast Cancer Cells by Stable Transfection of ABCB1 Gene. *Anticancer research* **35**, 2531–2538 (2015).

[175] Dong, X., Bai, X., Ni, J., Zhang, H., Duan, W., Graham, P., & Li, Y. Exosomes and breast cancer drug resistance. *Cell death & disease* **11**, 987 (2020).

[176] Hoosain, F. G., Choonara, Y. E., Tomar, L. K., Kumar, P., Tyagi, C., du Toit, L. C., & Pillay, V. Bypassing P-Glycoprotein Drug Efflux Mechanisms: Possible Applications in Pharmacoresistant Schizophrenia Therapy. *BioMed research international* **2015**, 484963 (2015).

[177] Ndungu, J. M., Lu, Y. J., Zhu, S., Yang, C., Wang, X., Chen, G., Shin, D. M., Snyder, J. P., Shoji, M., & Sun, A. Targeted delivery of paclitaxel to tumor cells: synthesis and in vitro evaluation. *Journal of medicinal chemistry* **53**, 3127–3132 (2010).

[178] Quirk, S. M., Cowan, R. G., Harman, R. M., Hu, C. L., & Porter, D. A. Ovarian follicular growth and atresia: the relationship between cell proliferation and survival. *Journal of animal science* **82** *E-Suppl*, E40–E52 (2004).

[179] Zhuang, X., Xiang, X., Grizzle, W., Sun, D., Zhang, S., Axtell, R. C., Ju, S., Mu, J., Zhang, L., Steinman, L., Miller, D., & Zhang, H. G. Treatment of brain inflammatory diseases by delivering exosome encapsulated anti-inflammatory drugs from the nasal region to the brain. *Molecular therapy: the journal of the American Society of Gene Therapy* **19**, 1769–1779 (2011).

CHAPTER 7

7. Supplementary information

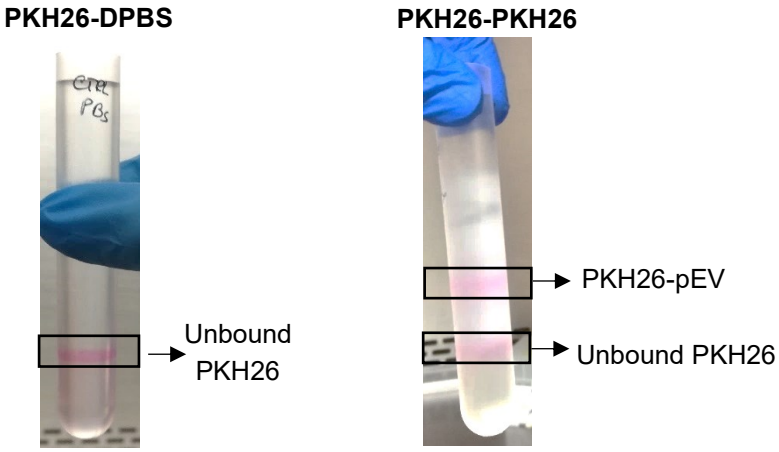

Figure 7.1: Separation of PKH26-pEV by DGUC. The presence of two bands marked in the figure indicates a clear separation of PKH26-pEV (upper band) at the level of fractions enriched in pEV (fractions 8 and 9) from the unbound dye (lower band) located at denser fractions.

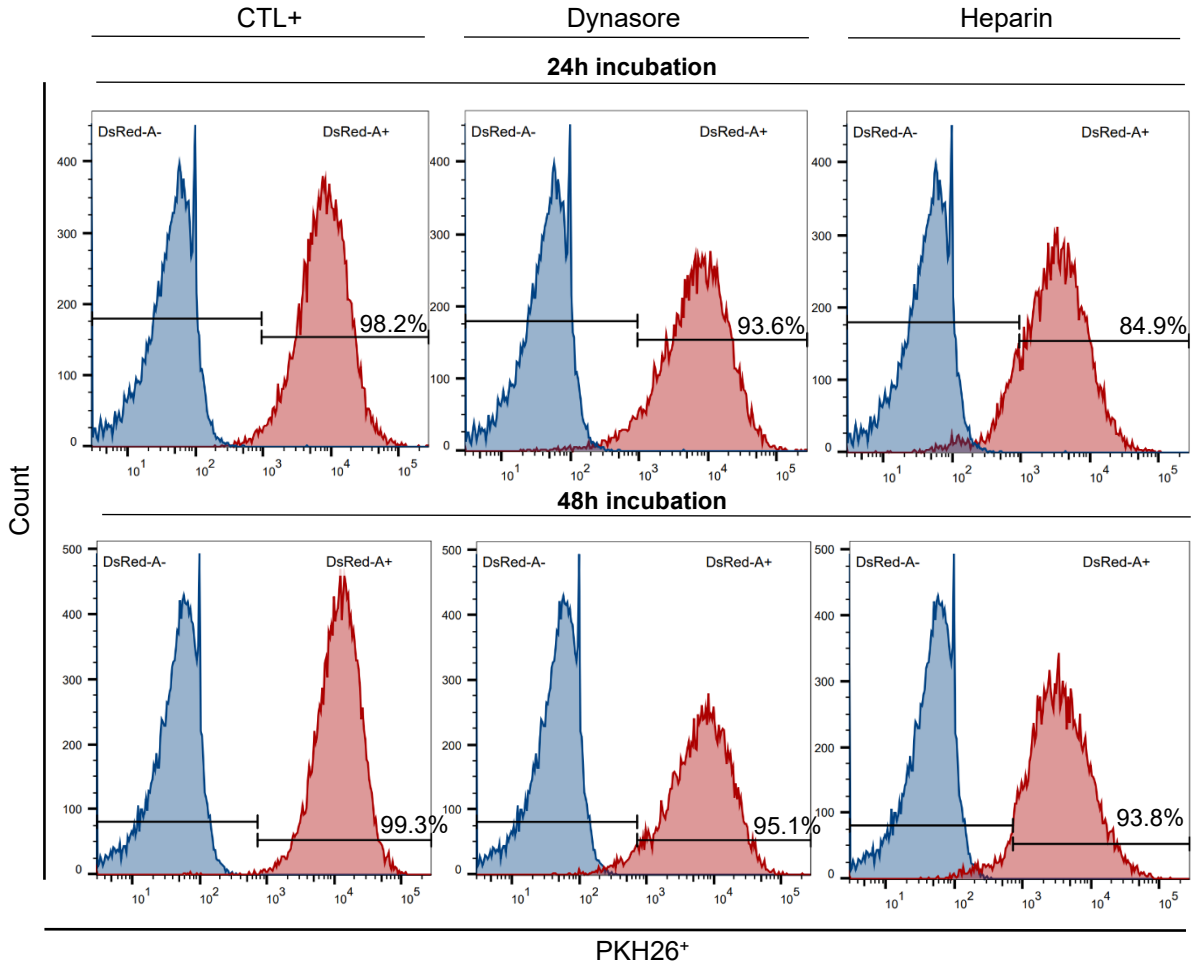

Figure 7.2: Quantification of EV uptake blocking in MDA-MB-231 cells by flow cytometry. Representative histograms showing PKH26 fluorescence intensity of cells incubated with PKH26-pEV (6000 pEV/cell) in the presence of the EV uptake chemical Inhibitors, dynasore (100 μM), and heparin (500 μg/mL) for 24 h and 48 h. Cells incubated only with PKH26-EV were used as positive control (CTL+) and cells completely untreated were used as negative control for both time points. Blue filled histograms show control negative population and red filled histograms represent the PKH26-pEV population. The x-axis represents the detection by the DsRed-A filter and y-axis represents pEV counts.

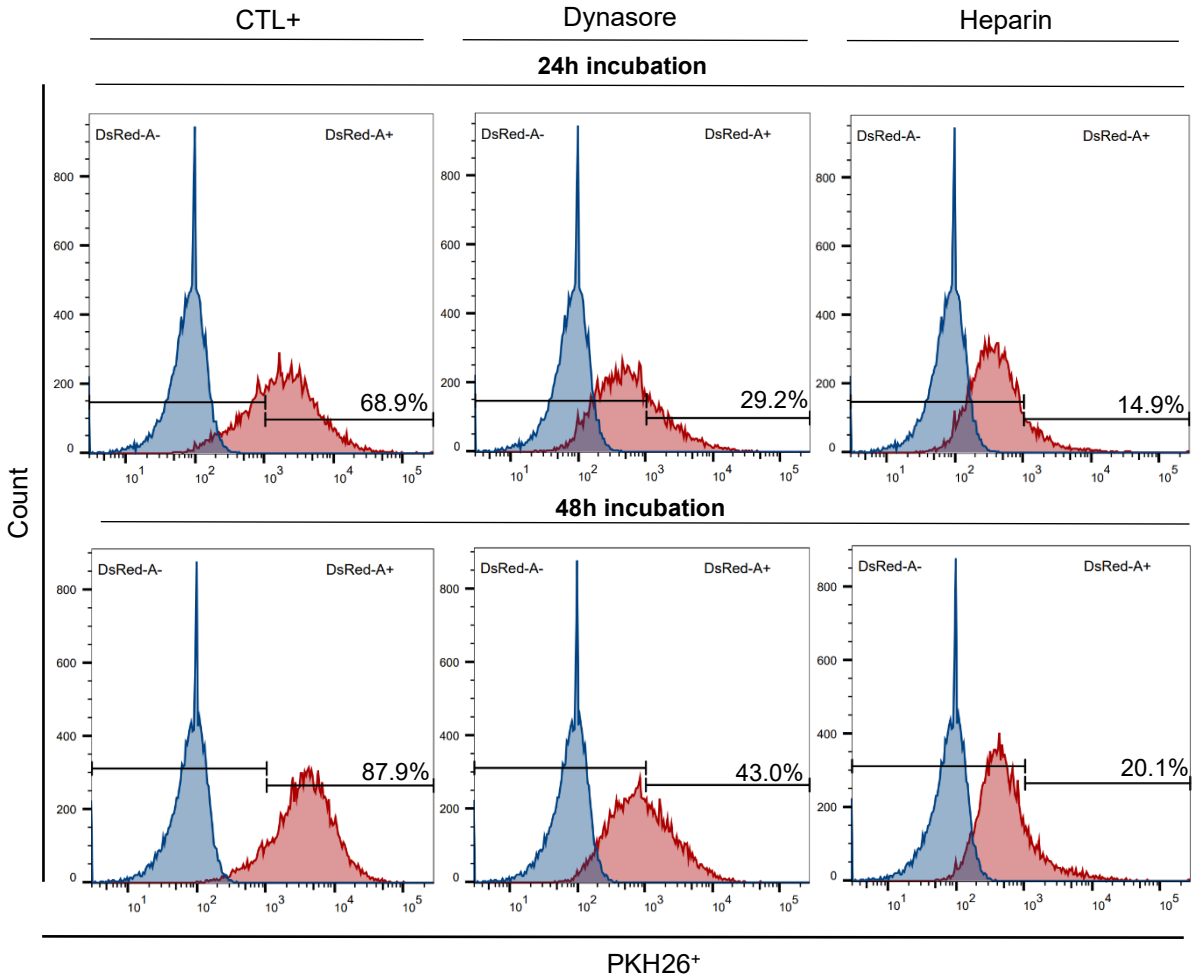

Figure 7.3: Quantification of EV uptake blocking in BT474 cells by flow cytometry. Representative histograms showing PKH26 fluorescence intensity of cells incubated with PKH26-pEV (6000 pEV/cell) in the presence of the EV uptake chemical Inhibitors, dynasore (100 μM), and heparin (500 μg/mL) for 24 h and 48 h. Cells incubated only with PKH26-EV were used as positive control (CTL+) and cells completely untreated were used as negative control for both time points. Blue filled histograms show control negative population and red filled histograms represent the PKH26-pEV population. The x-axis represents the detection by the DsRed-A filter and y-axis represents pEV counts.

2021

ANA EDUARDA LOPES MELICIANO

EMPOWERING THE THERAPEUTICAL POTENTIAL OF CLINICALLY EXPIRED PLATELET CONCENTRATES: A NEW SOURCE OF EXTRACELLULAR VESICLES

NOVA SCHOOL OF SCIENCE & TECHNOLOGY